Chem Soc Rev

Nanostructured Mo-based electrode materials for electrochemical energy storage

SCHOLARONE™
Manuscripts

Nanostructured Mo-based electrode materials for electrochemical energy storage

Xianluo Hu,* Wei Zhang, Xiaoxiao Liu, Yueni Mei, and Yunhui Huang*

State Key Laboratory of Materials Processing and Die &Mould Technology, School of

Materials Science and Engineering, HuazhongUniversity of Science and Technology,

Wuhan 430074, P. R. China

E-mail: huxl@mail.hust.edu.cn (X. L. Hu); huangyh@mail.hust.edu.cn (Y. H. Huang)

Abstract: The development of advanced energy storage devices is at the forefront of research geared towards a sustainable future. Nanostructured materials are advantageous in offering huge surface to volume ratios, favorable transport features, and attractive physicochemical properties. They have been extensively explored in various fields of energy storage and conversion. This review is focused largely on the recent progresses in nanostructured Mo-based electrode materials including molybdenum oxides (MoO_x, $2 \leq x \leq 3$), dichalconides (MoX_2, $X = S$, Se), and oxysalts for rechargeable lithium/sodium-ion batteries, Mg batteries, and supercapacitors. Mo-based compounds including MoO_2, MoO_3, MoO_{3-y} ($0 < y < 1$), MMo_xO_y ($M = Fe$, Co, Ni, Ca, Mn, Zn, Mg, or Cd; $x = 1$, $y = 4$; $x = 3$, $y = 8$), MoS_2, $MoSe_2$, $(MoO_2)_2P_2O_7$, $LiMoO_2$, Li_2MoO_3, *etc.* possess multiple valence states and exhibit rich chemistry. They are very attractive candidates for efficient electrochemical energy storage systems because of their unique physicochemical

properties, such as conductivity, mechanical and thermal stability, and cyclability. In this review, we aim to provide a systematic summary on the synthesis, modification, and electrochemical performance of nanostructured Mo-based compounds, as well as their energy storage applications in lithium/sodium-ion batteries, Mg batteries, and pseudocapacitors. The relationship between nanoarchitectures and electrochemical performances as well as the related charge-storage mechanism is discussed. Moreover, remarks on the challenges and perspectives of Mo-containing compounds for further development in electrochemical energy storage applications are proposed. This review sheds light on the sustainable development of advanced rechargeable batteries and supercapacitors with nanostructured Mo-based electrode materials.

1. Introduction

Nowadays the increasing environmental problems, such as global warming and pollution, give a great impetus to reduce the society's dependence on fossil fuels. It is preferable to produce energy from renewable and sustainable resources (e.g., solar and wind). The utilization of electricity generated from intermittent renewable sources requires efficient energy storage systems (ESSs). Among clean energy technologies, electrochemical ESSs are considered the most feasible, environmentally friendly, and sustainable.[1-6] Electrochemical ESSs such as rechargeable batteries and supercapacitors have been widely used in portable electronics, electric vehicles, and smart electrical grids.[7-12]

Lithium-ion batteries (LIBs) are one type of rechargeable energy-storage devices based on Li-ion shuffling between a negative electrode (also termed as anode) and a positive electrode (cathode). During discharge, Li ions carry the current from the anode to the cathode through the nonaqueous electrolyte and separator diaphragm, and the process reverses in charging. Since commercialization by Sony in 1991, LIBs have become one kind of the most popular rechargeable batteries for portable electronics (e.g., laptops, cell phones, and digital cameras), because of high energy density, no memory effect, and only a slow loss of capacity when not in use. Meanwhile, the advent of LIBs has ushered in the wireless revolution, and further stimulated a quest to power electric vehicles (EVs) and hybrid electric vehicles (HEVs). The electrode materials are the key components of LIBs that play crucial roles in the overall performance.[13-17] In order to power EVs or HEVs, five basic factors including energy density, power density, cost, life and safety need to be well balanced.

Dramatic developments in next-generation electrical transportation and large-scale ESSs for smart grids will require substantially greater amounts of materials to build large batteries. Li is not regarded as an abundant element. The mean mass fraction of Li in the earth's crust is estimated to be only 20 ppm. It is also witnessed that the price of the Li resource has been increasing in recent years, arising from more and more use of LIBs. In contrast, the abundance and low cost of Na in the earth will become advantageous when a large amount of materials are demanded for renewable energy

solutions.[18-23] Moreover, Na is the second-lightest and -smallest alkali metal next to Li. Therefore, the sacrifice in energy density is expected to be minimized if the same electrochemical insertion is utilized for discharge-charge cycling. Owing to the similarities in electrochemistry between Li and Na, the state-of-the-art advances in LIBs may pave the way for developing sodium-ion batteries (SIBs). Nevertheless, Na ion intercalation and storage mechanisms are also scientifically challenging, since Na^+ ions are ~70% larger in radius than Li^+ ions. It is highly desirable to explore suitable host materials to accommodate Na^+ ions and facilitate reversible insertion/extraction of Na^+ ions. In additionto Li, Mg is another abundant element in the earth's crust, leading to wider availability and much lower cost. Rechargeable Mg batteries are now gaining increasing interest especially after Aurbach's pioneering work.[24] Fundamentally, the science and technology of rechargeable Mg batteries are quite different from those of LIBs and SIBs.[25] The use of alkali metals such as Li and Na in rechargeable batteries is enabled by the formation of a solid electrolyte interface (SEI) layer on the surface of the electrodes via reacting with the electrolyte.[26,27] The passive SEI film hampers the transport of electrons, but is still permeable to Li^+ and Na^+ions. Compared to LIBs or SIBs, it is noted that the diffuse of alkaline earth metal cations like Mg^{2+} ions through interfacial passivation layers is much sluggish or even impossible. Meanwhile, Mg^{2+} ions have the divalent nature and Mg metal anodes are used in rechargeable Mg batteries. The divalent nature of Mg^{2+} ions enables a high theoretical specific capacity (2205 mA h g^{-1}).[28–30] In comparison to LIBs, however, the kinetically sluggish Mg intercalation/insertion and diffusion in cathode materials

as well as the incompatibility between the Mg anode and the electrolyte due to the high polarizing ability of the divalent Mg^{2+} ions, are the major obstacles for Mg rechargeable batteries.[31–32]

Supercapacitors, also known as electrochemical capacitors or ultracapacitors, have attracted much attention because of their fast charging capabilities, long charge-discharge cycles, and broad operating temperature ranges.[33] They can complement or even replace batteries in a wide variety of applications including electric vehicles, electronics and smart grids, when high power delivery or uptake is needed.[14, 34-37] Generally, supercapacitors can be classified into two categories based on the charge storage mechanism. One is the electrical double layer capacitor (EDLC), where electrical energy is stored by ion adsorption and desorption. The other type of supercapacitor is the so-called pseudocapacitor, in which electrical energy is stored by fast and reversible Faradic reactions.[35] The specific pseudo-capacitance often exceeds that of carbon materials used in EDLCs. The pseudo-capacitive behavior of the redox reactions is similar to the electrochemical reactions in rechargeable batteries. However, pseudo-capacitors often suffer from the drawbacks of a low power density (due to poor electrical conductivity), and a lack of stability during cycling. Moreover, hybrid capacitors with an asymmetrical electrode configuration, combining these two charge storage mechanisms (Faradaic and non-Faradaic), have recently aroused much interest. They offer an attractive alternative to conventional pseudo-capacitors or EDLCs by combining a battery-like electrode (energy source) with a capacitive-like electrode (power source) in the same cell, and the overall cell voltage, energy, and

power density can be improved.[38-48]

Nanomaterials with attractive chemical and physical properties are being explored for their potential in energy storage applications. The design and creation of new materials and substances that are chemically modified from the molecular and atomic level to sizes on the nanoscale would offer significantly enhanced functions for energy storage applications. Meanwhile, the development of advanced nanocharacterization techniques has facilitated the fundamental molecular-level understanding on structure-performance relationships, which are strongly related to the grain size and size distribution, shape, chemical composition, interfaces, surface (potentially with different electrolytes), and interactions between the constituent domains. This knowledge, together with effective synthetic strategies, has inspired the design and fabrication of novel nanostructured materials for a wide variety of energy-based applications. During the past decades, much effort has been particularly devoted to fabricating a great number of nanostructured materials as electrodes in a range of LIBs, SIBs, Mg batteries, and supercapacitors. This research trend has been evidenced by many important pioneering works published during the past decades.[37, 49-53] As expected, a notable improvement in performance has been achieved through recent advances in the development of advanced nanostructured materials and understanding on charge storage mechanisms.[54] In batteries and supercapacitors, nanostructuring of electrode materials may reduce diffusion/transport lengths for both ions and electrons, increase active sites, and relieve the volume expansion/contraction,

thus leading to improved capacity, and higher power/energy density, and longer cycle life. In some cases, new thermodynamics and/or kinetics allow enhanced phase transitions and rate capability during Li^+ intercalation/deintercalation. It is believed that new development in the field of nanomaterials chemistry holds the key to further breakthroughs in ESSs. Recently, many excellent reviews and reports on the preparation, modification, assembly, characterization, property, and engineering of nanostructured materials for energy storage applications have been published.[5, 55-65]

This article reviews recent advancements and trends in nanostructured molybdenum oxides (MoO_x, $2 \leq x \leq 3$), dichalconides (MoX_2, X = S, Se), and oxysalts for batteries and supercapacitors with high energy and power density. Their representative crystal structures are shown in Fig. 1. Mo-based oxides, dichalconides, and oxysalts possess multiple valence states and exhibit rich chemistry. Recent progress has demonstrated that nanostructured Mo-based compounds including MoO_2, MoO_3, MoO_{3-y} ($0 < y < 1$), MMo_xO_y (M = Fe, Co, Ni, Ca, Mn, Zn, Mg, or Cd; $x = 1$, $y = 4$; $x = 3$, $y = 8$), MoS_2, $MoSe_2$, $(MoO_2)_2P_2O_7$, $LiMoO_2$, Li_2MoO_3, *etc.* are very promising candidates for efficient electrochemical energy storage systems because of their unique physical and chemical properties, such as conductivity, mechanical and thermal stability, and cyclability. In this review, we present a summary on the synthesis, modification, and electrochemical performance of nanostructured Mo-based compounds. Also, their energy storage applications in the fields of LIBs, SIBs, Mg batteries, and pseudocapacitors are emphasized. The relationship between nanoarchitectures and electrochemical performances as well as related charge-storage mechanisms is

discussed. This review ends with an outlook of Mo-containing compounds for further development in electrochemical energy storage applications.
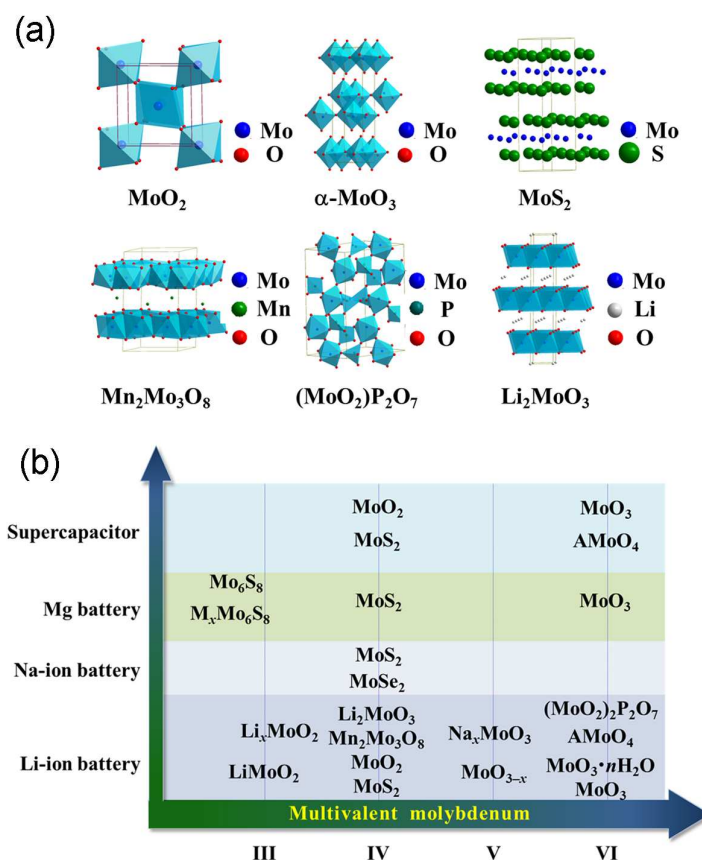
Fig. 1 (a) Cyrstal structures of monoclinic MoO_2, α-MoO_3, MoS_2, $Mn_2Mo_3O_8$, $(MoO_2)P_2O_7$, and Li_2MoO_3. (b) Multivalent Mo-based electrode materials with rich chemistry for electrochemical energy storage applications including LIBs, SIBs, Mg batteries, and supercapacitors.

2. Nanostructured Mo-based electrode materials for LIBs

2.1 MoO$_2$

In general, the Li-storage mechanisms for metal oxide-based anodes can be classified

into three types:[66,67] insertion reaction, alloying−dealloying, and conversion reaction.

A literature survey suggests that the oxides including early transition metal elements

such as TiO_2,[66-75] V_2O_5,[76, 77] and MoO_2[78, 79] are often found to be lithiated though the

insertion reaction. In contrast, the other ones like CoO,[80, 81] MnO,[82-85] and Fe_2O_3[86]

follow the conversion-reaction mechanism. The difference of their Li-cycling

reactions is probably related to the metal-oxygen bond strength. The conversion

reaction in metal oxides requires a heterogeneous charge transfer at the interfaces, Li^+

and O^{2-} in solid state, and M–O bond cleavage. The former group has a relatively

stronger metal-oxygen bond. For instance, the bond dissociation energy of Mo-O in

MoO_2 is about 678 kJ mol^{-1}, which is much higher than 368 kJ mol^{-1} for Co-O in

CoO.[87] Therefore, the insertion reaction occurs in MoO_2 without bond cleavage at

ambient temperature. MoO_2 crystallizes in a monoclinic cell as illustrated in Fig. 1. In

MoO_2 octahedra are distorted and Mo atoms are off-centre, leading to alternating

short and long Mo–Mo distances and Mo-Mo bonding.[88] MoO_2 has low metallic

electrical resistivity (8.8×10^{-5} Ω·cm at 300 K in bulk samples), high melting point,

and excellentchemical stability.[89] It has been extensively investigated in LIBs,

supercapacitors, solid state fuel cells, catalysis, sensors, recording media, and

electrochromic displays due to its efficient charge transport properties.[90-95]

2.1.1 Lithium-storage mechanism. As a matter of fact, the Li-insertion behavior in

MoO_2 was investigated 30 years ago.[96] However, its electrochemical Li-storage

performance receives little attention due to the sluggish kinetics in bulk MoO_2. So far,

several Li-cycling mechanisms for amorphous and crystalline MoO_2 anodes in LIBs

have been proposed, but some of them are still controversial at present. Actually, the

crystal size and crystallinity of MoO_2 materials should determine the specific

electrochemical reactions. Therefore, none of the given mechanisms is absolutely

suitable for all of the cases in MoO_2-based electrodes. As summarized as follows, four

representative Li-cycling mechanisms have been proposed for MoO_2.

(i) One-electron insertion (ordered Li$_x$MoO$_2$). Bulk or micrometer-sized MoO_2

accommodates Li usually through an insertion-type reaction with a theoretical

capacity of 209 mA h g^{-1}.[76]

$$MoO_2 + xLi^+ + xe^{-1} \leftrightarrow Li_xMoO_2 \text{ (crystalline ordered, } 0 < x < 1)$$
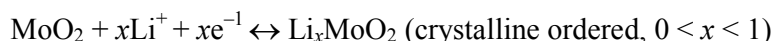
During electrochemical Li-cycling reactions, Li$^+$ storage sites are crystallographically

well-defined and the site amount determines Li$^+$ storage capacity. The bulk or

micrometer-sized MoO_2-based electrodes based on the insertion-reaction mechanism

(one-electron reduction) often suffers from poor cyclability and low capacity as a

result of the phase transition of Li$_x$MoO$_2$ from a monoclinic structure ($0 < x < 0.5$) to

an orthorhombic structure ($0.45 < x < 0.79$).[79]

(ii) Four-electron conversion. Oh and coworkers studied the high-temperature

lithiation behavior of the MoO_2 electrode.[97] It is found that the MoO_2 electrode is

lithiated with four-electron reduction by addition and continued conversion reactions

at elevated temperatures. By means of thermoelectrochemical activation, the

extension from one- to four-electron reduction is achieved. The initial crystalline

MoO_2 phase can be decomposed into a nanosized mixture of metallic Mo and Li_2O,

which is in turn converted to nanosized MoO_2 upon forthcoming delithiation. During

subsequent discharge-charge cycles, the as-formed nanosized MoO_2 is fully lithiated

up to four-electron reduction even at room temperature. Interestingly, the

newly-formed nanosized MoO_2 electrode through thermoelectrochemical activation

delivers a reversible specific capacity that is close to the theoretical four-electron

capacity 838 mA h g^{-1} with an excellent cycle performance at room temperature. In

this regard, nanosized MoO_2 as the initial active material would be preferable for a

high-capacity four-electron conversion reaction:

$$MoO_2 + 4Li^+ + 4e^- \leftrightarrow Mo + 2Li_2O$$

With the rapid development of nanomaterials synthesis in recent decades, various

well-defined MoO_2-based nanostructures have been fabricated by advanced

nanotechnology, offering elaborate candidates as high-capacity anodes for LIBs. As

expected, reducing the particle size of MoO_2 will enhance the kinetic barriers for the

conversion reaction, arising from not only the enhanced heterogeneous charge transfer

and solid-state Li^+ and/or O^{2-} diffusion, but also the weaker Mo–O bond strength of

nanosized MoO_2. In addition to thermoelectrochemical activation or nanostructuring,

increasing defect sites is another effective way to improve the electrochemical

performance of MoO_2-based electrodes.[98]

(iii) Coupled insertion-conversion reaction. For nanostructured MoO_2 materials,

there exists a general phenomenon that the specific capacities increase gradually

during initial charge and discharge cycles. Some researchers ascribed vaguely the

capacity increase upon cycling to the activation of the MoO_2 electrode. Recently,

Zhang *et al.*[99] and Guo *et al.*[100] investigated the Li storage mechanism of nanosized

MoO_2 in detail by *in-situ* or *ex-situ* X-ray diffraction (XRD) analysis. *In-situ* and *ex-situ* XRD results indicate that the intermediate phase of $Li_{0.98}MoO_2$ is generated during the first lithiation cycle at the potential from 3.0 to 1.0 V. When further discharged from 1.0 to 0.01 V, the crystal phase of $Li_{0.98}MoO_2$ is mainly retained in the lithiated product. Only a part of intermediate $Li_{0.98}MoO_2$ undergoes a conversion reaction and then decomposes into Mo and Li_2O during the first discharge cycle. The first discharge capacity is between 205 mA h g^{-1} ($Li_{0.98}MoO_2$) and 838 mA h g^{-1} (Li_4MoO_2). In the first delithiation process, both $Li_{0.98}MoO_2$ and Mo could be transformed into MoO_2. During the initial 30 discharge/charge cycles, most of $Li_{0.98}MoO_2$ can reversibly convert into MoO_2, while a part of $Li_{0.98}MoO_2$ is further reduced simultaneously to Li_2O and Mo upon Li^+ insertion.[99] After about 30 discharge/charge cycles, the lithiation reaction of MoO_2 shifts from an initial insertion type to a conversion mechanism, which is frequently observed in transition metal oxides. The overall electrochemical reactions of the MoO_2 electrode can be simplified as:

$$MoO_2 \leftrightarrow Li_{0.98}MoO_2 \leftrightarrow Mo + Li_2O$$

First principle calculations also provided an elementary explanation on the gradual increase in capacity upon cycling.[101] Their calculations including geometry and electronic structure calculation are performed by using density function theory (DFT) on the basis of projector augmented wave (PAW) method implemented in the VASP package. Average binding energy, density of states (DOS) and average cell voltage were calculated. Their calculation results showed that the binding energy in MoO_2 is

large, suggesting the stable nature of MoO_2. If the lithiation extent of Li_xMoO_2

increases, the average binding energy will decrease. Miao and coworkers also

calculated the formation energy of Mo vacancies.[101] The intercalation of Li in MoO_2

would weaken both the Mo–Mo bond and the charge polarization of Mo vacancies,

thus greatly reducing the formation energy of Mo vacancies in Li_xMoO_2. The

newly-formed Mo vacancies in Li_xMoO_2 provide new active sites for Li storage, and

therefore the capacity will be enhanced. Upon further continuous cycling, however,

the capacity decays because of the broken structure of MoO_2 as well as the

irrepressible structural change.

(iv) Structural defects induced Li$^+$ storage (disordering Li$_x$MoO$_2$). Recently, Oh's

group further demonstrated that structural defects in amorphous MoO_2 could also

serve as reversible Li^+ storage sites for rechargeable LIBs.[87] Amorphous MoO_2

(a-MoO_2) exhibits an unexpectedly high Li^+ storage capacity (up to four Li per MoO_2

unit), which is 4 times larger than that for the crystalline counterpart. Unexpectedly,

Mo and Li_2O in the lithiated a-MoO_2 are not generated upon Li-cycling. Meanwhile,

the local structural framework of a-MoO_2 is maintained, suggesting that the

conversion-type lithiation does not take place. The structural defects in a-MoO_2 both

facilitate Li^+ diffusion pathways and increase Li^+ mobility, which was evidenced by

^{7}Li nuclear magnetic resonance (NMR) analysis.[87]

$$MoO_2 + xLi^+ + xe^{-1} \leftrightarrow Li_xMoO_2 \text{ (disordered } Li^+, x < 4)$$

2.1.2 Nanostructured MoO$_2$. Several synthetic approaches, such as

hydrothermal/solvothermal process, magnetron-sputtering, rheological phase reaction, electrochemical deposition, and thermal evaporation, nanocasting, and thermal reduction, have been reported for preparing well-defined MoO_2 nanostructures including nanoparticles,[87, 87, 102-109] nanosheets,[110] nanorods,[100, 111] nanotubes,[99, 111] hollow spheres,[112-114] mesoporous structures,[115, 116] hierarchical architectures,[117-119] and thin films[120, 121] as anode materials for LIBs. Nanostructuring of MoO_2 can enhance the electrochemical performance, which cannot be achieved in bulk materials. In particular, the fabrication of a hierarchically nanostructure arouses much interest because of its extraordinarily high active surface/interface and robust stability. Electrode materials with hierarchical nanoarchitectures exhibit intriguing properties by taking advantage of both the nanometer-size effects and the high stability of the secondary-structure assemblies. Our group has reported a two-step method to grow a hierarchically nanostructured "cellulose" MoO_2 monolith as a binder-free anode for LIBs, whereby the cotton texture acts as both a template and a stabilizer (Fig. 2).[117] At first, a sheet of cotton cloth involving phosphomolybdic acid (PMA) was converted into a crystalline hierarchical MoO_3 replica through thermal treatment in air. Then, a hierarchically nanoparticle-organized MoO_2 monolith was obtained by thermal reduction in a (5%)H_2 /Ar atmosphere at 600 ºC. The electrode made of the "cellulose" MoO_2 monolith delivers a specific capacity of 719.1 mA h g^{-1} at 200 mA g^{-1}. Zhao *et al.*[114] reported a template-free one-step strategy to synthesize interconnected core–shell MoO_2 hierarchical microcapsules via a solvothermal route. The nanostructured MoO_2 capsules possess core–shell hierarchical architectures,

featuring hollow cavities, porous shells, and interconnected walls. When evaluated for

Li-storage properties, the hierarchical MoO_2 capsules exhibit a high specific capacity

of 749.3 mA h g^{-1} in the first discharge at 1 C and a high reversible capacity of 623.8

mA h g^{-1} after 50 cycles.
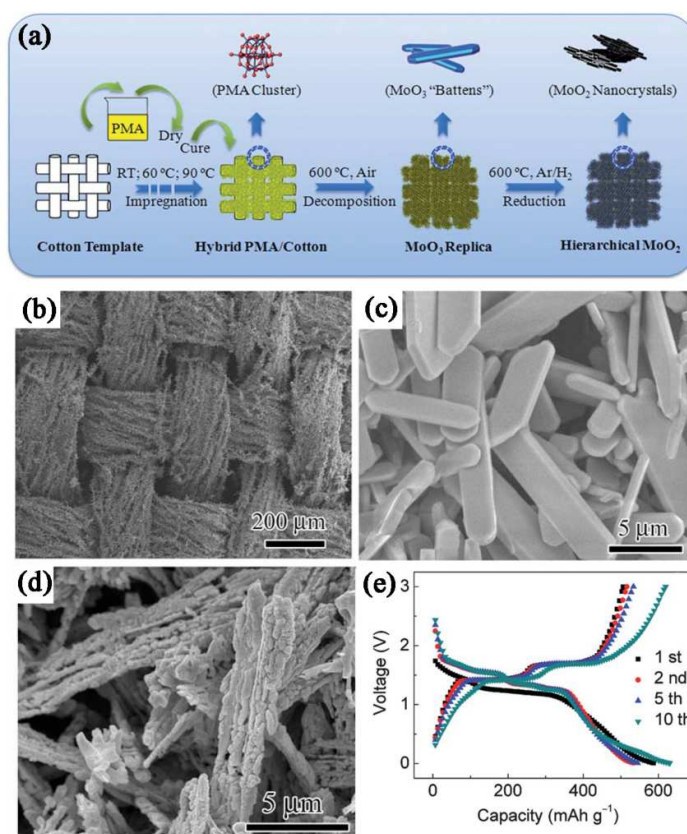
Fig. 2 (a) Schematic illustration of hierarchical MoO_2 formation. (b,c) FE-SEM

images of the MoO_3 replica obtained at 600 ºC for 4 h in air. (d) FE-SEM image and

(e) electrochemical performance of the MoO_2 product obtained at 600 ºC for 5 h in

H_2/Ar. Reproducedwith permission from ref. 117,Copyright (2012) by The Royal

Society ofChemistry.

Mesoporous MoO_2 materials have also attracted considerable interest as potential

electrode materials in LIBs.[116, 122-126] Mesoporous structures can reduce solid-state

diffusion lengths for both Li^+ and e^- due to the nanosized walls (< 10 nm), efficiently

facilitate solvated Li^+ transport through the mesopore channels (> 2 nm), and improve

the charge capacity because of intrinsic high surface areas. Hu and coworkers[116]

synthesized highly ordered crystallized MoO_2 with a three-dimensional (3D)

bicontinuous cubic symmetry *(Ia3d)* mesostructure via a nanocasting strategy. The

mesoporous silica template KIT-6 filled with PMA was thermally treated at 500–700

ºC in a diluted H_2 gas flow (10% H_2 + 90% Ar), and the template was subsequently

removed by HF. Electrochemical testing showed that this electrode made of

mesoporous MoO_2 had a typical metallic conductivity with low resistivity and

exhibited a reversible capacity as high as 750 mA h g^{-1} at C/20 (41.9 mA g^{-1}) after 30

cycles. Similarly, tungsten-doped MoO_2 was also synthesized by the nanocasting

method using a sacrificing template of mesoporous KIT-6.[115] W-doping could help

mesoporous MoO_2 to fully react with Li and the ''activation process'' disappeared.

The W-doped MoO_2 material created an optimized electrode configuration by

combining the advantages of the high theoretical capacity of MoO_2 and the high

electroactivity of WO_2. This leads to an overall performance that is better than that of

MoO_2 or WO_2. However, those mesoporous MoO_2-based nanostructures are

carbon-free, and the MoO_2 nanocrystals are unprotected. During the continuous Li^+

insertion/extraction cycles, especially for the conversion reaction involving ultrafine

Mo and Li_2O, the structural stability of the whole electrode would be problematic,

thus resulting in rapid capacity fading. To further improve cyclability and rate

capability, ordered mesoporous carbon (OMC) was used as both the nanoreactor and the reduction agent for the fabrication of MoO_2/OMC nanocomposites.[127, 128] OMC could act as the branches to connect MoO_2 nanoparticles and build up a network to ensure good electrical contact of MoO_2–MoO_2 and MoO_2–C to increase reaction kinetics. At the same time, OMC with a mechanical buffer function alleviated the volume expansion and contraction and prevented the agglomeration of MoO_2 nanoparticles during Li^+ insertion/extraction processes.[128] By using mesoporous carbon CMK-3 as both the template and the reactant, Zhang et al.[111] recently reported the synthesis of hierarchical porous MoO_2/Mo_2C heteronanotubes through a one-step carbothermal reduction method (Fig. 3a and 3b). Instead of carbon, conducting Mo_2C with a high conductivity (1.02×10^2 S cm^{-1}) was introduced into the final nanocomposite of porous MoO_2/Mo_2C heteronanotubes. Cycled at 200 and 1000 mA g^{-1} for 140 cycles, the discharge capacity of MoO_2/Mo_2C heteronanotubes could remain at 790 and 510 mA h g^{-1}, respectively (Fig. 3c and 3d). Nevertheless, Mo_2C in the nanocomposite MoO_2/Mo_2C heteronanotubes is electrochemically inactive, which will reduce the energy density of the electrode. Moreover, transition metal nitrides (e.g., Mo_2N, WN, and TiN) also have high conductivity, in addition to high chemical resistance, hardness, mechanical strength and high melting points. Liu et al.[129] reported a carbon-free nanocoating strategy for large-scale synthesis of Mo_2N-nanolayer-coated MoO_2 hollow nanostructures. The as-formed Mo_2N-nanolayer-coated MoO_2 hollow nanostructures exhibit highly reversible capacity of 815 mA h g^{-1} after 100 cycles, good cyclability, and high rate capability.

17

The carbon-free nanocoating of Mo_2N is effective, and endows electrode materials with high surface stability and long cycle life, in comparison to the carbon nanocoating commonly used in other electrode materials.
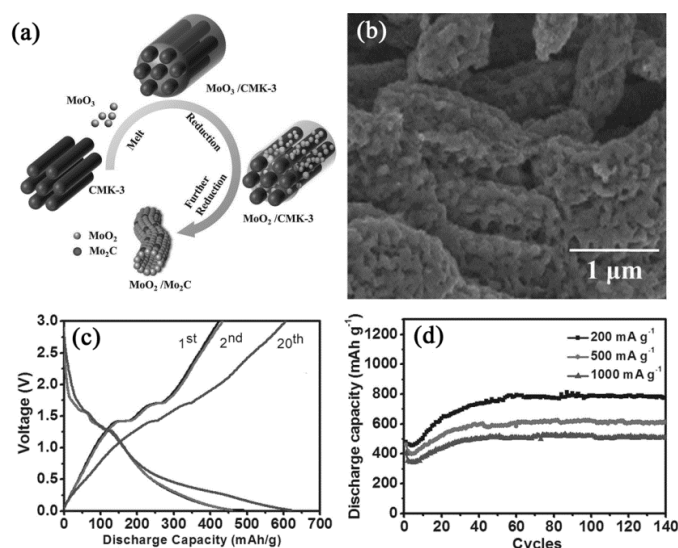
Fig. 3 MoO_2/Mo_2C heteronanotubes: (a) schematic illustration for the preparation process, (b) SEM image, (c) galvanostatic charge/discharge curves at a 200 mA g^{-1}, and (d) cycling performance. Reproduced with permission from ref. 111, Copyright (2014) by Wiely-VCH.

2.1.3 MoO_2/carbon nanohybrids. Based on literature studies and our own research on MoO_2 in the past several years, reducing the particle size, for example, to nanosize, is possible to achieve high specific capacity via a conversion-reaction mechanism or coupled insertion-conversion reactions. However, the long-term Li cyclability in MoO_2 is normally found to be poor, and severe capacity fading occurs upon 10–30 discharge-charge cycles. This is mainly due to the aggregation and/or pulverization of

the highly active electrode involving ultrafine particles, the volume change, and intensive side reactions between the electrode and the electrolyte. It is well known that carbonaceous hybridization of nanostructured MoO_2 would effectively both enhance the Li-insertion kinetics and improve the Li-cyclability. To date, a variety of carbon-based MoO_2 nanocomposites with unique architectures have been reported. Some of the recent data on the Li-cycling properties of nanocomposite MoO_2/C are list in Table 1. For the metal oxides based on the conversion reaction mechanism, the large volume change could result in pulverization and aggregation of the active materials, thus decreasing the reversible capacity upon cycling. Also, those transition metal oxides are normally electrically insulting. We and others have shown that it is highly desirable to grow small metal oxide nanoparticles on (or in) a carbon-based matrix to shorten diffusion length of ions and expedite electron transport, enhancing the capacity, rate capability and cycle life.[130-132] Among the various carbonaceous materials, graphene typically exhibits superior electrical conductivity, large surface area, structural flexibility, and chemical stability. It can host nanostructured electrode materials for energy applications.[133-135] The graphene layers can offer a support for anchoring nanoparticles and work as a highly conductive matrix providing good contact between them. Importantly, graphene layers prevent the volume expansion/contraction and the aggregation of nanoparticles effectively during charge and discharge processes. Meanwhile, the integration of inorganic nanostructures with the graphene layers may reduce the restacking of graphene sheets and consequently maintain the high surface area.[45] In this regard, both the lithium-storage capacity and

the cycling performance of graphene-based nanomaterials will be improved. We reported the large-scale fabrication of unprecedented self-assembled hierarchical MoO$_2$/graphene nanoarchitectures through a facile solution-based method combined with a subsequent reduction process (Fig. 4a), where nanostructured MoO$_2$ was first stabilized by reduced graphene oxide sheets.[136] PMA and graphene oxide (GO) reacted with hydrazine hydrate in solution to produce a Mo-precursor/graphene composite. Then, the resulting composite was further annealed at 500 ºC for 5 h in a reducing H$_2$/Ar atmosphere, and self-assembled hierarchical MoO$_2$/graphene nanoarchitectures were finally formed. Our results showed that the electrode made of the resulting hierarchical MoO$_2$/graphene delivered a high capacity of 597.9 mA h g^{-1} over 70 cycles with a Coulombic efficiency of ~98% at a high current density of 1000 mA g^{-1} (Fig. 4b and 4c). In order to buffer the volume effect arising from the conversion reaction, we further proposed a simple impregnation–reduction–carbonization (IRC) route for the assembly of ultrafine MoO$_2$ nanoparticles (< 2 nm) into a carbon cloth.[137] Interestingly, the MoO$_2$/C composite exhibited excellent cycling stability (600 cycles) and a high reversible capacity of 734 mA h g^{-1} as an anode material for LIBs. Our results showed ultrafine MoO$_2$ nanoparticles embedded in the nanoporous carbon matrix would be highly favorable for the conversion reaction. The MoO$_2$ nanoparticles with high surface area and abundant surface defects may enhance the heterogeneous charge transfer kinetics, ion diffusion, and capacity. In particular, the nanoporous nature of the as-formed hybrid could not only facilitate fast Li-ion and electron transport but also act as an

elastic buffer to prevent the mechanical failure and volume effect, thus leading to the

high stability during the conversion reaction process. Another important progress is

that Bhaskar *et al.*[138] improved cyclability by uniform entrapment of MoO_2

nanoparticles in 2D graphene scaffolds. The unique layered nanostructure and the

conductive matrix provided uninhibited conducting pathways for fast charge transfer

and transport between the oxide nanoparticles and graphene which are responsible for

the high rate capability, a large Li-ion capacity of 770 mA h g^{-1}, and an excellent

cycling stability (550 mA h g^{-1} reversible capacity retained even after 1000 cycles) at

a current density of 540 mA g^{-1}.
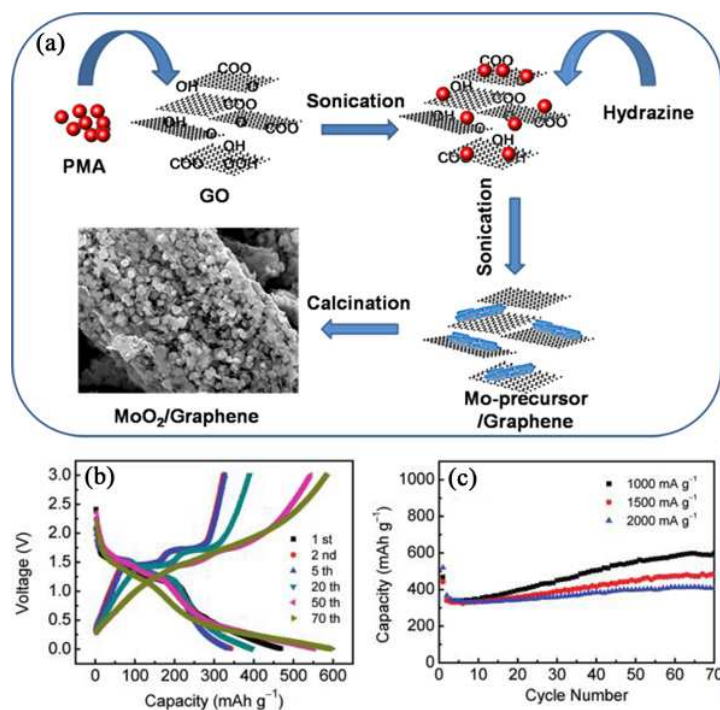
Fig. 4 MoO_2/graphene nanocomposite: (a) schematic representation of the fabrication

process, (b) discharge and charge curves at 1000 mA g^{-1}, and (c) cycling performance

at different current densities. Reproduced with permission from ref. 136, Copyright

(2011) by American Chemical Society.

.

Table 1. Morphology and electrochemical performances of carbon-based MoO_2 nanocomposites prepared by different methods.

Carbon-based MoO_2 nanocomposites	Methods	Current density (mA/g)	Capacity (mA h/g)	cycle number	Ref.
Hierarchical MoO_2/graphene nanoarchitecture	Solution and annealed	1000	600	70	136
MoO_2 nanoparticles embedded in carbon nanofibers	Solution and annealed	50	734	350	137
Carbon-coated MoO_2 nanofibers	Electrospinning	50	762.7	50	138
MoO_2/graphene thin film	Layer-by-layer self-assembly	47.8	675.9	100	139
Hierarchical carbon/MoO_2 core-shell spheres	Hydrothermal	167.6	600	60	140
MoO_2-ordered mesoporous carbon hybrids	Solvothermal	100	1049.1	50	128
Graphene-MoO_2 hierarchical nanoarchitecture	In-situ reduction	167.6	997.1	50	140
3D graphene supported MoO_2	Chemical vapor deposition	200	986.9	150	142
Cage-like MoO_2/carbon	Hydrothermal	200	692.5	80	143
MoO_2@C nanoparticles	Hydrothermal	100	730	60	144
MoO_2-ordered mesoporous carbon	Carbon thermal reduction	50	689	50	145
Hierarchical MoO_2/C spheres	Hydrothermal	200	812	150	146
Mesoporous carbon-MoO_2	Carbothermal reduction	83.8	581	30	127
MoO_2/multiwalled carbon nanotubes	Hydrothermal	100	1143	200	147
Carbon-coated MoO_2nanospheres	Hydrothermal and annealing	838	650	30	146
MoO_2/graphite oxide	Solvothermal	100	720	30	149
Interconnected MoO_2 nanocrystals with carbon	Hydrothermal	200	640	70	150

nanocasting

MoO_2/graphene	Hydrothermal	540	550	1000	138
Nanosized MoO_2/C	Spray pyrolysis	83.8	225	2	151
MoO_2- porous carbon hollow spheres	Solution and annealing	50	640	80	152
MoO_2/carbon nanowires	Oil bath and calcination	200	500	20	153
Carbon/MoO_2 composite	Template	83	760	20	154
MoO_2/graphene	Solution and annealing	200	640	50	155
MoO_2/graphene	Hydrothermal and calcination	100	1009.9	60	156
Carbon coated MoO_2 nanobelts	Hydrothermal and calcination	100	617.2	30	157

2.1.4 MoO_2 additive. In addition to the direct use as active materials, MoO_2 is attractive as a conducting additive to modify other electrode materials for LIBs because of its high electric conductivity and chemical stability. For instance, we prepared MoO_2 -modified TiO_2 nanofibers, comprising a core of TiO_2 nanofibers and a thin metal-like MoO_2 nanolayer, through electrospinning and layer-by-layer (LBL) self-assembly processes.[158] The thickness of the MoO_2 nanolayer could be tuned easily by altering the precursor concentration or the LBL cycles. Results showed that the electrochemical performance of surface-modified TiO_2 was distinctively improved, compared with the pure TiO_2 nanofibers. The MoO_2-modified TiO_2 nanofibers exhibited a high discharge capacity of 514.5 mA h g^{-1} at 0.2 C over 50 cycles and excellent rate capability. This also demonstrates that enhanced physical and/or chemical properties can be achieved through proper surface modification. Besides, MoO_2 was also reported to modify the surface of the $LiFePO_4$/C electrode materials.[159] Despite of the low electric resistivity of MoO_2, its own structural

instability needs to be evaluated when it is employed as an additive or modification agent to improve the surface nature of other electrode materials. In particular, MoO_2 may be oxidized to a higher oxidation state, when used at a high potential. Also, the thickness and the uniformity of the MoO_2 layer are crucial to the Li^+ storage performance of MoO_2-modifed nanocomposite electrode materials.

2.1.5 Other MoO_2-based nanocomposites. Other carbon-stabilized MoO_2 anode materials for LIBs include carbon-coated MoO_2 nanoparticles,[144,148,150] nanofibers,[153,160] and nanobelts,[157] nanosized MoO_2 in porous carbon,[127, 128, 145, 152] MoO_2/multiwalled carbon nanotubes,[148] and MoS_2 coated MoO_2 nanonetworks.[161] The $MoO_2@MoS_2$ nanocomposite is composed of nanocrystalline - nanoporous MoO_2 partially covered with few atomic layers of MoS_2.[161] The obtained porous $MoO_2@MoS_2$ networks delivered a reversible capacity as high as 1163 mA h g^{-1} at a current density of 100 mA g^{-1} after 80 cycles. Reversible capacities of 1125 and 654 mA h g^{-1} were also achieved at current densities of 200 and 500 mA g^{-1} after 80 cycles, respectively. Yoon and Manthiram[162] reported a microwave-assisted hydrothermal process to prepare carbon-decorated WO_x-MoO_2 (x = 2 and 3) nanorods as anode materials. The WO_x-MoO_2 anodes showed excellent capacity retention as the carbon could provide an elastic matrix for absorbing the volume expansion–contraction smoothly and prevent aggregation of the WO_x-MoO_2 nanorods during cycling.

2.2 MoO_3

24

2.2.1 Crystal structure. MoO_3 is an attractive example of a prospective electrode material for LIBs with high capacity. It has been investigated as both cathode and anode materials because of its unique layered structure.[163-165] Two basic polymorphs of MoO_3 include thermodynamically stable orthorhombic α-phase and metastable monoclinic β-phase with a ReO_3-type structure (Fig. 5).[166] The most important characteristic of α-MoO_3 is the structural anisotropy. The crystal phase of α-MoO_3 possesses an orthorhombic layered structure parallel to (010) planes. Each layer is composed of two interleaved sub-layers, each of which is formed by corner-sharing octahedra along [001] and [100]; the two sub-layers stack together by sharing the edges of the octahedra along [001].[167] An alternate stack of these layered sheets along [010] would lead to the formation of α-MoO_3, where a van der Waals interaction would be the major binding force between the piled sheets.[168]
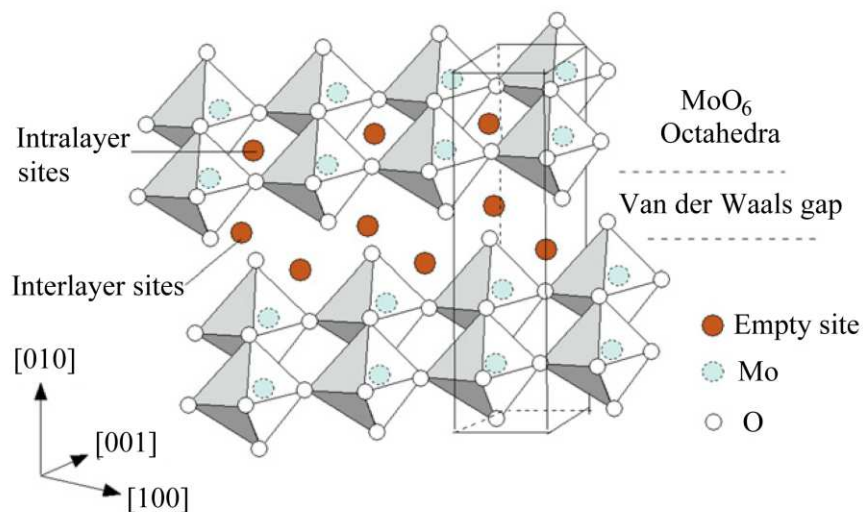
Fig. 5 Structure of α-MoO_3 showing the available empty sites for Li insertion. Reproduced with permission from ref. 166, Copyright (2012) by Elsevier.

2.2.2 MoO$_3$ cathodes. In 1970s MoO$_3$ was proposed as a cathode material for secondary solid-state ion batteries.[163, 164, 169-175] As shown in Fig. 6, two types of empty sites are available for hosting foreign ions like Li$^+$.[166] The interlayer distance has been determined to be 6.929 Å.[176] The reversible electrochemical behaviour of MoO$_3$ electrodes can be explained on the grounds of topotactic redox reactions. The interleaved sheets of MoO$_6$ octahedra are retained as two-dimensional matrix units during the insertion and deinsertion processes. Although the guest ions can be well accommodated without structural change in principle, the spacing between the interlayers in the MoO$_3$ host could be enlarged due to lithium uptake.[177-179] The overall redox reaction of intercalation could be described as:[176]

$$MoO_3 + xLi^+ + xe^- \leftrightarrow Li_xMoO_3$$
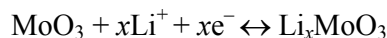
The kinetically accessible charge range amounts to $0.1 \leq x < 1.5$ with the lower limit of x depending on the precedent cathodic load.[170] At the initial cathodic stage of Li$^+$ uptake, it is proved that two phases of MoO$_3$ and Li$_x$MoO$_3$ ($x < 0.25$) coexist at a potential of around 2.8 V $vs.$ Li. A second cathodic stage involves the solid solution of Li$_x$MoO$_3$ ($0.25 < x < 0.5$) at the potentials ranging from 2.8 to 2.4 V. At the final cathodic stage, the solid solution of Li$_x$MoO$_3$ ($1 < x < 1.5$) is present at the potential lower than 2.4 V. Reduction beyond $x = 1.5$ would result in irreversible changes in the oxide structure. Also, complete re-oxidation (Li$^+$ extraction) to the binary oxide is kinetically hindered presumably, as a result of small structural changes. It has been reported that the accessible range of reversible Li$^+$ intercalation/deintercalation is 0.1

26

$\leq x < 1.5.$[180] The electronic conductivity of Li_xMoO_3 depends on the x value.[181] In general, the conductivity increases with x up to a maximum value, and then drops significantly on further Li^+ intercalation. Namely, the conductivity is relatively poor at the end of discharge. On the other side, the completely charged state, the oxide MoO_3 is practically an insulator. The specific conductivity of Li_xMoO_3 (prepared by lithiation with n-butyl lithium) in the range of $0.3 \leq x \leq 0.9$ was in the order of 10^{-1} S cm^{-1}, with a maximum value at $x = $ about $0.6.$[181] The electronic and Li^+-ionic conductivity of Li_xMoO_3 varies with x by orders of magnitude. Mai and coworkers[182] proved that the electroactivity of MoO_3 nanobelts was highly improved through lithiation. The lithiated MoO_3 nanobelts exhibited excellent cycling capability, with a capacity retention rate of 92 % after 15 cycles, while the non-lithiated nanobelts retained only 60% (Fig. 6). Transport measurements also showed that the conductivity of a lithiated MoO_3 nanobelt (10^{-2} S cm^{-1}) is increased by nearly two orders of magnitudes compared to that of a non-lithiated MoO_3 nanobelt (10^{-4} S cm^{-1}).
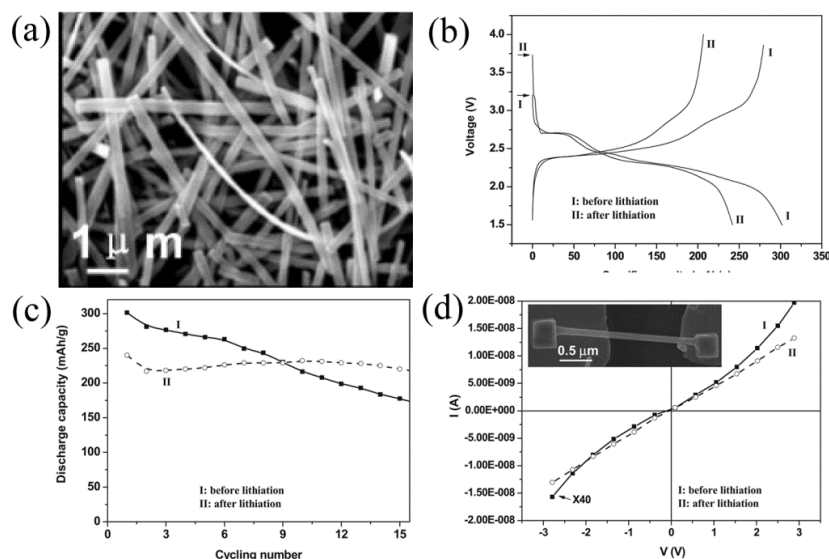
Fig. 6 (a) SEM image for the MoO$_3$ nanobelts. (b) Potential vs. capacity curves for the first cycle of charge-discharge process of the nanobelts before and after lithiation. (c) The discharge capacity as a function of the cycle number for the MoO$_3$ nanobelts before and after lithiation. (d) I-V transport measurements of single nanobelt fabricated devices using the samples before and after lithiation. Reproduced with permission from ref. 182, Copyright (2007) by Wiley-VCH.

2.2.3 MoO$_3$ anodes. Utilization of MoO$_3$ as an anode material has been paid much attention during the past decade. When tested in the potential window of 0.01–3.0 V vs. Li, MoO$_3$ has been found to follow the conversion-reaction mechanism:[183]

$$MoO_3 + 6Li^+ + 6e^- \leftrightarrow 3Li_2O + Mo$$
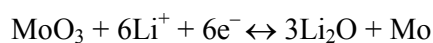
The theoretical specific capacity reaches as high as 1117 mA h g^{-1}, which approximates three times larger than that of graphite. However, poor ionic and electronic conductivity of MoO$_3$ often limits its electrochemical performance. Nanostructuring, carbon hybridization, and pre-lithiation are the general strategies for

28

improving the capacity, rate capability and cycle life.[183-199] For instance, Choi and

Kang employed the crumpled graphene sheets as substrates to grow MoO_3

nanoparticles by spray pyrolysis and subsequent thermal treatment.[184] The initial

discharge capacity of ~1490 mA h g^{-1} at a current density of 2000 mA g^{-1} was

achieved, and the capacity of 975 mA h g^{-1} could be maintained after 90 cycles. Lou

et al.[184] prepared ultralong MoO_3 nanobelts with an average length of 200−300 μm

and uniform width of around 0.6−1.5 μm via a hydrothermal method. They also

proposed the use of sodium carboxymethyl cellulose (Na-CMC) as the binder for

assembly of the MoO_3 electrode, which delivered a high specific capacity of over 730

mA h g^{-1} for over 200 cycles at a 0.2 C rate. Even cycled at high rates of 1−2 C, high

capacities of around 430−650 mA h g^{-1} could still be retained. As demonstrated, the

Na-CMC binder should play a crucial role in improving the cyclability of MoO_3. The

Na-CMC binder can dissolve in water with a fully stretched molecular conformation

because of the rigid long chains and the electrostatic repulsive interactions between

ionized carboxy groups. Therefore, homogeneous 3D networks between the

conductive agent and active material particles may be formed, leading to a tightened

electrode architecture. These findings demonstrate that selecting a suitable polymer

binder would help to optimize the performance of metal oxide electrodes, especially

for those undergoing drastic volume and structure changes upon lithiation. Hassan et

al.[187] prepared carbon-coated MoO_3 nanobelts that exhibited a high capacity of about

1000 mA h g^{-1} at 0.1 C. Dillon's group[188] investigated the reversible Li^+-insertion

behaviour of MoO_3 nanoparticles prepared by a hot-wire chemical vapor deposition

(HWCVD) technique. The anode made of MoO_3 nanocrystals displayed both a durable reversible capacity of 630 mA h g^{-1} and durable high rate capability. The capacity did not decay after 150 cycles at a C-rate of C/2 between 3.5 and 0.005 V, compared to micrometer-sized MoO_3 particles where the capacity faded quickly. First-principle calculations by Dillon *et al.*[188] also indicated that the MoO_3 nanoparticles maintained some structural integrity due to the heavy Mo-framework, in spite of a large volume expansion. Combining the XRD results with the theoretical calculations, Dillon *et al.*[188] considered that amorphization of MoO_3, instead of conversion reactions, could occur during the Li-cycling processes.

2.3 MoO$_{3-x}$

Substoichiometric molybdenum oxide (MoO_x, $2 < x < 3$) or reduced molybdenum oxide is another attractive electrode material and possesses all the advantages that MoO_3 has.[200-206] Moreover, the conductivity can be improved as a result of the intrinsic oxygen vacancies, compared to MoO_3. However, those oxygen deficient structures in early studies were limited by low recharge efficiency and poor cycling stability. Christian *et al.*[200] studied the electrochemical behaviour of Mo_4O_{11} ($MoO_{2.75}$), $Mo_{17}O_{47}$ ($MoO_{2.765}$), Mo_8O_{23} ($MoO_{2.889}$), and Mo_9O_{26} ($MoO_{2.875}$) cathode materials using a $LiClO_4$/propylene carbonate electrolyte. Among them, $Mo_{17}O_{47}$ exhibited the greatest reversible capacity (1.5 Li/Mo) after several deep discharge-charge cycles in the potential range between 2.9 and 1.4 V. It was also found that the Li^+-diffusion coefficients and the variations of lattice parameters of the

non-stoichiometric Mo oxides depended on the depth of discharge.[207] Fuentes and

coworkers synthesized reduced molybdenum oxide, Mo_4O_{11}, by a solid state reaction

between MoO_3 and MoO_2.[205] Two polymorphs of orthorhombic γ-Mo_4O_{11} and

monoclinic γ'-Mo_4O_{11} were investigated as the cathode materials. They incorporated a

similar number of Li^+ per metal atom (Li/Mo = 2.12 and 2.25, respectively). Detailed

studies on the insertion reaction kinetics suggested that the insertion-induced

reduction of γ-Mo_4O_{11} and γ'-Mo_4O_{11} went through different mechanisms.[205]

Solid-state lithium batteries fabricated by the thin film technology are attracting

interest as micro-batteries. Ohtsuka et al.[204] prepared Li/MoO_{3-x} thin film batteries by

using a RF sputtering method, in which MoO_{3-x} has a larger specific capacity than

other cathode films (e.g., $LiMn_2O_4$ film). At the discharge current density of 10 μA

cm^{-2}, the thin-film Li/MoO_{3-x} batteries had discharge capacities of 290 mA h cm^{-2},

and hold the promise for flexible energy-storage devices as well as further

miniaturization. Jung et al.[202] prepared nanostructured MoO_{3-y} powders as anode

materials by ball-milling. Oxygen deficiency increased with the milling time. The

ball-milled MoO_{3-y} could uptake more than 6 Li/Mo by an addition reaction followed

by a conversion reaction, wherein the reactivity was strongly dependent on the

oxygen deficiency. The ball-milled MoO_{3-y} samples exhibited a high initial discharge

capacity of 1100 mA h g^{-1} with capacity fading upon cycling (~620 mA h g^{-1} after 35

cycles). Compared to bulk MoO_3, ball-milled MoO_{3-y} powders displayed significantly

improved cyclability, possibly arising from the smaller crystallite size and/or low

crystalline nature. Sunkara et al.[203] grew vertical nanowire arrays of MoO_{3-x} on

metallic substrates in a hot-filament chemical vapor deposition reactor. At a current density of 50 mA g^{-1}, the nanowire arrays of MoO$_{3-x}$ showed high-capacity retention of ~630 mA h g^{-1} for up to 20 cycles. Besides the progresses in electrode materials for Li$^+$-ion batteries, the substoichiometric molybdenum oxides have been recently used to enhance hole exchange in optoelectronic devices based on organic semiconductors (OSCs), such as organic light-emitting diodes (OLEDs) and organic photovoltaics (OPVs), because of their improved n-type conductivity originated from intrinsic oxygen vacancies.[208]

2.4 Hydrated Mo-based oxides

Li insertion in hydrated Mo-based oxides has been investigated as cathodes for LIBs. As described above (Fig. 5), anhydrous MoO$_3$ contains double sheets of MoO$_6$ octahedra. In contrast, single sheets are found in hydrated MoO$_3$ (MoO$_3 \cdot$H$_2$O, MoO$_3 \cdot$2H$_2$O).[175] By dehydration, the intercalated water could be first lost, and then neighboring sheets condense into double sheets as the final water is lost.[209] Julien *et al.*[210-213] performed in-depth studies of hydrated MoO$_3$ for cathode applications. Polycrystalline MoO$_3 \cdot$0.5H$_2$O and amorphous MoO$_3 \cdot$H$_2$O were prepared by an ionic resin exchange technique.[210] It was found that the chemical diffusion coefficient of Li$^+$ ions for polycrystalline MoO$_3 \cdot$0.5H$_2$O decreased from ~3 × 10^{-8} to 3 × 10^{-9} cm^2 s^{-1} as the number of inserted Li$^+$ increased from 0.05 to 1.5. For amorphous MoO$_3 \cdot$H$_2$O, however, the diffusion coefficient remained nearly the same with Li insertion at a higher value of ~3 × 10^{-8} cm^2 s^{-1}. The decrease in the diffusion

coefficient for $MoO_3 \cdot 0.5H_2O$ probably is as a result of the interfacial blocking effect

in the polycrystalline material.[210] In addition, $MoO_3 \cdot 2/3H_2O$ was found to show a

maximum diffusion coefficient of $\sim 5 \times 10^{-9}$ $cm^2 s^{-1}$ at the Li-inserting extent of 0.7

Li^+/MoO_3.[211] Electrochemical Li-insertion results on amorphous $MoO_3 \cdot 2H_2O$ showed

that its reaction kinetics was superior to that both anhydrous MoO_3 and other hydrated

Mo-based oxides. However, its initial Coulombic efficiency was only 55%, which

could be attributed to the irreversible reaction between the inserted Li and the

coordinated water in the hydrate host.[214, 215]

2.5 Mo-containing oxysalts

2.5.1 $MMoO_4$ (M = Fe, Co, Ni, Ca, Mn, or Zn). Mo-containing mixed oxides are

attractive as "hosts" for lithium insertion while the combination of two metals in

oxide-matrices produces the materials with new structures and chemical properties

compared to that of binary metal oxides.[216-226] In particular, ternary metal oxides can

form flexible crystal structures or phases depending on the synthetic conditions and

compositions, and thus a large variety of systems could be modeled and explored.

Calcium molybdate, $CaMoO_4$, adopts a tetragonal scheelite structure with the Mo in

tetrahedral O-coordination.[222, 224, 225] Chowdari's group prepared carbon-coated

nanophase $CaMoO_4$ by solution precipitation and sol-gel methods.[225] The *in-situ*

C-coating during the precipitation of $CaMoO_4$ produced uniform and smooth particles

of 1–2 μm in size. Well-separated $CaMoO_4$ nanocrystallites with sizes in the range of

50–80 nm were obtained by the sol-gel synthesis. Galvanostatic cycling was carried

out over 50 cycles in the range of 0.005–2.5 V at a current rate of 10 mA g^{-1} for the first two cycles and at 60 mA g^{-1} for all other cycles. Cycling was also performed with upper cutoff voltages of 2.0 and 3.0 V for the sol-gel and C-coated $CaMoO_4$. It was found that the cutoff voltage of 2.5 V exhibited the best performance. The C-coating enabled high inter-particle electronic conductivity of the otherwise insulating $CaMoO_4$, leading to the best performance of carbon-coated $CaMoO_4$ nanoparticles with a specific capacity of 508 mA h g^{-1} and a Coulombic efficiency higher than 98%. A plausible mechanism involving the formation - decomposition of the oxide bronze "Li_xMoO_y" was proposed for the first discharge and subsequent charge – discharge cycling of $CaMoO_4$.

Yu and coworkers[218] reported a general hydrothermal route for preparing different phases and morphologies of molybdate hydrates $MMoO_4 \cdot nH_2O$ (M = Co, Ni, Mn, n = 0, 3/4, 1) nano/microcrystals, whereby $NiMoO_4 \cdot H_2O$ microflowers, $MnMoO_4 \cdot H_2O$ microparallelogram plates, and $CoMoO_4 \cdot 3/4H_2O$ microrods could be selectively synthesized (Fig. 7). After further annealing at a temperature of 500–550 ºC, they could be transformed into anhydrous molybdates. The electrochemical Li-storage performances of $MMoO_4$ (M = Ni, Co) nanorod bundles and $MnMoO_4$ microrods were evaluated. The first reversible discharge specific capacity for $NiMoO_4$ could reach up to 850 mA h g^{-1} at 0.1 mA cm^{-2} within a potential range of 1.2–4.0 V, which is higher than those for $CoMoO_4$ (130 mA h g^{-1}) and $MnMoO_4$ (180 mA h g^{-1}). It was proposed that such a high capacity of $NiMoO_4$ was assigned to a large amount of vacancies in

the structure of $NiMoO_4$ nanorod bundles, in which Li^+ ions could be reversibly incorporated.
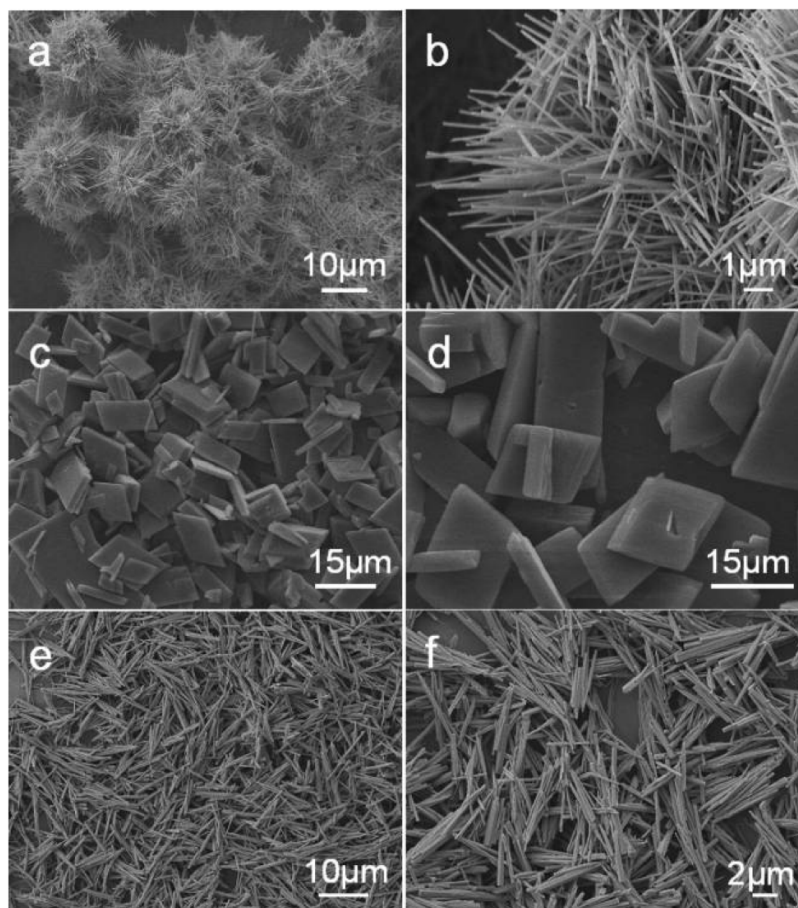
Fig. 7 FE-SEM images of $MMoO_4 \cdot nH_2O$ (M = Co, Ni, Mn, n = 0, 3/4, 1) nanostructures and microstructures: (a, b) $NiMoO_4 \cdot H_2O$ microflowers, (c, d) $MnMoO_4 \cdot H_2O$ microparallelogram plates, (e, f) $CoMoO_4 \cdot 3/4H_2O$ microrods. Reproduced with permission from ref. 218, Copyright (2008) by American Chemical Society.

Oriented 1D nanomaterials are acknowledged as one of the promising solutions to future-generation LIBs with high performances because of their large surface area,

short transport path for ions and electrons, and buffering function for volume change.[51, 53, 227] Lou's group reported the synthesis of $AMoO_4 \cdot nH_2O$ (A = Ni, Co) nanorods through a hydrothermal method.[228] The size of the nanorods could be easily controlled, and self-assembled growth of oriented $NiMoO_4 \cdot nH_2O$ nanorod arrays on Ti-foil substrates was achieved. The resulting $AMoO_4$ (A = Ni, Co) was investigated as the cathode materials for LIBs (Fig. 8). The capacities of about 120 mA h g^{-1} could be retained after 50 cycles. Kim $et\ al.$[229] obtained $Ni_xCo_{1-x}MoO_4$ ($0 \leq x \leq 1$) nanowire electrodes by employing a hydrothermal method with post-annealing. The electrodes made of $Ni_{0.75}Co_{0.25}MoO_4$ nanowires delivered a high reversible capacity of about 520 mA h g^{-1} after 20 cycles at a current densityof 196 mA g^{-1}. This enhanced electrochemical performance of $Ni_{0.75}Co_{0.25}MoO_4$ nanowires with high Ni content was ascribed to their larger surface area and efficient electron transport path facilitated by their 1D nanostructure.
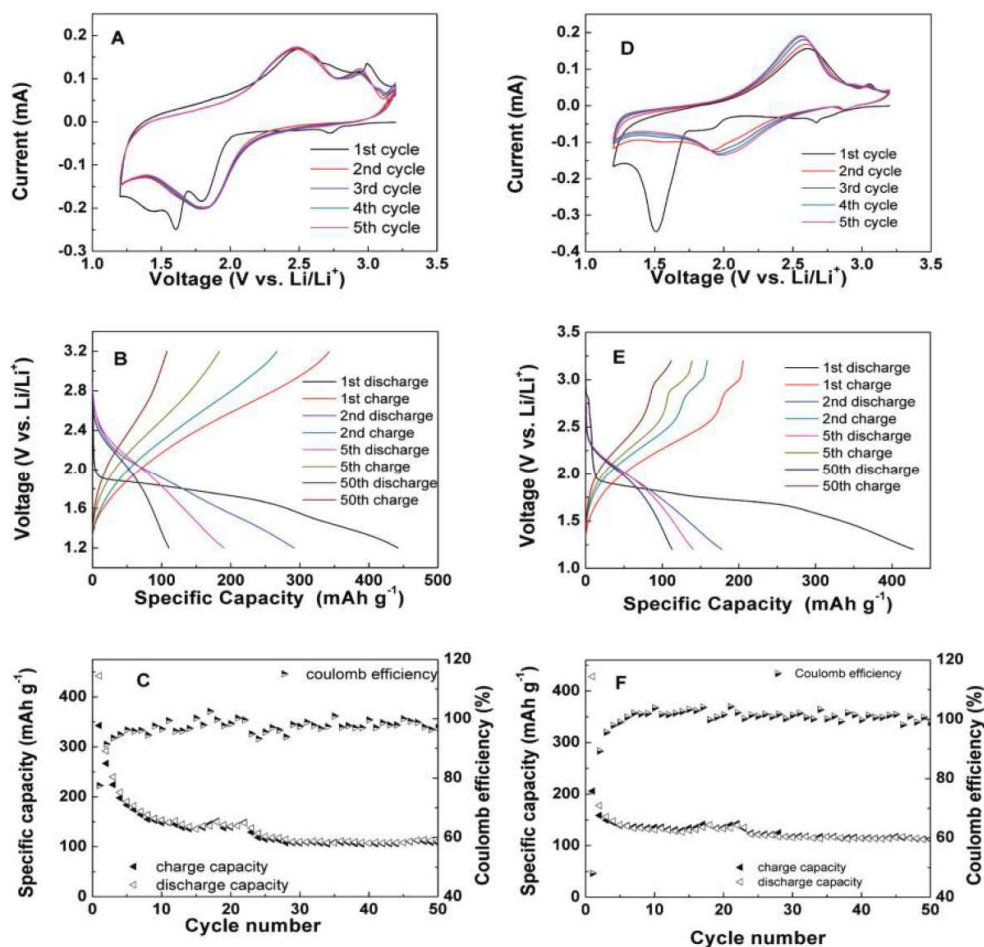
Fig. 8 Cyclic voltammograms with a scan rate of 0.5 mV s^{-1} for the first five cycles, voltage-capacity profiles with a current density of 50 mA g^{-1}, and cycling performances of NiMoO$_4$ (A, B, and C) and CoMoO$_4$ (D, E, and F) nanorod electrodes between 1.2 and 3.2 V (vs Li$^+$/Li). Reproduced with permission from ref. 228, Copyright (2008) by American Chemical Society.

2.5.2 Mo-cluster oxysalts. In recent years, a number of interesting pioneer works on hexagonal Mo-cluster compounds including LiHoMo$_3$O$_8$, A$_2$Mo$_3$O$_8$ (A = Zn, Co), LiYMo$_3$O$_8$, and Mn$_2$Mo$_3$O$_8$ as anode materials have been published by Chowdari's group.[230, 231] These studies are very important for understanding the Li-cycling

mechanisms of the Mo-cluster oxides, and their potential applications in Li-storage devices. We recently prepared hierarchically nanostructured $Mn_2Mo_3O_8$–graphene nanocomposites in large quantities through a facile two-step reduction approach.[232] Typically, phosphomolybdic acid and manganese acetate reacted with hydrazine hydrate in solution, accompanied with the reduction of graphene oxide to graphene by hydrazine hydrate, leading to the formation of a Mn-Mo-precursor–graphene composite. Then, this intermediate product was further treated at 550 ºC for 5 h in a reducing H_2/Ar atmosphere to obtain the final product. As displayed in Fig. 9, a large number of hierarchical architectures consisting of secondary micro-spheres of ~3–5 μm in diameter, are clearly observed. The high-magnification SEM images in Fig. 9a and 9b indicate that the hierarchical architectures are built from $Mn_2Mo_3O_8$ nanosheets with a thickness of 10–15 nm and a width of 80–120 nm. The reversible capacity of the nanocomposite electrode reached 920 ± 5 mA h g^{-1}atthe 20th cycle with a Coulombic efficiency of ~98%. As shown in Fig. 9c, the reversible specific capacity gradually increased in the initial cycles and kept steady in the following cycles. After 40 discharge and charge cycles, the composite electrode still exhibited a reversible capacity of 950 ± 5 mA h g^{-1} at a current density of 200 mA g^{-1}. Fig. 9d shows the cycling behaviour of the $Mn_2Mo_3O_8$–graphene hybrid at different charge-discharge current densities. Even at a high current density of 1500 mA g^{-1}, the specific capacity was as high as 671 ± 5 mA h g^{-1}, indicating the excellent rate capability. The enhanced capacity and cyclability of the nanocomposite could benefit from the synergistic effects of the nanohybridization: the unique hierarchical

nanoarchitectures composed of the primary $Mn_2Mo_3O_8$ nanocrystals and ultrathin graphene sheets. The role of graphene during cycling reaction, and the Li-cycling mechanism for the hierarchically structured $Mn_2Mo_3O_8$–graphene nanohybrid are worth further investigation. Furthermore, we recently develop a facile and scalable strategy to prepare the $Fe_2Mo_3O_8$/reduced graphene oxide (rGO) nanocomposites through a solution-based method combined with a subsequent heat treatment process.[233] $Fe_2Mo_3O_8$ nanoparticles of 10–15 nm were uniformly distributed on the rGO nanosheets. The $Fe_2Mo_3O_8$/rGO electrode delivered a high specific capacity of 835 mA h g^{-1} after 40 discharge/charge cycles at 200 mA g^{-1}. A possible Li-cycling mechanism was proposed based on *in-situ* XRD analyses. It was found that the reversible conversion reaction involved the decomposition of $Fe_2Mo_3O_8$ and the formation of metallic Mo, Fe and Li_2O upon cycling.
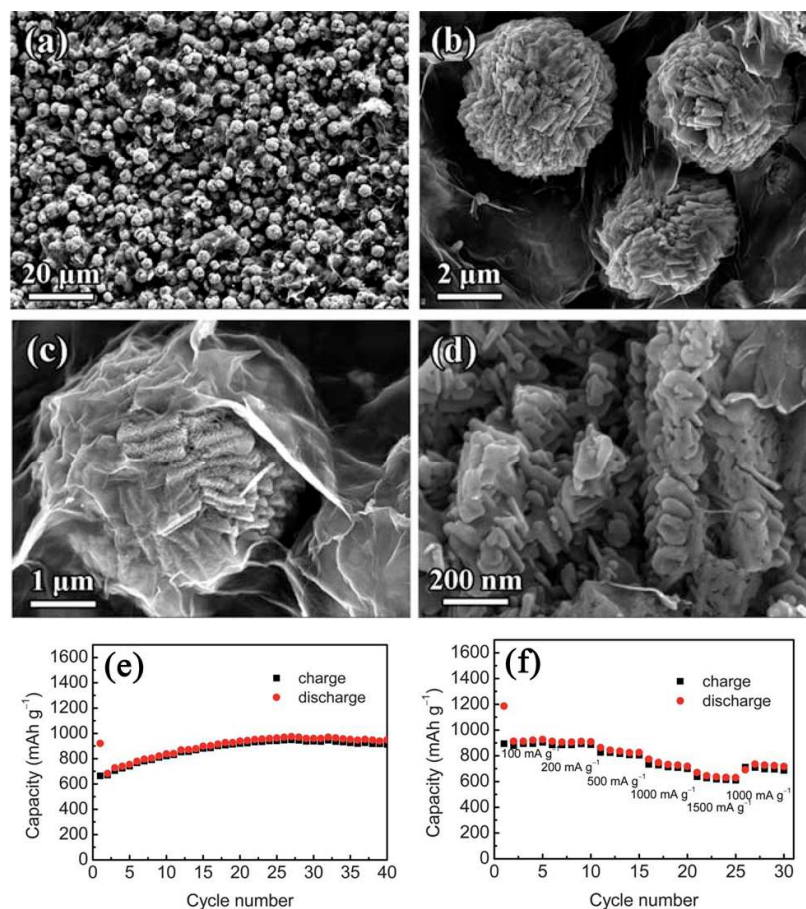
Fig. 9 (a–d) FESEM images of the hierarchical $Mn_2Mo_3O_8$–graphene hybrid. (e)Cycling performance of the $Mn_2Mo_3O_8$–graphene composite electrodes cycled in the voltage range of 3–0.01 V *vs.* Li at 200 mA g^{-1}. (f) Capacity retention of the $Mn_2Mo_3O_8$–graphene composite at various current densities of 100, 200, 500, 1000 and 1500 mA g^{-1}. Reproduced with permission from ref. 232, Copyright (2011) by The Royal Society of Chemistry.

2.5.3 Bronze Mo-based oxides. As well known, α-MoO_3 readily takes part in topotactic reactions because of its unique layered crystal structure.[163, 170, 177] Mo-based

bronzes (A_xMoO$_3$, A = H, Li, Mg, etc.) can be formed though intercalation of group

IA and IIA ions, where α-MoO$_3$ reacts with solids (e.g. LiI), vapors (e.g. CH$_3$OH),

and liquids (e.g. *n*-butyl lithium solutions), electrochemically in aqueous and

nonaqueous media.[134, 179, 234] The interlayer spacing (*d*) between the MoO$_3$ slabs in the

host structure is usually enlarged as a result of the foreign-ion uptake, but the guest

ions would not disrupt the primary Mo–O bonding within the individual MoO$_3$-type

slabs. The electrochemical Li-insertion properties of bronze Mo-based oxides have

aroused much attention for LIB applications. Combined electrochemical, NMR, and

X-ray absorption spectroscopy (XAS) research by Nazar*et al.*[235] provided in-depth

insight into the Li-cycling mechanism for (bronze Na$_{0.25}$MoO$_3$). The Li-insertion

behavior in Na$_{0.25}$MoO$_3$ at low potential can be summarized as:

$$\text{Na}_{0.25}\text{MoO}_3 + 7.8\ (\text{Li}^+ + \text{e}^-) \rightarrow y(\text{Na, Li})_2\text{O} + \text{Li}_z\text{MoO}_{3\text{-}y}\ (2y + z = 7.8)$$

Nazar*et al.*[236] also developed a general "*chimie douce*" method to prepare A$_{0.25}$MoO$_3$

(Na, Li, Sn) as anodes for LIBs. These materials presented large reversible charge

capacities (> 900 mA h g^{-1}) with good cyclability. The volumetric capacities, on the

order of 4000 mA h cm^{-3} (density for MoO$_3$ is of 4.69), were three to four times

greater than for carbon materials and twice that of Sn oxide-based glasses. It was also

found that a soft heat treatment and an appropriate discharge cut-off potential would

stabilize the charge capacity upon cycling (600 mA h g^{-1} after 100 cycles). However,

the loss of irreversible capacity and the high charge potential are the main

disadvantages in these bronze A$_{0.25}$MoO$_3$ materials. Introduction of Sn into the layered

Mo-containing bronzes via an exchange process could lower the charge potential of

the $A_{0.25}MoO_3$ materials.

2.5.4 Mo-based phosphates. Mo-based phosphates have rich crystal chemistry with a large number of structures containing tunnels, cages and micropores.[237, 238] So far, hundreds of molybdenum phosphates have been reported, and many of them with large surface areas can be used in ion exchange, catalysis, and separations.[239, 240] They consist of varied phosphate groups including monophosphate (PO_4^{3-}), diphosphate ($P_2O_7^{4-}$), metaphosphate (PO_3^{-}), oxyphosphates, and even their mixture. Most structures of Mo-based phosphates are based on MoO_6 octahedra that share their corners with PO_4 tetrahedra to build up frameworks. Owing to the varied oxidation states and rich chemistry of Mo, Mo-based phosphates have been explored as potential cathodes with two or more electron transfers (unlike $LiFePO_4$ with one-electron transfer per $Fe^{2+/3+}$ redox center) for LIBs.[241] Recent results of *ab initio* calculations by Hautier *et al.*[242] suggest that Mo ($Mo^{3+/4+}$, $Mo^{4+/5+}$, $Mo^{5+/6+}$) and V ($V^{2+/3+}$, $V^{3+/4+}$, $V^{4+/5+}$) among thousands of known and virtual phosphate compounds are the only two multiple-valence elements that can possibly enable two or more electron transfers within the acceptable voltage window (3–4.5 V). Uebou *et al.*[241] first investigated the electrochemical Li-insertion behaviours of γ-$(MoO_2)_2P_2O_7$ that possesses a 3D structure (Fig. 10). A specific capacity up to 250 mA h g^{-1} was achieved in the first discharge cycle. Intercalation processes at a current density of 0.2 mA cm^{-2} could be reversible with the Li-insertion extent of $0.85 < x < 4.0$. More recently, Whittingham and coworkers reported a cathode material of layer-structured

δ-$(MoO_2)_2P_2O_7$ that was prepared by heating a $MoO_2HPO_4 \cdot H_2O$ precursor at 560 °C.[243] Electrochemical evaluation revealed that up to four Li ions per formula unit could be intercalated into δ-$(MoO_2)_2P_2O_7$ upon discharge to 2 V (Fig. 11). Three voltage plateaus were observed at 3.2, 2.6, and 2.1 V. The first plateau corresponds to the intercalation of 1.2 Li, forming δ-$Li_{1.2}(MoO_2)_2P_2O_7$. Intercalation of the second Li leads to a different lithiated structure that is also reversible, delivering the capacity of 110 mA h g^{-1} at a potential range of 2.3–4 V. More Li^+-intercalation would result in the loss of crystallinity and structural instability.[243] Those results confirmed that Mo-based phosphates could provide a multi-electron redox center. However, the redox potential drops fast to below 3 V upon reduction of Mo to 5+, and the structure of δ-$(MoO_2)_2P_2O_7$ does not tolerate more than two Li^+ per formula unit as its structure becomes amorphous. It still remains a significant challenge to use both $Mo^{6+/5+}$ and $Mo^{5+/4+}$ redox pairs, which could be achieved in the future by designing a novel structure. Moreover, it is expected that nanostructuring and hybridization of Mo-based phosphates may have unique properties and new applications.
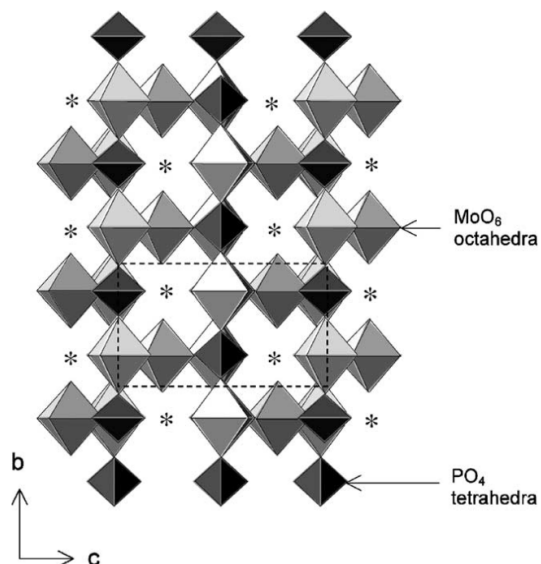
Fig. 2. The structure of $(MoO_2)_2P_2O_7$. The possible cavities for lithium or sodium insertion are indicated as (∗).

Fig. 10 Crystal structure of γ-$(MoO_2)_2P_2O_7$. The possible cavities for Li insertion are indicated as (*). Reproduced from with permission ref. 241, Copyright (2003) by Elsevier.
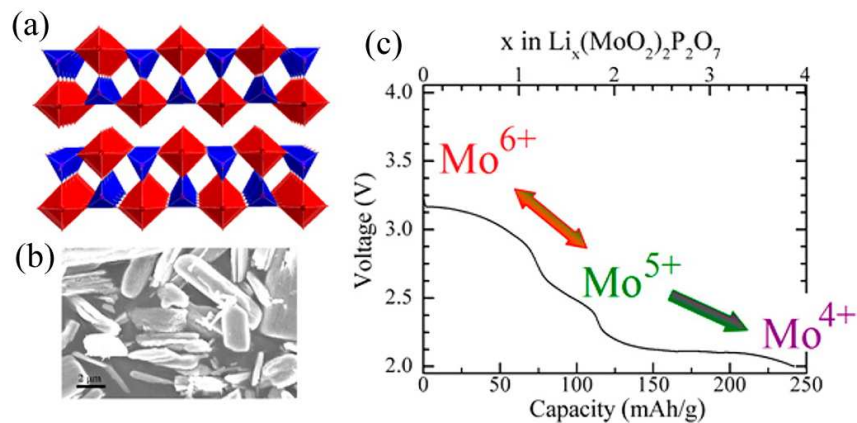
Fig. 11 (a) Layered structure of δ-$(MoO_2)_2P_2O_7$. MoO_6 octahedra are red and PO_4tectrahedra are blue. (b) SEM image of the δ-$(MoO_2)_2P_2O_7$ product. (c) Galvnostatic discharge curve for δ-$(MoO_2)_2P_2O_7$ at 0.04 mA cm^{-2} over a potential range of 2.0–4.0 V. Reproduced with permission from ref. 243, Copyright (2013) by

American Chemical Society.

2.5.5 Lithium molybdenum oxides. Considering the Li–Mo–O phase diagram as shown in Fig. 12, several phases appear to be stable in the MoO_2–Li–MoO_3 systems including $LiMoO_2$, Li_2MoO_3, $Li_4Mo_3O_8$, and $Li_{0.74}MoO_2$.[244–247] $LiMoO_2$, isostructural to widely known $LiMO_2$ (M = Co, Mn, Ni, Fe) cathode materials for LIBs, holds the promise to be a Li storage material. Up to 0.85 Li per unit of "MoO_2" can be reversible accommodated in layered $LiMoO_2$ at an average potential of 3 V with an initial capacity of about 200 mA h g^{-1}.[248] In comparison to $LiCoO_2$, $LiMoO_2$ has some different features although their crystal structures are similar. It is known that Li_xCoO_2 ($x \leq 0.8$) has a tendency to release oxygen and transform into Co_3O_4, whereas Li-free Li_xMoO_2 could be obtained electrochemically or by soft oxidation with Br_2 or I_2.[249] In addition, the existence of metallic Mo–Mo bonding in the Li_xMoO_2 polymorph may influence the Li-insertion/extraction behaviors, but there are no metallic Co–Co bonds in $LiCoO_2$. Recently, detailed in-situ structural analysis by synchrotron diffraction in Mikhailova's group revealed that a multi-phase extraction/intercalation mechanism in Li_xMoO_2 over the composition range of $0.15 \leq x \leq 1.0$ with some single-phase regions.[248]
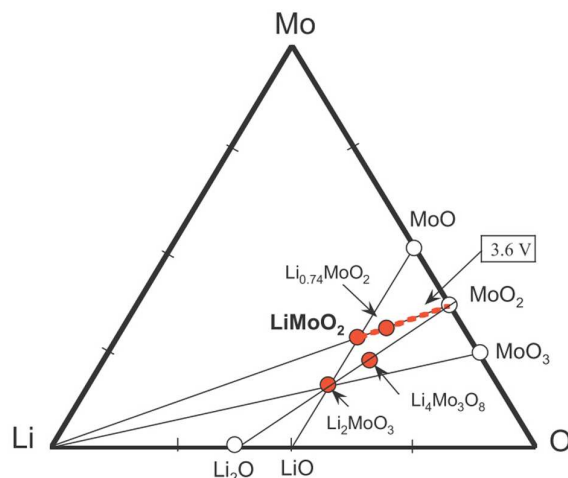
Fig. 12 Phase diagram of the Li–Mo–O system. Reproduced with permission from ref. 244, Copyright (2012) by Elsevier.

James and Goodenough first reported the basic electrochemical Li-storage properties of Li_2MoO_3 and determined its structure by neutron Rietveld analysis.[249] Li_2MoO_3 has the rhombohedral symmetry close to the α-NaFeO₂ structure.[250,251] The Mo^{4+}/Mo^{6+} redox couple of Li_2MoO_3 can exchange multiple electrons and deliver a theoretical capacity up to 339 mA h g^{-1}.[252] $LiFeO_2$-incorporated Li_2MoO_3 was investigated as a cathode additive to improve the electrochemical performance of $LiCoO_2$-based cathode systems.[253] More recently, Ma *et al.*[252,254] have successfully demonstrated the feasibility of replacing conventional Li_2MnO_3 with Li_2MoO_3 in building new layer-structured $xLi_2MoO_3 \cdot (1 - x)LiMO_2$ (M = Mn, Co, Ni, etc.) cathode materials. Interestingly, several attractive features of Li_2MoO_3 are demonstrated including the nearly reversible Mo-ion migration to/from the Li vacancies, absence of oxygen evolution, and reversible phase transition during initial (de)lithiation. Therefore, Li_2MoO_3 would be an ideal replacement of Li_2MnO_3 in constructing Li_2MoO_3-based

Li-rich cathode materials with high energy densities.Combined with advanced

nanofabrication and nanocharacterization strategies, it is expected that some novel

Li_2MoO_3-based Li-rich electrode materials with stronger structural stability and

higher cycling reversibility would be developed for high-energy LIBs applications.

Nearly all previously reported Li-Mo-O cathodes for LIBs possess ordered structures

in which Li and Mo occupy distinct sites.[244–251] Cation-disordered materials are

routinely ignored as cathodes, considering that the disordered structures often hinder

lithium diffusion in solid. Excitingly, this logic has been recently overturned by Lee *et*

al.[255] They found that lithium diffusion can be facile in disordered

$Li_{1.211}Mo_{0.467}Cr_{0.3}O_2$ (LMCO) materials. LMCO with a layered rocksalt structure was

synthesized though standard solid-state procedures, but transformed to a disordered

rocksalt after just a few charge-discharge cycles. With the help of ab initio

computations, such an unexpected behavior is attributed to percolation of a certain

type of active diffusion channels in disordered Li-excess materials. These great

findings will shed light on understanding and designing disordered-electrode

materials with high capacity and higher energy density.

2.6 Mo-based dichalconides

Molybdenum dichalcogenides (MoX_2, X = S, Se, Te) is layered transition-metal

dichalcogenides that belong to a large two-dimensional (2D) family of the general

formula MX_2. Individual sandwiched X–Mo–X layers are held together by weak van

der Waals interactions in hexagonally packed structures that are similar to the graphene layers in graphite. MoX_2 occurs in the polytypes of hexagonal $2H–MoX_2$ and rhombohedral $3R–MoX_2$. Also, tetragonal $1T-MoS_2$ has been observed for single layers exfoliated from $2H–$ or $3R–MoS_2$ crystals.[256] Because of the layered structure, a pronounced anisotropy of electrical conduction is observed, which is considerably (two or three orders of magnitude) larger parallel to the planes. Perpendicular to the planes, conduction occurs by a hopping mechanism. As summarized in the recent comprehensive reviews,[44, 257-261] MoX_2 exhibits a remarkably diverse range of unique optical, electrochemical, and mechanical properties. They have been widely used as functional materials in diverse fields of lubrication,[262] electronic transistors,[263] batteries,[264] photovoltaics,[265] catalysis,[266] and sensing.[267]

2.6.1 MoS$_2$ nanostructures. MoS_2 is an attractive host for ion intercalation because of its rich intercalation chemistry and structural peculiarities. The application of MoS_2 as a cathode for LIBs was patented and commercialized by Moli Energy in 1980.[206, 268-274] However, the lithiation voltage of MoS_2 as a cathode is lower than that of other commercial cathode materials such as $LiCoO_2$, thus reducing the energy density of a full cell. Even worse, the secondary Li/MoS_2 batteries using MoS_2 as the cathode and Li as the anode are prone to the growth Li dendrites from the anode, which results in serious safety problems and poor cyclability. In contrary, MoS_2 is becoming the hot subject of significant attention as an anode material for LIBs. In particular, the emergence of diverse nanostructures has recently led to a variety of high-performance

anodes using MoS_2 nanostructures and MoS_2 nanocomposites. Nanostructuring and nanocarbon incorporation have been demonstrated as two effective approaches to improvethe electrochemical performance of MoS_2-based electrode materials. To date, various MoS_2 nanostructured materials with diverse geometric shapes and morphologies, such as nanoflakes, nanotubes, nanoflowers, and hierarchical tubular architectures, have been intensively explored to enhance the cycling stability. [15, 275-283] Nevertheless, those nanostructures were often found to be destroyed upon continuous discharge-charge cycling. Graphene has been successfully demonstrated as one of the most important supports to enhancethe performance of MoS_2.[195, 284-299] For instance, Chang and Chen[287] prepared layered MoS_2/reduced graphene oxide (MoS_2/rGO) composites by an L-cysteine-assisted solution-phase method. The resulting MoS_2/rGO (1:2) composite displayed a 3D architecture composed of a large number of scaled and curved sheets in the range 100–200 nm (Fig. 13a), and the layered MoS_2 was supported on the surface of rGO (Fig. 13b). Compared to the electrodes made of pristine MoS_2, MoS_2/rGO (1:1), and MoS_2/rGO (1:4), the MoS_2/rGO (1:2) electrode delivered the highest specific capacity of $\sim$1100 mA h g^{-1} at a current density of 100 mA g^{-1} without capacity fading after 100 cycles (Fig. 13c). Even at a high current density of 1000 mA g^{-1}, the specific capacity of the MoS_2/rGO (1:2) electrode remained at $\sim$900 mA h g^{-1}, indicating an excellent rate capability (Fig. 13d). Moreover, amorphous carbon, carbon nanotubes, carbon fibers, polyaniline nanowires, and so on. have been explored as the elastic buffer layers/supports to enhance the stability of the MoS_2-based anode materials.[300-324]
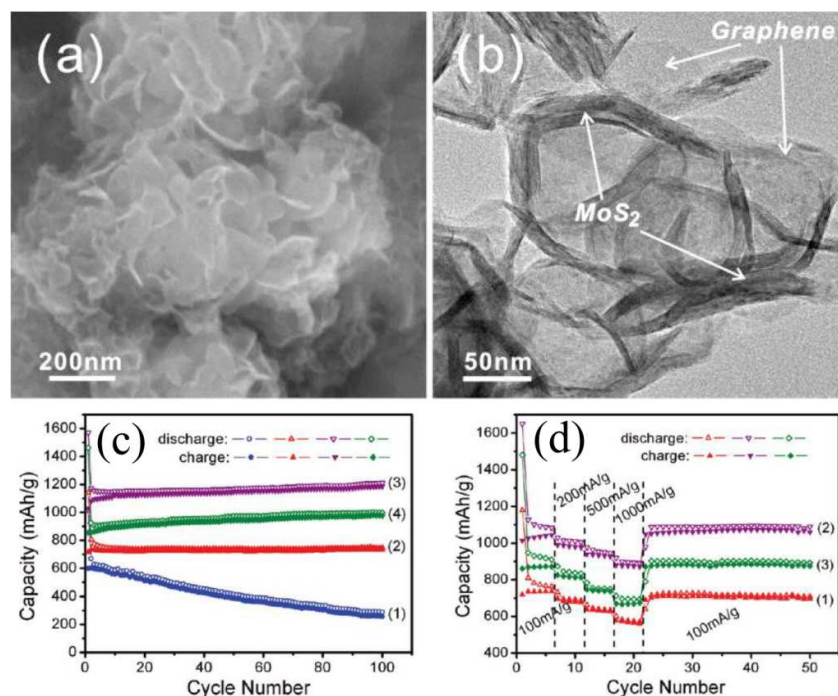
Fig. 13 (a) SEM image and (b) TEM image for the representative MoS$_2$/rGO (1:2)

nanocomposite. (c) Cycling behavior of samples for 2 h at a current density of 100

mA/g: (1) MoS$_2$; (2) MoS$_2$/rGO (1:1); (3) MoS$_2$/rGO (1:2); (4) MoS$_2$/rGO (1:4). (d)

Rate capability of MoS$_2$/rGO samples at different current densities: (1) MoS$_2$/rGO

(1:1); (2) MoS$_2$/rGO (1:2); (3) MoS$_2$/rGO (1:4). Reproduced with permission from ref.

287, Copyright (2011) by American Chemical Society.

The Li-cycling mechanism of MoS$_2$ as an anode has so far not been well understood,

especially below the potential of 1.1 V $vs.$ Li/Li$^+$. The recent comprehensive review

by Stephenson et $al.$[260] has discussed the Li-insertion reactions in MoS$_2$ in detail.

Normally, intercalation of Li$^+$ into MoS$_2$ is known to occur within the potential range

of 3–0 V *vs.* Li/Li$^+$. Li$^+$ insertion is considered to be fully reversible in the potential

range of 3.0–1.1 V, and the electrochemical reaction can be described as:[296, 311, 314]

$$MoS_2 + xLi^+ + xe^- \rightarrow Li_xMoS_2 \ (\sim1.1 \ \text{V vs. Li/Li}^+)$$

Where x is in the range of $0 \leq x \leq 1$. The theoretical specific discharge capacity of the

above reaction is calculated to be 167 mA h g^{-1} (corresponding to LiMoS$_2$). When the

potential is below the plateau of ~1.1 V, there takes place one or several

disproportionation reactions together with the presence of intermediate metastable

sulfide species. For example, the lower plateau at about 0.6 V during the first

discharge process has been assigned to the following reversible conversion reaction

from MoS$_2$ to Li$_2$S and Mo:[299, 311, 314]

$$Li_xMoS_2 + (4 - x)Li^+ + (4 - x)e^- \rightarrow Mo + 2Li_2S \ (\sim0.6 \ \text{V vs. Li/Li}^+)$$
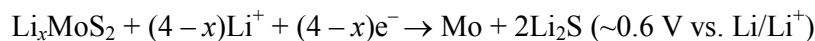
The theoretical specific capacity for the full conversion reaction (MoS$_2$ + 4Li$^+$ + 4e$^-$

$\rightarrow$ Mo + 2Li$_2$S) is 669 mA h g^{-1}. During the first delithiation cycle, a pronounced

peak at ~2.3 V was attributed to the delithiation of Li$_2$S into S.[278, 304]

$$Li_2S \rightarrow 2Li^+ + S + 2e^- \ (\sim2.3 \ \text{V vs. Li/Li}^+)$$
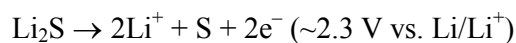
During the second lithiation cycle, two new plateaus at ~1.9 and 1.2 V appeared. The

dominant cathodic peak at ~1.9 V is well known in Li-S batteries. It is attributed to

the formation of Li$_2$S, and the smaller peak at ~1.2 V could be the conversion of

residual S$_8^{2-}$ into Li$_2$S. In the charge (delithiation) process, only one plateau at ~2.2 V

was observed, corresponding to the oxidation of Li$_2$S into S. After the first

lithiation–delithiation cycle, the electrode could be changed into a mixture of S and

Mo, instead of MoS$_2$, based on the following reversible reaction that yields a

theoretical capacity of 1675 mA h g^{-1} (if the weight of Mo is not taken into account):[325]

$$Li_2S + Mo \leftrightarrow 2Li + S + Mo$$
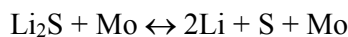
The functions of Mo as well as the additives like carbon allotropes in the nanocomposite electrode materials need to be further explored. Sometimes, the MoS$_2$-based electrodes have exhibited high specific capacities that are larger than the theoretical value for the conversion reaction of $MoS_2 + 4Li^+ + 4e^- \rightarrow Mo + 2Li_2S$. Although the exact Li-cycling mechanism for MoS$_2$ remains still unclear at present, even some controversial, it is expected that the advanced *in-situ* analytic techniques such as solid-state NMR and XAS, together theoretical simulations will help unveil the details.

2.6.2 MoSe$_2$ nanostructured materials. As a close analogue to the layer structured MoS$_2$, the electrochemical Li-storage performance of MoSe$_2$ has seldom been reported.[326, 327] More recently, Shi *et al.*[328] prepared highly ordered mesoporous crystalline MoSe$_2$ by using mesoporous silica SBA-15 as a hard template via a nanocasting strategy (Fig. 14). The obtained products displayed a highly ordered hexagonal mesostructure and a rod-like particle morphology. When evaluated as an anode material, mesoporous MoSe$_2$ delivered a reversible lithium-storage capacity of 630 mA h g^{-1} for at least 35 cycles without any evident decrease. It was found that the rate performance of mesoporous MoSe$_2$ was much better than that of analogously synthesized mesoporous MoS$_2$, making it a promising anode for the lithium-ion

battery. Also, the as-obtained mesoporous $MoSe_2$ as a photocatalyst showed remarkable photocatalytic activity for the degradation of organic compound in aqueous solution under visible light irradiation.[328] Nanocarbon hybridization may also be a useful method to improve the properties of $MoSe_2$ nanostructures, and may find new applications in optoelectronics, catalysis and sensing.
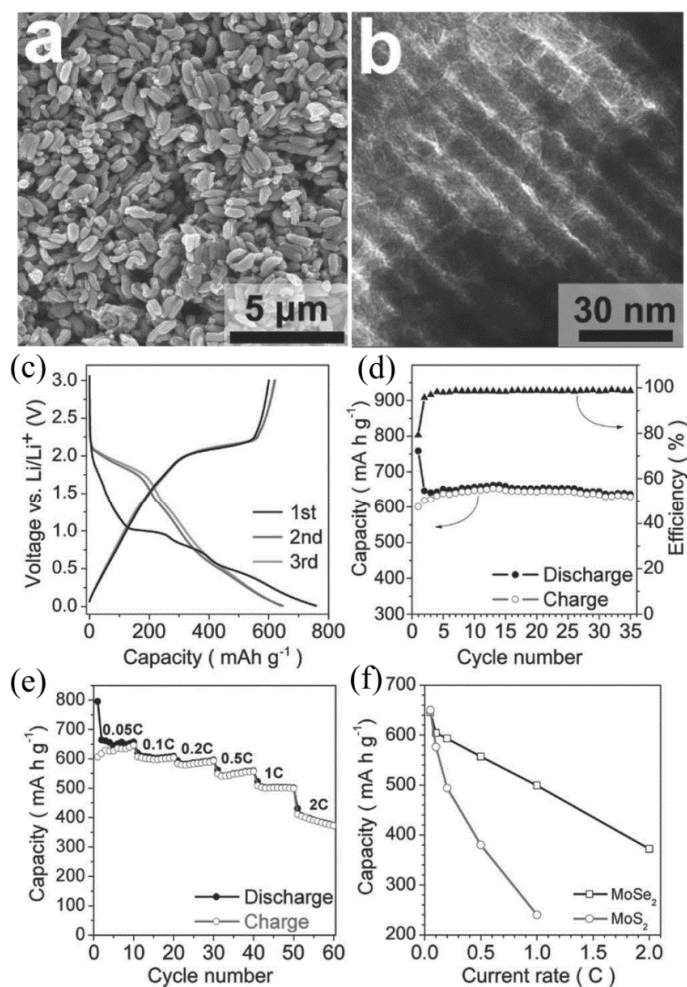
Fig. 14 (a) SEM and (b) TEM images of the synthesized mesoporous $MoSe_2$ materials using SBA-15 as the template via a nanocasting method. c) The discharge/charge curves of the first three cycles for the mesoporous $MoSe_2$ electrode at a current rate of

0.05 C between 0.01 and 3.00 V. (d) Cycling performance of the mesoporous

MoSe$_2$electrode at a current rate of 0.05 C. e) Rate performance of the mesoporous

MoSe$_2$ electrode between 0.01 and 3.00 V. f) Comparison of the rate performance

between mesoporous MoSe$_2$ and MoS$_2$ electrodes. Reproduced with permission from

ref. 328, Copyright (2013) by WILEY-VCH.

3. Mo-based nanostructures as electrode materials for SIBs

SIBs have recently drawn increasing attention because of the cheap raw material.

Compared to LIBs, however, the larger size of Na$^+$ (1.02 Å $vs.$ 0.76 Å for Li$^+$)

hampers electrochemical reaction kinetics. Therefore, reversible electrode materials

are required to possess large enough channels and/or interstitial sites. Particularly for

the anodes of SIBs, the main issues include large polarization and rapid capacity

fading. Considering the extreme reactivity of Na metal, it is also very crucial to find

an alternative anode material to secure battery safety and realize the practical

utilization of this energy-storage system. Recent findings have shown that the anode

materials for SIBs based on alloy-type (e.g., Si, Sn, Ge, and SnO$_2$) and

conversion-type (e.g., CuO, Fe$_2$O$_3$, and FeS$_2$) exhibited high initial capacity, but

suffered from poor cyclability most likely due to the large volume change and the

sluggish kinetics. In addition, some non-graphitic carbon (e.g., hard carbon and

carbon spheres), organic anode materials (e.g., Na$_2$C$_8$H$_4$O$_4$), and titanium-based

intercalation compounds (e.g., amorphous TiO$_2$ and Na$_2$Ti$_3$O$_7$) have been investigated

as anode materials for SIBs. These anode materials have demonstrated a maximum

reversible capacity in the range of 100–300 mA h g^{-1}.

A large class of layered materials, namely, transition metal dichalcogenides are a potentially useful alternative to graphite as anodes for SIBs. For example, the atomic structure of layered MoX_2 (X = S, Se and Te) is similar to graphite, characteristic of a strong in-plane covalent bonding and weak van der Waals interactions between X layers. Also, MoX_2 have a larger interlayer slab space (e.g., ~6.2 Å for MoS_2) than graphite, offering a wide range of electron affinity for the intercalation of a guest ion. Among transition metal dichalcogenides, MoS_2 with a well-defined layered structure has been intensively investigated as anode materials for rechargeable batteries. According to the terminal discharge voltage, the reactions in a Na-MoS_2 battery proceed in two steps: intercalation and conversion, as described as follows:

$$MoS_2 + xNa = Na_xMoS_2 \text{ (above 0.4 V, } x < 2)$$

$$Na_xMoS_2 + (4 - x)Na = Mo + 2Na_2S \text{ (below 0.4 V)}$$

Park et al.[329] reported the possibility of using commercial MoS_2 for Na-ion storage, and demonstrated a capacity of 85 mA h g^{-1} at 0.4–2.6 V over 100 cycles based on an intercalation/deintercalation reaction. Recently, *ab initio* calculations on Na-intercalation in all structural polytypes of MoS_2 were conducted by Medhekar *et al.*[330] Their findings revealed that Na ions are generally found to occupy octahedral or distorted octahedral sites within the interlayer van der Waals spaces upon intercalation. Na-ion intercalation in MoS_2 causes a phase transformation at $x = 0.39$ from the 2H to

1T phase. However, it is thermodynamically stable across the entire concentration range of $0 < x < 1$ against the phase separation of Na. The calculated energy barrier of 0.68 and 0.28 eV for Na-ion diffusion in 2H- and 1T-MoS$_2$, indicating moderately fast charge and discharge rates, respectively. These results suggest that 1T polytype obtained via exfoliation of 2H polytype has better electrochemical performance arising from its inherent metallic electronic structure, higher capacity for Na ions and their fast motilities.[330] Therefore, exfoliating layered structure into few-layer sheets or individual monolayers can allow for an enhanced adsorption of Na$^+$ on both sides and faster diffusion rates. More recently, Chen *et al.*[331] reported the synthesis of unique graphene-like MoS$_2$ nanoflowers with expanded layers by a hydrothermal method (Fig. 15). By controlling the cut-off voltage to the range of 0.4–3 V, it was found that the reversible Na-insertion in MoS$_2$ followed an intercalation mechanism, instead of a conversion mechanism. The electrode made of graphene-like MoS$_2$ nanoflowers showed high discharge capacities of 350 mA h g^{-1} at 0.05 A g^{-1}, 300 mA h g^{-1} at 1 A g^{-1}, and 195 mA h g^{-1} at 10 A g^{-1} over up to 1500 cycles, indicating excellent rate capability and superior cyclability (Fig. 15). It is believed that the expanded and gradually exfoliated interlayers have contributed to the decreased barrier for Na$^+$ insertion and extraction, thus reducing the charge transfer resistance and offering more active sites for Na$^+$ storage. In addition, Choi et *al.*[332] reported a liquid-phase exfoliation method to improve the exfoliation efficiency for single-layer MoS$_2$ sheets in 1-methyl-2-pyrrolidinone (NMP) with an assistant of NaOH. The exfoliated MoS$_2$ electrode showed a Na-intercalation capacity 161 mA h g^{-1} at 20 mA g^{-1} over 50

cycles.
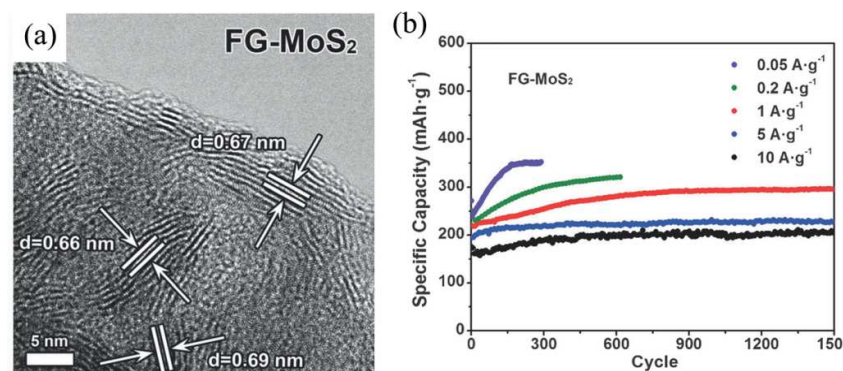
Fig. 15 (a) High-resolution TEM image and (b) electrochemical performances for the electrode made of MoS_2 nanoflowers. Reproduced with permission from ref. 331, Copyright (2014) by Wiely-VCH.

Besides Na-ion intercalation, pristine MoS_2 has been proven to be converted into Mo and Na_2S with additional substantial gain in capacity (~3 Na^+ reaction, ~501 mA h g^{-1}) when further deeply discharged to lower voltage (0.01 V).[333] The discharge product, Na_2S, could afford better conductivity than Na_2O as typically formed from a deep conversion reaction of metal-oxide compounds.[334] Another work by Chou et al.[335] is that an exfoliated MoS_2–C composite (E-MoS_2–C) was prepared via simple chemical exfoliation and a hydrothermal reaction. The MoS_2 nanoflowers electrode exhibited a capacity of ~400 mA h g^{-1} at 0.25 C (100 mA g^{-1}) over 100 cycles. To address the issues of large volume change during the conversion reaction resulting in the formation of internal cracks, loss of electrical contact, and eventual failure of the electrode, nanostructuring or nanocarbon incorporation of MoS_2 may be an effective

strategy. For instance, Kim and coworkers proposed an electrospinning method to prepare 1D MoS_2 nanofibers with a vine-like shape composed of MoS_2 nanoflakes to improve Na-storage properties. Singh et al.[336] fabricated layered free-standing paper composed of acid-exfoliated few-layer MoS_2 and rGO flakes as a self-standing flexible electrode in SIBs. The electrode showed good Na cycling ability with a stable charge capacity of approximately 230 mA h g^{-1} with respect to total weight of the electrode. More recently, Maier et al.[324] prepared single-layered MoS_2 ultrasmall nanoplates embedded in carbon nanowires by electrospinning. The nanohybrid delivered specific capacities of 854 mA h g^{-1} at 0.1 A g^{-1}, 484 mA h g^{-1} at 1 A g^{-1}, and 253 mA h g^{-1} at 10 A g^{-1} over 100 cycles, demonstrating the excellent rate capability of the MoS_2/C nanocomposite anode for SIBs.

Compared to MoS_2, $MoSe_2$ has been seldom studied as an anode material for SIBs. Tirado et al.[327] demonstrated the possibility of Na^+ intercalation in $MoSe_2$ based on a Na-intercalation/deintercalation reaction mechanism. Recently, Kang et al.[337] prepared yolk–shell-structured $MoSe_2$ microspheres via a simple selenization process of MoO_3 microspheres. The yolk–shell-structured $MoSe_2$ and MoO_3 microspheres delivered initial discharge capacities of 527 and 465 mA h g^{-1}, respectively, in the voltage range of 0.001–3 V vs. Na/Na^+ at 0.2 A g^{-1}. Their discharge capacities were kept to be 433 and 141 mA h g^{-1} after 50 cycles, respectively. The hierarchical yolk–shell structure comprised of wrinkled nanosheets facilitated fast Na-ion and electron kinetics, and buffered the large volume changes encountered during conversion-type cycling.

4. Mo-based nanostructures as cathode materials for Mg batteries

Mg batteries have been long pursued as a highly promising technology for energy storage and conversion. The first working Mg rechargeable battery prototypes were successfully developed in 2000,[24] using ethereal solutions containing magnesium halo-alkyl aluminate complex electrolytes. Since then, more profound understanding on several types of complex solutions in which Mg electrodes are reversible has been achieved. Despite these advances, two main obstacles of kinetically sluggish Mg intercalation/diffusion in cathodes and incompatibility between Mg anodes and electrolytes prohibit Mg batteries from practical applications.[29] A variety of candidates have been proposed in recent years for rechargeable Mg batteries. In particular, Mo-containing cathode materials are intensively explored among those Mg-intercalation cathode materials. For instance, molybdenum chalcogenides, $M_xMo_6T_8$ (M = metal, T = S, Se, Te, or their combination), also known as Chevrel phases, can intercalate various divalent ions.[338–346] They possess a special crystallographic structure comprising pseudo-cubic cavities between Mo_6T_8 blocks (i.e. octahedral clusters of Mo atoms in side cubic anionic framework). It has been demonstrated that Mo_6S_8 can intercalate Mg^{2+} ions reversibly according to the reaction: $Mo_6S_8 + 2Mg^{2+} + 4e^- \leftrightarrow Mg_2Mo_2S_8$.[28] As shown in Fig. 16,[28] the unique crystal structure of Mo_6S_8 facilitates the fast insertion kinetics of bivalent Mg^{2+} ions, benefiting from a large number of vacant sites, short distances between them, and the metallic Mo_6 clusters that easily compensates the charge-unbalance due to the
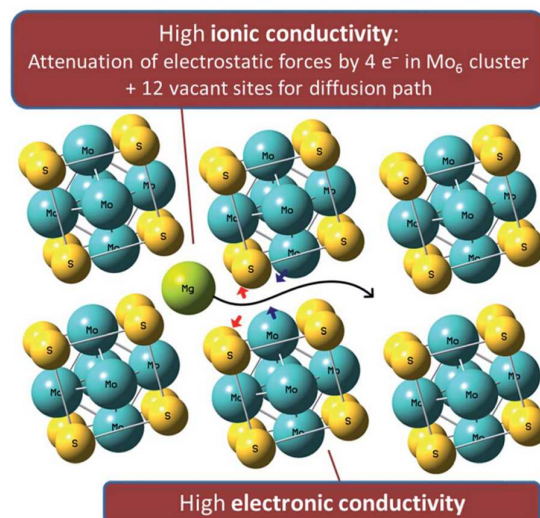
Fig. 16 A schematic explanation for the fast solid-state diffusion of Mg^{2+} ions in Chevrel phase electrodes. Reproduced with permission from ref. 28, Copyright (2013) by The Royal Society of Chemistry.

Recently, nanostructured MoO_3 and MoS_2 with a layered crystal structure have been developed as promising cathode materials for Mg batteries, because of their structural flexibility to accommodate the severe structural deformation upon insertion of bivalent Mg^{2+} ions. Chen *et al.*[347] prepared graphene-like MoS_2 (G-MoS_2) via a solvothermal route from the reaction of MoO_3 with thioacetamide in pyridine. Combined with the use of ultrasmall Mg nanoparticles of ~2.5 nm in size as the anode, the G-MoS_2 cathode achieved a high operating voltage of 1.8 V, an initial discharge capacity of 170 mA h g^{-1}, and capacity retention of 95% upon 50 discharge/charge cycles. Based on a formula unit of $Mo_{20}S_{40}$ (a width of ~1.2 nm) as a representative

model for a MoS_2 monolayer, density functional theory calculations show that each

Mg atom could be coordinated by three S atoms at a distance of about 2.5 Å, and a

formula unit of $Mg_4Mo_6S_{12}$ is derived.[348] The electrochemical reactions in the cathode

of single-layered MoS_2 in Mg batteries could be simplified as: $6MoS_2 + 4Mg^{2+} + 8e^-$

$\leftrightarrow Mg_4Mo_6S_{12}$. Li's group[349] reported the solution synthesis of MoS_2 hollow-cage

fullerene-like nanoparticles, fibrous floccus, and spherical nanovesicles. The

electrodes made of these MoS_2 nanostructures showed enhanced reversibility upon

Mg-ion intercalation/extraction cycling compared to bulk MoS_2 powders. More

recently, Jiao et al.[350] demonstrated that sandwich-structured MoS_2/rGO serving as a

cathode in Mg batteries delivered 104.2 and 74.1 mA h g^{-1} after 30 and 50 cycles,

respectively.

Aurbach's group[351] performed detailed investigations by electrochemical and

spectroscopic analysis of Mg^{2+} intercalation into thin-film electrodes of layered MoO_3.

It was found that thin-film electrodes of MoO_3 delivered a high reversible capacity of

220 mA h g^{-1} at a potential of 1.8 V vs Mg^{2+}/Mg. A two-phase reaction may occur

during the magnesium of MoO_3. In contrast to Li^+ ions, higher overpotential is needed

for intercalation/deintercalation of Mg^{2+} in the MoO_3 host. Besides aforementioned

systems, the search for a suitable nanostructured cathode and a less passivated

anode/electrolyte configuration is intrinsically urgent for developing rechargeable Mg

batteries. For more details, please refer to the recent review articles on rechargeable

Mg batteries, which have comprehensively summarized and discussed the cathode

materials as well as the Mg anodes and electrolytes.[25–32]

5. Mo-based nanostructures as electrode materials for supercapacitors

It is well known that electrode materials based on an EDLC mechanism often have limited specific capacitance, usually in the range of 10–50 mF cm^{-2} for a real electrode surface.[35, 352] Since pseudocapacitance may be 10–100 times larger, supercapacitors made of redox-active electrode materials bearing pseudocapacitance are highly desirable for next-generation electrochemical energy storage applications.[353] Besides charge storage in the double layer, the pseudocapacitors rely on fast and reversible surface redox reactions (faradaic reactions). The most widely used active electrode materials with pseudocapacitance are conducting polymers and transition metal oxides.[353] Among the redox-active materials, Mo-based compounds, featuring high specific capacitance, low cost, natural abundance, and environmental benignity, have attracted significant interest as active electrodes for supercapacitors.

5.1 Molybdenum oxides

5.1.1 MoO$_2$. MoO$_2$ has been demonstrated as a candidate for electrochemical pseudocapacitors because its low metallic resistivity and different oxidation state of Mo. Actually, several MoO$_2$-based nanostructures such as MoO$_2$ nanorods, mesoporous MoO$_2$, and MoO$_2$-based nanohybrids have been reported for supercapacitors.[354-360] Several examples of MoO$_2$-based electrode materials and their

electrochemical properties are given in Table 2. It was reported that MoO_2 not only served as an active material, but also could function as a conducting support. For example, Mai *et al.*[357] prepared a nanostructured MoO_2 thin film that was coated by $Co(OH)_2$ nanoflakes on a 3D nickel foam scaffold by successive electrodeposition. The MoO_2 thin film could serve as a conductive layer for electron transport, while $Co(OH)_2$ nanoflakes allowed fast ion diffusion due to their large interlayer space. It was observed that the electrode made of the $MoO_2/Co(OH)_2$ nanohybrid exhibited a high capacitance of 800 F g^{-1} at 20 A g^{-1} as well as largely enhanced cyclability with only 3% capacitance loss after 5000 cycles as compared with each counterpart of MoO_2 (53%) and $Co(OH)_2$ (61%). The superior electrochemical performances of nanocomposite $MoO_2/Co(OH)_2$ electrode materials were mainly attributed to: (i) the hierarchical architecture allowing synergistic contribution of both materials with increased ion diffusion and fast electron transport; (ii) stable $MoO_2/Co(OH)_2$ interface relieving the destruction of the electrode upon charge/discharge cycling.

Table 2 Specific capacitance of MoO_2-based electrode materials

Electrode materials	Specific capacitance (F/g)	Electrolyte	Voltage window (V)	Current load or scan rate	Ref.
MoO_2 nanorods	140 (3-electrode)	1.0 M H_2SO_4	−0.3–0.4 (*vs.* Ag|AgCl)	1 mA cm^{-2}	354
MoO_2/SWNT	597 (3-electrode)	1.0 M Na_2SO_4	0–1 (*vs.* SCE)	10 mV s^{-1}	355
MoO_2 nanorods on the Cu foil	250.3 (3-elelctrode)	1.0 M Na_2SO_4	−0.2–1 (*vs.* SCE)	1 mA	359
OMC/MoO_2	395 (3-elelctrode)	1.0 M H_2SO_4	−0.2–0.6 (*vs.* SCE)	2 mV s^{-1}	360
rGO/MoO_2	624 (2-electrode)	1 M $LiPF_6$ in EC:DEC	0.005–3 (vs. Li/Li^+)	50 mA g^{-1}	356
$Co(OH)_2$nanoflakes on MoO_2 thin film	800 (3-elelctrode)	2.0 KOH	−0.2–0.45 (*vs.* SCE)	20 A g^{-1}	357
Ordered mesoporous	146 (3-elelctrode)	1.0 LiOH	−1.2– −0.5 (*vs.* SCE)	5 mV s^{-1}	358

MoO$_2$

Note: SWNT: single-walled carbon nanotube; OMC: ordered mesoporous carbon; rGO: reduced graphene oxide; SCE: saturated calomel electrode; EC: ethylene carbonate; DEC: diethyl carbonate.

5.1.2 MoO$_3$. As discussed above, α-MoO$_3$ is a typical electroactive 2D layered material that can accommodate up to 1.5 Li/Mo, and comprises alternately stacked layers held together by weak van der Waals forces along [010]. As a result, α-MoO$_3$ could be an ideal material that has the potential to deliver both redox and intercalation pseudocapacitance, thus optimizing both energy density and power density in a single material. In order to demonstrate the capacitive behaviour in such a layered structure of α-MoO$_3$, Dunn *et al.*[361] prepared mesoporous films through an evaporation-induced self-assembly process (Fig. 17). It was found that the capacitive charge-storage properties of mesoporous films of iso-oriented α-MoO$_3$ were superior to those of either mesoporous amorphous material or non-porous crystalline α-MoO$_3$. Both crystalline and amorphous mesoporous MoO$_3$ showed redox pseudocapacitance, but the iso-oriented layered crystalline domains enabled lithium ions to be inserted into the van der Waals gaps of the α-MoO$_3$. Dunn *et al.*[361] proposed that extra capacitance contribution arising from a unique intercalation pseudocapacitance would take place on the same timescale as redox pseudocapacitance. Significantly, the charge-storage capacity was unusually increased in mesoporous crystalline α-MoO$_3$, but the charge/discharge kinetics was not scarified. Inspired by this research, researchers may come up with new ideas to develop unique pseudocapacitive materials that offer increased energy density while still maintaining their high-power-density advantages. In recent years, other nanostructures including

MoO$_3$nanoparticles,[362] nanorods,[363] nanowires,[364] nanoplates,[365] and nanobelts,[366, 367] as well as ZnO/MoO$_3$,[368] polypyrrole/MoO$_3$,[369] and MWCNT/MoO$_3$[370] have been reported as electrode materials for electrochemical pseudocapacitor applications, and exhibited enhanced capacitive properties.
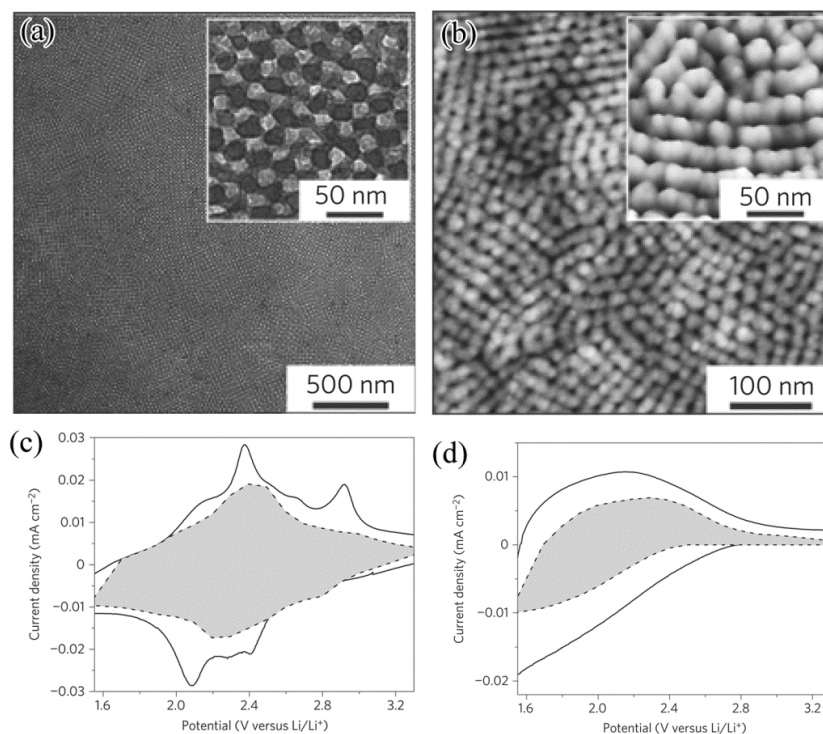
Fig. 17 (a) TEM and (b) tapping-mode AFM images for mesoporous α-MoO$_3$ with highly oriented crystalline walls. (c, d) Capacitive and diffusion-controlled contributions to charge storage. Voltammetric responses for mesoporous MoO$_3$ films at a sweep rate of 0.1 mV s^{-1}. The capacitive contribution to the total current is shown by the shaded region. For mesoporous α-MoO$_3$ (c), some 70% of the total charge is capacitive, whereas for the mesoporous amorphous MoO$_3$ (d), only 35% is capacitive. Reproduced with permission from ref. 361, Copyright (2010) by Nature Publishing Group.

5.1.3 MoO$_{3-x}$. During the past three years, MoO$_{3-x}$ ($0 < x < 1$) has been investigated as a negative electrode material that shows high specific capacitance in neutral or slightly acidic aqueous solution with high specific capacitance. Zhang's group prepared MoO$_{3-x}$ thin films by magnetron sputtering and core-shell Ti@MoO$_{3-x}$ nanorod arrays by electrodeopsition.[371-373] Recently, Zhou and coworkers[374] reported a nanocomposite negative electrode of WO$_{3-x}$/MoO$_{3-x}$core@shell nanowires on carbon fabrics by physical evaporation deposition and a subsequent electrodeposition process. A flexible all-solid-state supercapacitor was assembled based on polyaniline as the positive electrode and the resulting hybrid WO$_{3-x}$/MoO$_{3-x}$ as the negative electrode. It exhibited stable performance between 0 and 1.9 V, a high areal capacitance of about 216 mF cm^{-2}, an energy density of 0.0019 Wh cm^{-3}, and high rate capability. This work offers the possibilities of using the WO$_{3-x}$/MoO$_{3-x}$nanohybrids for applications in energy storage, flexible electronics, and other consumer electronics. Another work by Zhou *et al.*[375] is that freestanding films of carbon nanotubes were used as positive electrodes, assembled with freestanding CNT/MoO$_{3-x}$ negative electrodes to fabricate carbon nanotube-based solid-state asymmetric supercapacitors. Such a unique device showed a high volumetric capacitance of 3.0 F cm^{-3}, energy and power density of 1.5 mWh cm^{-3} and 4.2 W cm^{-3}, respectively. Very interestingly, a pack of supercapacitors have also been assembled in this work to drive a homemade wireless transport system successfully, demonstrating the potential of this solid-state system for future applications in the fields of portable/wearable electronics.[375]

5.2 Molybdenum molybdates

Recently, $AMoO_4$-type metal molybdates (A = Co, Ni, Mn, Fe, etc.) have emerged as prospective effective and scalable electrode materials for supercapacitors because of their low cost, environmental friendliness, and abundant resources. Purushothaman *et al.*[376] synthesized α-$MnMoO_4$ nanorods by using a sol–gel spin coating method and obtained a specific capacitance of 998, 784, and 530 F g^{-1} in H_2SO_4, *para*-toluene sulfonic acid, and HCl electrolytes, respectively. Kong *et al.*[377] demonstrated a high capacitance of 326 F g^{-1} at 5 mA cm^{-2} for $CoMoO_4 \cdot 0.9H_2O$ nanorods prepared by a hydrothermal process. Selvan*et al.*[378] reported that $MnMoO_4$, $CoMoO_4 \cdot xH_2O$, and $NiMoO_4$ based on solution-combustion synthesis provided a high specific capacitance at 5 mA cm^{-2} of 126, 401, and 1116 F g^{-1}, respectively. Likewise, Wang *et al.*[379] reported a template-free hydrothermal route for the preparation of $CoMoO_4$ nanoplate arrays on Ni, and achieved a high specific capacitance of 1.26 F cm^{-2} at 4 mA cm^{-2} and 0.78 F cm^{-2} at 32 mA cm^{-2} with an excellent cyclability upon 4000 cycles. Hierarchical bismuth molybdate nanowires synthesized by an electrodeposition-heat method demonstrated its suitability as a negative electrode material for pseudocapacitors, showing a capacitance 1075 F g^{-1} at 0.1 A g^{-1} and excellent cycle life up to 1000 cycles.[380] Besides, several other nanostructures with 1D morphologies (e.g., $MnMoO_4$ nanorods,[381] $NiMoO_4$ nanorods,[382] nanowires[383, 384] and nanosheets,[385] $NiMoO_4 \cdot xH_2O$ nanorods[386, 387]) and conducting graphene (or polyaniline)-stabilized nanohybrids (graphene/$NiMoO_4 \cdot nH_2O$,[388] graphene/α-$MnMoO_4$,[389]

graphene/CoMoO$_4$,[390] and polyaniline/CoMoO$_4$•0.75H$_2$O[391]) have been investigated for redox-active supercapacitors.

Recently, coupled metal molybdates have also been explored as electrode materials for supercapacitors.[392-395] Coupled metal molybdates can provide an improvement in electrochemical performances due to the synergistic effect of individual metal molybdates.[392, 394, 395] For example, Mai *et al.*[394] reported a simple refluxing method to prepare heterostructured MnMoO$_4$–CoMoO$_4$ nanowires that exhibited a capacitance of 187.1 F g^{-1} and excellent stability (Fig. 18). This capacitance is higher than MnMoO$_4$ (9.7 F g^{-1}) and CoMoO$_4$ (62.8 F g^{-1}). Selvan and coworkers[395] prepared nanosized β-NiMoO$_4$–CoMoO$_4$•xH$_2$O composites by a solution-combustion method. The NiMoO$_4$–CoMoO$_4$•xH$_2$O nanocomposite with a Ni : Co weight ratio of 3 : 1 exhibited a maximum specific capacitance of 1472 F g^{-1} at 5 mA cm^{-2}. Liu et al. obtained an improvement in electrochemical performance for CoMoO$_4$–NiMoO$_4$•xH$_2$O bundles compared to the corresponding individual metal molybdates.[393] The composite with a Ni–Co mass ratio of 1.4 : 0.6 took advantages of both CoMoO$_4$ (rate capability) and NiMoO$_4$•xH$_2$O (high specific capacitance, 1039 F g^{-1}). More recently, Wang *et al.*[392] synthesized NiCo$_2$O$_4$ nanowire@CoMoO$_4$ nanoplate core/shell arrays on Ni foam. With an optimized preparation condition, the hybrid material showed a high areal capacitance of 14.67 F cm^{-2} at 10 mA cm^{-2}, which was several times larger than the pristine NiCo$_2$O$_4$ electrode (1.42 F cm^{-2}). Despite those recent advances, the synergistic effects for the coupled electrodes of

mixed metal molybdates as well as cycling stability need to be further explored. In particular, the cyclability is important for pseudocapacitive materials, where the capacity decay could be resulted from agglomeration of small nanoparticles of active materials or fractions of the active materials losing electrical contact with the current collector. Functionalized graphene sheets or carbon nanotubes may not only stabilize the nanosized active materials by hybridization but also provide a 3D conducting network for the active materials. The systems based carbon-stabilized mixed metal molybdates for high-performance pseudocapacitors are worth investigating.
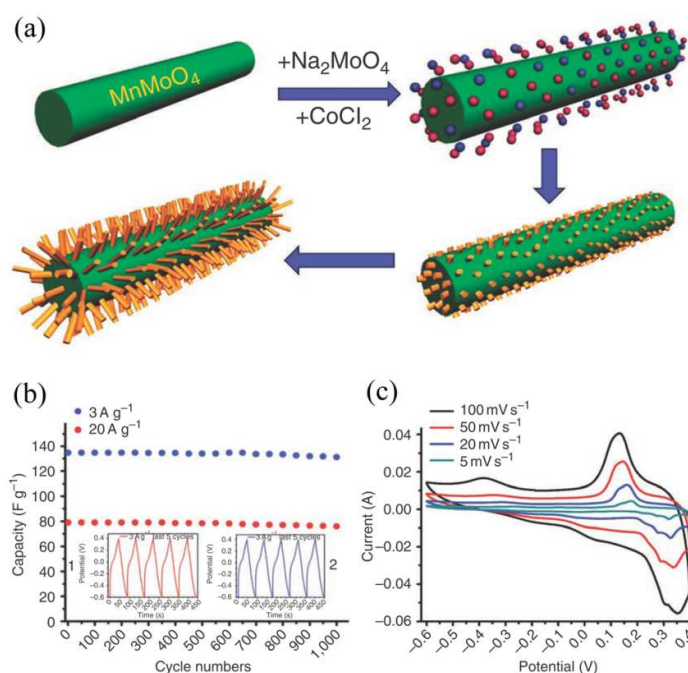
Fig. 18 (a) The construction of hierarchical $MnMoO_4/CoMoO_4$ nanowires, where the green rod represents the backbone $MnMoO_4$ nanowire, and orange rods represents the $CoMoO_4$ nanorods. Red and blue balls are different ions dispersed in the aqueous solution. (b) Charge–discharge cycling test of $MnMoO_4/CoMoO_4$ (3D) electrodes at

the current density of 3 and 20 A g^{-1}, showing 2% loss after 1,000 cycles; inset shows

the galvanostatic charge–discharge cyclic curves of the first and last five cycles at 3 A

g^{-1}. (c) Cyclic voltammogram curves of MnMoO$_4$/CoMoO$_4$ (3D) electrodes.

Reproduced with permission from ref. 394, Copyright (2011) by Nature Publishing

Group.

5.3 Molybdenum dichalconides

MoS$_2$ can potentially store charge by intersheet and intrasheet double-layers over

individual atomic MoS$_2$ layers and faradaic charge transfer processes due to several

oxidation states of Mo.[396-409] Recently, Leite and coworkers[397] have demonstrated a

microwave-assisted route to fabricate a MoS$_2$/rGO hybrid with MoS$_2$ layers

covalently bonded on the surface of the rGO. Electrochemical characterizations

indicated that this electroactive nanocomposite could be cycled reversibly in the range

of 0.25–0.8 V in 1 M HClO$_4$ for the hybrids with low concentrations of MoS$_2$ layers

(LCMoS$_2$/rGO), and in the range of 0.25–0.65 V for medium (MCMoS$_2$/rGO) and

high concentrations (HCMoS$_2$/rGO) of MoS$_2$ layers on graphene. The specific

capacitance at 10 mV s^{-1} were 128, 265, and 148 F g^{-1} for the MoS$_2$/rGO with low,

medium, and high concentrations of MoS$_2$, respectively. Ajayan *et al.*[396] demonstrated

film-based microsupercapacitors via spray painting of MoS$_2$ nanosheets and

subsequent laser patterning. It was found that the optimum MoS$_2$-based

micro-supercapacitor exhibited excellent electrochemical performance for energy

storage with aqueous electrolytes, with a high area capacitance of 8 mF cm^{-2}

(volumetric capacitance of 178 F cm^{-3}) and excellent cyclic performance. Soon and coworkers[406] proposed that MoS$_2$ sheet arrays provided a large surface area for double-layer charge storage. Nevertheless, a low specific capacitance was obtained, probably as a result of the low conductivity of the MoS$_2$ molybdenite phase. Since Ni$_3$S$_2$ is a good metallic conductor leading to ease in transportation for ions and electrons, it can be used for enhanced electrochemical performance of supercapacitors. Lin and coworkers[392] have recently demonstrated a facile one-step solution method to synthesize Ni$_3$S$_2$@MoS$_2$ core/shell nanoarrays directly grown on Ni foam. As expected, the as-formed Ni$_3$S$_2$@MoS$_2$ heterostructured electrode exhibited about 2 times the capacitance (848 F g^{-1}) compared to the pristine Ni$_3$S$_2$ sample (425 F g^{-1}), excellent rate capability (46.6% capacity retention at 20 A g^{-1}) and outstanding cycling stability (91% retention after 2000 cycles). Compared to MoS$_2$, little research has been done on MoSe$_2$ as an electroactive material for pseudocapacitors.

6. Summary and outlook

In this review article, we have attempted to chart the significant progresses in nanostructured Mo-based molybdenum oxides, dichalconides, and oxysalts for rechargeable LIBs/SIBs, Mg batteries, and pseudocapacitors. The rational and creative design of unique nanoarchitectures help address the significant issues encountered during the electrochemical reactions, thus dramatically enhancing the capacity, rate capability, and cycle life of Mo-based electrodes. These developments greatly enrich Mo-based chemistry and represent promising steps towards viable

energy storage devices. Moreover, a deeper and broader understanding of the Li/Na-storage mechanisms and electrochemical reaction pathways has been achieved based on several *in situ* and *ex situ* nanocharacterization techniques. While these progresses over the past decade have been impressive, a comprehensive understanding on the Mo-based chemistry is still urgent. The complex structural and composition evolution of Mo-based compounds with varied valence states often takes place during the electrochemical reactions, especially in the cases of nanosized domains, which makes it difficult to characterize the details of the microstructure and composition. Therefore, many details of the electrochemical mechanisms on Mo-based compounds remain controversial and unclear. It is anticipated that future investigations, especially advanced *in situ* nanotechnologies, would help build a thorough understanding on the reaction mechanisms and would facilitate an optimized design and engineering of nanostructured electrode materials.

Besides further improving the capacity and cyclability of the Mo-based nanostructures, another topic to explore is how to reduce irrepressible capacity, especially in the cases of nanostructured electrodes. Usually, substantial irreversible capacity occurs during the first cycle, namely, not all the charge passed on first inserting Li/Na into the electrode is extracted on subsequent Li/Na deintercalation. It is known that irreversible capacity loss is crucial to real full cells, compromising the energy density and even the effect of nanostructuring. In general, the irreversible capacity loss is mainly caused by two aspects including (i) reduction of the electrolyte on the

electrode surface and (ii) the inability to remove all the Li^+ (or Na^+) charge that is inserted on the first discharge.[17] Notably, in contrast to bulk electrodes, irreversible capacity is a more serious issue for the nanostructured materials, in which high surface area of nanomaterials prompts the surface reactions. For the currently developed nanostructured electrode materials, the initial irreversible capacity loss has not been taken seriously. By virtue of the modern analytic techniques on the atomic or molecular level, the investigation on increasing initial coulombic efficiency of nanostructured electrode materials needs to be emphasized, since it is important for the commercialization of nanostructured materials for rechargeable LIBs/SIBs, Mg batteries, and supercapacitors.

Although it is still significantly challenging on the road to viable energy storage devices based on nanostructured Mo-based materials, the great stride has been achieved during the past decade, especially the past three years. Major advances have been made in materials synthesis, enhancing electrochemical performances, unveiling the intrinsic structure–property relationships, and understanding on the charge-transport mechanism of Mo-based electrode materials for LIBs/SIBs, Mg batteries, and pseudocapacitors. It would be reasonable to believe that a further exploration in this field will lead to more exciting achievements and eventually practicability of those promising Mo-based compounds in advanced energy storage devices.

Undoubtedly, the fundamental understanding on electrode structures, the electrode/electrolyte interface, and charge-storage mechanisms is essential for future Mo-based electrochemical research. Meanwhile, the transport of electrons and ions in active electrode materials and electrolytes should be well investigated by theoretical calculations. The applications of nanotechnology in energy storage are currently in the stage of research and development. For realization of wide industrial applications of nanostructured Mo-based electrode materials in the energy-storage fields, future work is required to achieve large-scale preparation (even in low lost), improve volumetric energy density (i.e., increase the tap density), and maintain high compatibility between electrodes with electrolytes as well as device systems.

References:

1 A. S. Arico, P. Bruce, B. Scrosati, J. M. Tarascon and W. Van Schalkwijk, *Nat. Mater.*, 2005, **4**, 366-377.

2 B. Dunn, H. Kamath and J. M. Tarascon, *Science*, 2011, **334**, 928-935.

3 A. Manthiram, A. V. Murugan, A. Sarkar and T. Muraliganth, *Energy Environ. Sci.*, 2008, **1**, 621-638.

4 M. V. Reddy, G. V. Subba Rao and B. V. Chowdari, *Chem. Rev.*, 2013.

5 Y.-G. Guo, J.-S. Hu and L.-J. Wan, *Adv. Mater.*, 2008, **20**, 2878-2887.

6 Z. Yang, J. Zhang, M. C. Kintner-Meyer, X. Lu, D. Choi, J. P. Lemmon and J. Liu, *Chem. Rev.*, 2011, **111**, 3577-3613.

7 M. Armand and J. M. Tarascon, *Nature*, 2008, **451**, 652-657.

8 P. G. Bruce, S. A. Freunberger, L. J. Hardwick and J. M. Tarascon, *Nat. Mater.*, 2012, **11**, 19-29.

9 G. N. Zhu, Y. G. Wang and Y. Y. Xia, *Energy Environ. Sci.*, 2012, **5**, 6652-6667.

10 B. Scrosati, J. Hassoun and Y. K. Sun, *Energy Environ. Sci.*, 2011, **4**, 3287-3295.

11 C.-X. Zu and H. Li, *Energy Environ. Sci.*, 2011, **4**, 2614.

12 A. Zhamu, G. Chen, C. Liu, D. Neff, Q. Fang, Z. Yu, W. Xiong, Y. Wang, X. Wang and B. Z. Jang, *Energy Environ. Sci.*, 2012.

13 H. Li, Z. Wang, L. Chen and X. Huang, *Adv. Mater.*, 2009, **21**, 4593-4607.

14 M. Winter and R. J. Brodd, *Chem. Rev.*, 2004, **104**, 4245-4269.

15 R. Dominko, D. Arcon, A. Mrzel, A. Zorko, P. Cevc, P. Venturini, M. Gaberscek, M. Remskar and D. Mihailovic, *Adv. Mater.*, 2002, **14**, 1531-1534.

16 C. M. Park, J. H. Kim, H. Kim and H. J. Sohn, *Chem. Soc. Rev.*, 2010, **39**, 3115-3141.

17 S. Brutti, V. Gentili, H. Menard, B. Scrosati and P. G. Bruce, *Adv. Energy Mater.*, 2012, **2**, 322-327.

18 H. L. Pan, Y. S. Hu and L. Q. Chen, *Energy Environ. Sci.*, 2013, **6**, 2338-2360.

19 Y. S. Wang, X. Q. Yu, S. Y. Xu, J. M. Bai, R. J. Xiao, Y. S. Hu, H. Li, X. Q. Yang, L. Q. Chen and X. J. Huang, *Nat. Commun.*, 2013, **4**.2365.

20 J. F. Qian, X. Y. Wu, Y. L. Cao, X. P. Ai and H. X. Yang, *Angew. Chem. Int. Ed.*, 2013, **52**, 4633-4636.

21 M. D. Slater, D. Kim, E. Lee and C. S. Johnson, *Adv.. Funct.. Mater.*, 2013, **23**, 947-958.

22 V. Palomares, P. Serras, I. Villaluenga, K. B. Hueso, J. Carretero-Gonzalez and T. Rojo, *Energy Environ. Sci.*, 2012, **5**, 5884-5901.

23 S. W. Kim, D. H. Seo, X. H. Ma, G. Ceder and K. Kang, *Adv.. Energy Mater.*, 2012, **2**, 710-721.

24 D. Aurbach, Z. Lu, A. Schechter, Y. Gofer, H. Gizbar, R. Turgeman, Y. Cohen, M. Moshkovich and E. Levi, *Nature*, 2000, **407**, 724-727.

25 D. Aurbach,G. S. Suresh, E. Levi, A. Mitelman, O. Mizrahi, O. Chusidand M. Brunelli, *Adv. Mater.*, 2007, **19**, 4260–4267.

26 J. Chen and F. Y. Cheng, *Acc. Chem. Res.*, 2009, **42**, 713-723.

27 B. Peng and J. Chen, *Coordin. Chem. Rev.*, 2009, **253**, 2805-2813.

28 H. D. Yoo, I. Shterenberg, Y. Gofer, G. Gershinsky, N. Pour and D. Aurbach, *Energy Environ. Sci.*, 2013, **6,** 2265-2279.

29 E. Levi, Y. Gofer and D. Aurbach, *Chem. Mater.*, 2010, **22**, 860-868.

30 D. Aurbach, I. Weissman, Y. Gofer and E. Levi, *Chem. Record*, 2003, **3**, 61-73..

31 J. Muldoon, C. B. Bucur and T. Gregory, *Chem. Rev.*, 2014, **114**, 11683-11720.

32 P. Saha, M. K. Datta, O. I. Velikokhatnyi, A. Manivannan, D. Alman and P. N. Kumta, *Prog. Mater. Sci.*, 2014, **66**, 1-86.

33 P. Simon, Y. Gogotsi and B. Dunn, *Science*, 2014, **343**, 1210-1211.

34 P. Simon and Y. Gogotsi, *Nat. Mater.*, 2008, **7**, 845-854.

35 G. Wang, L. Zhang and J. Zhang, *Chem. Soc. Rev.*, 2012, **41**, 797-828.

36 Y. W. Zhu, S. Murali, M. D. Stoller, K. J. Ganesh, W. W. Cai, P. J. Ferreira, A. Pirkle, R. M. Wallace, K. A. Cychosz, M. Thommes, D. Su, E. A. Stach and R. S. Ruoff, *Science*, 2011, **332**, 1537-1541.

37 X. Y. Lang, A. Hirata, T. Fujita and M. W. Chen, *Nat. Nanotechnol.*, 2011, **6**, 232-236.

38 A. E. Fischer, K. A. Pettigrew, D. R. Rolison, R. M. Stroud and J. W. Long, *Nano*

Lett., 2007, **7**, 281-286.

39 H. L. Wang, Z. W. Xu, Z. Li, K. Cui, J. Ding, A. Kohandehghan, X. H. Tan, B. Zahiri, B. C. Olsen, C. M. B. Holt and D. Mitlin, *Nano Lett.*, 2014, **14**, 1987-1994.

40 H. Kim, K. Y. Park, M. Y. Cho, M. H. Kim, J. Hong, S. K. Jung, K. C. Roh and K. Kang, *Chemelectrochem*, 2014, **1**, 125-130.

41 K. Karthikeyan, S. Amaresh, S. N. Lee, V. Aravindan and Y. S. Lee, *Chem. Asian J.*, 2014, **9**, 852-857.

42 Y. Cai, B. T. Zhao, J. Wang and Z. P. Shao, *J. Power Sources*, 2014, **253**, 80-89.

43 X. B. Chen, C. Li, M. Gratzel, R. Kostecki and S. S. Mao, *Chem. Soc. Rev.*, 2012, **41**, 7909-7937.

44 M. R. Gao, Y. F. Xu, J. Jiang and S. H. Yu, *Chem. Soc. Rev.*, 2013, **42**, 2986-3017.

45 H. L. Wang and H. J. Dai, *Chem. Soc. Rev.*, 2013, **42**, 3088-3113.

46 Y. Yang, G. Y. Zheng and Y. Cui, *Chem. Soc. Rev.*, 2013, **42**, 3018-3032.

47 J. T. Zhang and C. M. Li, *Chem. Soc. Rev.*, 2012, **41**, 7016-7031.

48 Q. F. Zhang, E. Uchaker, S. L. Candelaria and G. Z. Cao, *Chem. Soc. Rev.*, 2013, **42**, 3127-3171.

49 J. Chmiola, C. Largeot, P. L. Taberna, P. Simon and Y. Gogotsi, *Science*, 2010, **328**, 480-483.

50 D. Pech, M. Brunet, H. Durou, P. H. Huang, V. Mochalin, Y. Gogotsi, P. L. Taberna and P. Simon, *Nat. Nanotechnol.*, 2010, **5**, 651-654.

51 K. T. Nam, D. W. Kim, P. J. Yoo, C. Y. Chiang, N. Meethong, P. T. Hammond, Y. M. Chiang and A. M. Belcher, *Science*, 2006, **312**, 885-888.

52 H. Wu, G. Chan, J. W. Choi, I. Ryu, Y. Yao, M. T. McDowell, S. W. Lee, A. Jackson, Y. Yang, L. B. Hu and Y. Cui, *Nat. Nanotechnol.*, 2012, **7**, 309-314.

53 C. K. Chan, H. L. Peng, G. Liu, K. McIlwrath, X. F. Zhang, R. A. Huggins and Y. Cui, *Nat. Nanotechnol.*, 2008, **3**, 31-35.

54 D. R. Rolison, J. W. Long, J. C. Lytle, A. E. Fischer, C. P. Rhodes, T. M. McEvoy, M. E. Bourg and A. M. Lubers, *Chem. Soc. Rev.*, 2009, **38**, 226.

55 F.-F. Cao, Y.-G. Guo and L.-J. Wan, *Energy Environ. Sci.*, 2011, **4**, 1634.

56 M. G. Kim and J. Cho, *Adv. Funct. Mater.*, 2009, **19**, 1497-1514.

57 H.-K. Song, K. T. Lee, M. G. Kim, L. F. Nazar and J. Cho, *Adv. Funct. Mater.*, 2010, **20**, 3818-3834.

58 Y. Wang and G. Cao, *Adv. Mater.*, 2008, **20**, 2251-2269.

59 P. G. Bruce, B. Scrosati and J.-M. Tarascon, *Angew. Chem. Int. Ed.*, 2008, **47**, 2930-2946.

60 L. Ji, Z. Lin, M. Alcoutlabi and X. Zhang, *Energy Environ. Sci.*, 2011, **4**, 2682.

61 S. W. Lee, B. M. Gallant, H. R. Byon, P. T. Hammond and Y. Shao-Horn, *Energy Environ. Sci.*, 2011, **4**, 1972.

62 T. Djenizian, I. Hanzu and P. Knauth, *J. Mater. Chem.*, 2011, **21**, 9925.

63 Y. Huang, J. Liang and Y. Chen, *Small*, 2012.

64 A. G. Dylla, G. Henkelman and K. J. Stevenson, *Acc. Chem. Res.*, 2013, **46**, 1104-1112.

65 K. Zhang, X. Han, Z. Hu, X. Zhang, Z. Tao and J. Chen, *Chem. Soc. Rev.*, 2014.

66 P. Poizot, S. Laruelle, S. Grugeon, L. Dupont and J. M. Tarascon, *Nature*, 2000, **407**, 496-499.

67 J. Cabana, L. Monconduit, D. Larcher and M. R. Palacín, *Adv. Mater.*, 2010, **22**, E170-E192.

68 Y. Qiao, X. L. Hu, Y. Liu, C. J. Chen, H. H. Xu, D. F. Hou, P. Hu and Y. H. Huang, *J. Mater. Chem. A*, 2013, **1**, 10375-10381.

69 C. J. Chen, X. L. Hu, P. Hu, Y. Qiao, L. Qie and Y. H. Huang, *Eur. J. Inorg. Chem.*, 2013, **2013**, 5320-5328.

70 Y. Qiao, X. L. Hu and Y. H. Huang, *J. Nanopart. Res.*, 2012, **14**.

71 Y. Qiao, X. L. Hu, Y. Liu, G. Liang, M. C. Croft and Y. H. Huang, *J. Mater. Chem. A*, 2013, **1**, 15128-15134.

72 C. J. Chen, X. L. Hu, Y. Jiang, Z. Yang, P. Hu and Y. H. Huang, *Chem. Eur. J.*, 2014, **20**, 1383-1388.

73 C. J. Chen, X. L. Hu, Z. H. Wang, X. Q. Xiong, P. Hu, Y. Liu and Y. H. Huang, *Carbon*, 2014, **69**, 302-310.

74 M. Wagemaker, A. P. M. Kentgens and F. M. Mulder, *Nature*, 2002, **418**,

397-399.

75   A. R. Armstrong, G. Armstrong, J. Canales, R. Garcia and P. G. Bruce, *Adv. Mater.*, 2005, **17**, 862-865.

76   C. K. Chan, H. L. Peng, R. D. Twesten, K. Jarausch, X. F. Zhang and Y. Cui, *Nano Lett.*, 2007, **7**, 490-495.

77   E. Morales and J. L. Acosta, *Solid State Ionics*, 1997, **95**, 269-274.

78   J. J. Auborn and Y. L. Barberio, *J. Electrochem. Soc.*, 1987, **134**, 638-641.

79   J. R. Dahn and W. R. McKinnon, *Solid State Ionics*, 1987, **23**, 1-7.

80   Y. M. Sun, X. L. Hu, W. Luo and Y. H. Huang, *J. Mater. Chem.*, 2012, **22**, 13826-13831.

81   Y. M. Sun, X. L. Hu, W. Luo and Y. H. Huang, *J. Phys. Chem. C*, 2012, **116**, 20794-20799.

82   Y. M. Sun, X. L. Hu, W. Luo and Y. H. Huang, *J. Mater. Chem.*, 2012, **22**, 19190-19195.

83   W. Luo, X. L. Hu, Y. M. Sun and Y. H. Huang, *ACS Appl. Mater. Interfaces*, 2013, **5**, 1997-2003.

84   Y. M. Sun, X. L. Hu, W. Luo, F. F. Xia and Y. H. Huang, *Adv. Funct. Mater.*, 2013, **23**, 2436-2444.

85   B. Liu, X. L. Hu, H. H. Xu, W. Luo, Y. M. Sun and Y. H. Huang, *Sci. Rep.*, 2014, **4**. 4229.

86   J. Chen, L. N. Xu, W. Y. Li and X. L. Gou, *Adv. Mater.*, 2005, **17**, 582-586.

87   J. H. Ku, J. H. Ryu, S. H. Kim, O. H. Han and S. M. Oh, *Adv. Funct. Mater.*, 2012, **22**, 3658-3664.

88   K. M. Mackay and R. A. Mackay, *Introduction to Modern Inorganic Chemistry*, 4th edn., Blackie ; Prentice Hall, London, Englewood Cliffs, N.J., 1989.

89   D. B. Rogers, R. D. Shannon, A. W. Sleight and J. L. Gillson, *Inorg. Chem.*, 1969, **8**, 841-849.

90   L. Z. Zhuang, Q. H. Li, S. X. Chen, X. N. Hou and J. T. Lin, *J. Mater. Sci.*, 2014, **49**, 5606-5616.

91   W. J. Zhou, D. M. Hou, Y. H. Sang, S. H. Yao, J. Zhou, G. Q. Li, L. G. Li, H. Liu

and S. W. Chen, *J. Mater. Chem. A*, 2014, **2**, 11358-11364.

92   Y. Oh, H. Vrubel, S. Guidoux and X. L. Hu, *Chem. Commun.*, 2014, **50**, 3878-3881.

93   J. Liu, Z. Zhang, C. Pan, Y. Zhao, X. Su, Y. Zhou and D. Yu, *Mater. Lett.*, 2004, **58**, 3812-3815.

94   B. W. Kwon, C. Ellefson, J. Breit, J. Kim, M. G. Norton and S. Ha, *J. Power Sources*, 2013, **243**, 203-210.

95   B. Hu, L. Mai, W. Chen and F. Yang, *ACS Nano*, 2009, **3**, 478-482.

96   D. W. Murphy, F. J. Di Salvo, J. N. Carides and J. V. Waszczak, *Mater. Res. Bull.*, 1978, **13**, 1395-1402.

97   J. H. Ku, Y. S. Jung, K. T. Lee, C. H. Kim and S. M. Oh, *J. Electrochem. Soc.*, 2009, **156**, A688-A693.

98   A. Manthiram, J. Kim and C. Tsang, in *Materials for Electrochemical Energy Storage and Conversion Ii-Batteries, Capacitors and Fuel Cells*, eds. D. S. Ginley, D. H. Doughty, B. Scrosati, T. Takamura and Z. M. J. Zhang, 1998, vol. 496, pp. 421-426.

99   H. J. Zhang, J. Shu, K. X. Wang, X. T. Chen, Y. M. Jiang, X. Wei and J. S. Chen, *J. Mater. Chem. A*, 2014, **2**, 80-86.

100 B. K. Guo, X. P. Fang, B. Li, Y. F. Shi, C. Y. Ouyang, Y. S. Hu, Z. X. Wang, G. D. Stucky and L. Q. Chen, *Chem. Mater.*, 2012, **24**, 457-463.

101 X. Ji, Y. Liu, X. Yu, K. Yang, J. Wu, L. Miao and J. Jiang, *Acta Chim Sinica*, 2013, **71**, 405.

102 Y. L. Liu, H. Zhang, P. Ouyang and Z. C. Li, *Electrochim. Acta*, 2013, **102**, 429-435.

103 J. Park, I. Choi, M. J. Lee, M. H. Kim, T. Lim, K. H. Park, J. Jang, S. M. Oh, S. K. Cho and J. J. Kim, *Electrochim. Acta*, 2014, **132**, 338-346.

104 D. Koziej, M. D. Rossell, B. Ludi, A. Hintennach, P. Novak, J. D. Grunwaldt and M. Niederberger, *Small*, 2011, **7**, 377-387.

105 Y. Liang, S. Yang, Z. Yi, J. Sun and Y. Zhou, *Mater. Chem. Phys.*, 2005, **93**, 395-398.

106 Y. G. Liang, Z. H. Yi, S. J. Yang, L. Q. Zhou, J. T. Sun and Y. H. Zhou, *Solid State Ionics*, 2006, **177**, 501-505.

107 Y. G. Liang, S. J. Yang, Z. H. Yi, X. F. Lei, J. T. Sun and Y. H. Zhou, *Mater. Sci. Eng. B*, 2005, **121**, 152-155.

108 L. C. Yang, Q. S. Gao, Y. Tang, Y. P. Wu and R. Holze, *J. Power Sources*, 2008, **179**, 357-360.

109 S. Yoon, K. N. Jung, C. S. Jin and K. H. Shin, *J. Alloy Compd.*, 2012, **536**, 179-183.

110 H. X. Zhang, L. X. Zeng, X. M. Wu, L. F. Lian and M. D. Wei, *J. Alloy Compd.*, 2013, **580**, 358-362.

111 H. J. Zhang, K. X. Wang, X. Y. Wu, Y. M. Jiang, Y. B. Zhai, C. Wang, X. Wei and J. S. Chen, *Adv. Funct. Mater.*, 2014, **24**, 3399-3404.

112 X. F. Zhang, X. X. Song, S. Gao, Y. M. Xu, X. L. Cheng, H. Zhao and L. H. Huo, *J. Mater. Chem. A*, 2013, **1**, 6858-6864.

113 Y. Z. Lei, J. C. Hu, H. W. Liu and J. L. Li, *Mater. Lett.*, 2012, **68**, 82-85.

114 X. Y. Zhao, M. H. Cao, B. Liu, Y. Tian and C. W. Hu, *J. Mater. Chem.*, 2012, **22**, 13334-13340.

115 X. P. Fang, B. K. Guo, Y. F. Shi, B. Li, C. X. Hua, C. H. Yao, Y. C. Zhang, Y. S. Hu, Z. X. Wang, G. D. Stucky and L. Q. Chen, *Nanoscale*, 2012, **4**, 1541-1544.

116 Y. F. Shi, B. K. Guo, S. A. Corr, Q. H. Shi, Y. S. Hu, K. R. Heier, L. Q. Chen, R. Seshadri and G. D. Stucky, *Nano Lett.*, 2009, **9**, 4215-4220.

117 Y. M. Sun, X. L. Hu, J. C. Yu, Q. Li, W. Luo, L. X. Yuan, W. X. Zhang and Y. H. Huang, *Energy Environ. Sci.*, 2011, **4**, 2870-2877.

118 L. C. Yang, Q. S. Gao, Y. H. Zhang, Y. Tang and Y. P. Wu, *Electrochem. Commun.*, 2008, **10**, 118-122.

119 N. H. Zhao, L. J. Fu, L. C. Yang, T. Zhang, G. J. Wang, Y. P. Wu and T. van Ree, *Pure Appl. Chem.*, 2008, **80**, 2283-2295.

120 Y. L. Liu, H. Zhang, P. Ouyang, W. H. Chen, Y. Wang and Z. C. Li, *J. Mater. Chem. A*, 2014, **2**, 4714-4721.

121 F. F. Ferreira, T. G. S. Cruz, M. C. A. Fantini, M. H. Tabacniks, S. C. de Castro, J.

Morais, A. de Siervo, R. Landers and A. Gorenstein, *Solid State Ionics*, 2000, **136**, 357-363.

122 H. S. Zhou, S. M. Zhu, M. Hibino, I. Honma and M. Ichihara, *Adv. Mater.*, 2003, **15**, 2107-2111.

123 F. Jiao, J. L. Bao, A. H. Hill and P. G. Bruce, *Angew. Chem. Int. Ed.*, 2008, **47**, 9711-9716.

124 J. Y. Luo, Y. G. Wang, H. M. Xiong and Y. Y. Xia, *Chem. Mater.*, 2007, **19**, 4791-4795.

125 Y. Ren, L. J. Hardwick and P. G. Bruce, *Angew. Chem. Int. Ed*, 2010, **49**, 2570-2574.

126 H. S. Zhou, D. L. Li, M. Hibino and I. Honma, *Angew. Chem. Int. Ed*, 2005, **44**, 797-802.

127 Y. Zhou, I. Lee, C. W. Lee, H. S. Park, H. Son and S. Yoon, *Bull. Korean Chem. Soc.*, 2014, **35**, 257-260.

128 A. L. Chen, C. X. Li, R. Tang, L. W. Yin and Y. X. Qi, *Phys. Chem. Chem. Phys.*,2013, **15**, 13601-13610.

129 J. Liu, S. S. Tang, Y. K. Lu, G. M. Cai, S. Q. Liang, W. J. Wang and X. L. Chen, *Energ Environ Sci*, 2013, **6**, 2691-2697.

130 Y. M. Sun, X. L. Hu, W. Luo, H. H. Xu, C. C. Hu and Y. H. Huang, *ACS Appl. Mater. Interfaces*, 2013, **5**, 10145-10150.

131 F. Zou, X. L. Hu, L. Qie, Y. Jiang, X. Q. Xiong, Y. Qiao and Y. H. Huang, *Nanoscale*, 2014, **6**, 924-930.

132 F. Zou, X. L. Hu, Y. M. Sun, W. Luo, F. F. Xia, L. Qie, Y. Jiang and Y. H. Huang, *Chem. Eur. J.*, 2013, **19**, 6027-6033.

133 V. Georgakilas, M. Otyepka, A. B. Bourlinos, V. Chandra, N. Kim, K. C. Kemp, P. Hobza, R. Zboril and K. S. Kim, *Chem. Rev.*, 2012, **112**, 6156-6214.

134 S. Han, D. Wu, S. Li, F. Zhang and X. Feng, *Small*, 2013, **9**, 1173-1187.

135 X. Huang, Z. Yin, S. Wu, X. Qi, Q. He, Q. Zhang, Q. Yan, F. Boey and H. Zhang, *Small*, 2011, **7**, 1876-1902.

136 Y. M. Sun, X. L. Hu, W. Luo and Y. H. Huang, *ACS Nano*, 2011, **5**, 7100-7107.

137 Y. Zhong, Y. Zhang, G. X. Zhang, R. Y. Li and X. L. Sun, *Appl. Surf. Sci.*, 2012, **263**, 410-415.

138 A. Bhaskar, M. Deepa, T. N. Rao and U. V. Varadaraju, *J Power Sources*, 2012, **216**, 169-178.

139 F. F. Xia, X. L. Hu, Y. M. Sun, W. Luo and Y. H. Huang, *Nanoscale*, 2012, **4**, 4707-4711.

140 J. Besnardiere, X. Petrissans, C. Surcin, V. Buissette, T. Le Mercier, M. Morcrette, D. Portehault and S. Cassaignon, *RSC Adv.*, 2014, **4**, 21208-21215.

141 Y. J. Chen, X. P. Di, C. Ma, C. L. Zhu, P. Gao, J. Q. Li, C. W. Sun and Q. Y. Ouyang, *RSC Adv.*, 2013, **3**, 17659-17663.

142 Z. X. Huang, Y. Wang, Y. G. Zhu, Y. M. Shi, J. I. Wong and H. Y. Yang, *Nanoscale*, 2014, **6**, 9839-9845.

143 B. Liu, X. Zhao, Y. Tian, D. Zhao, C. Hu and M. Cao, *Phys. Chem. Chem. Phys.*, 2013, **15**, 8831-8837.

144 Y. L. Liu, H. Zhang, P. Ouyang, W. H. Chen and Z. C. Li, *Mater. Res. Bull.*, 2014, **50**, 95-102.

145 L. X. Zeng, C. Zheng, C. L. Deng, X. K. Ding and M. D. Wei, *ACS Appl. Mater. Interfaces*, 2013, **5**, 2182-2187.

146 H. J. Zhang, T. H. Wu, K. X. Wang, X. Y. Wu, X. T. Chen, Y. M. Jiang, X. Wei and J. S. Chen, *J. Mater. Chem. A*, 2013, **1**, 12038-12043.

147 A. Bhaskar, M. Deepa and T. N. Rao, *ACS Appl. Mater. Interfaces*, 2013, **5**, 2555-2566.

148 Z. Y. Wang, J. S. Chen, T. Zhu, S. Madhavi and X. W. Lou, *Chem. Commun.*, 2010, **46**, 6906-6908.

149 Y. Xu, R. Yi, B. Yuan, X. F. Wu, M. Dunwell, Q. L. Lin, L. Fei, S. G. Deng, P. Andersen, D. H. Wang and H. M. Luo, *J. Phys. Chem. Lett.*, 2012, **3**, 309-314.

150 L. Zhou, H. B. Wu, Z. Wang and X. W. Lou, *ACS Appl. Mater. Interfaces*, 2011, **3**, 4853-4857.

151 W. Cho, J. H. Song, J. H. Kim, G. Jeong, E. Y. Lee and Y. J. Kim, *J. Appl. Electrochem.*, 2012, **42**, 909-915.

152 H. Gao, C. L. Liu, Y. Liu, Z. H. Liu and W. S. Dong, *Mater. Chem. Phys.*, 2014, **147**, 218-224.

153 Q. S. Gao, L. C. Yang, X. C. Lu, J. J. Mao, Y. H. Zhang, Y. P. Wu and Y. Tang, *J. Mater. Chem.*, 2010, **20**, 2807-2812.

154 X. L. Ji, S. Herle, Y. H. Rho and L. F. Nazar, *Chem. Mater.*, 2007, **19**, 374-383.

155 K. H. Seng, G. D. Du, L. Li, Z. X. Chen, H. K. Liu and Z. P. Guo, *J. Mater. Chem.*, 2012, **22**, 16072-16077.

156 Q. W. Tang, Z. Q. Shan, L. Wang and X. Qin, *Electrochim. Acta*, 2012, **79**, 148-153.

157 L. C. Yang, L. L. Liu, Y. S. Zhu, X. J. Wang and Y. P. Wu, *J. Mater. Chem.*, 2012, **22**, 13148-13152.

158 W. Luo, X. L. Hu, Y. M. Sun and Y. H. Huang, *J. Mater. Chem.*, 2012, **22**, 4910-4915.

159 J. C. He, H. B. Wang, C. L. Gu and S. X. Liu, *J. Alloy Compd.*, 2014, **604**, 239-244.

160 W. Luo, X. L. Hu, Y. M. Sun and Y. H. Huang, *Phys. Chem. Chem. Phys.*, 2011, **13**, 16735-16740.

161 Z. W. Xu, H. L. Wang, Z. Li, A. Kohandehghan, J. Ding, J. Chen, K. Cui and D. Mitlin, *J. Phys. Chem. C*, 2014, **118**, 18387-18396.

162 S. Yoon and A. Manthiram, *J. Mater. Chem.*, 2011, **21**, 4082-4085.

163 L. Campanella and G. Pistoia, *J. Electrochem. Soc.*, 1971, **118**, 1905-1908.

164 W. Li, F. Cheng, Z. Tao and J. Chen, *J. Phys. Chem. B*, 2006, **110**, 119-124.

165 A. M. Hashem, H. Groult, A. Mauger, K. Zaghib, J. Trottier and C. M. Julien, *ECS Transactions*, 2013, **50**, 131-136.

166 A. M. Hashem, H. Groult, A. Mauger, K. Zaghib and C. M. Julien, *J. Power Sources*, 2012, **219**, 126-132.

167 M. Baldoni, L. Craco, G. Seifert and S. Leoni, *J. Mater. Chemis. A*, 2013, **1**, 1778-1784.

168 J. Swiatowska-Mrowiecka, S. de Diesbach, V. Maurice, S. Zanna, L. Klein, E. Briand, I. Vickridge and P. Marcus, *J. Phys. Chem. C*, 2008, **112**, 11050-11058.

169 L. Campanella and G. Pistoia, *J. Electrochem. Soc.*, 1973, **120**, 383-384.

170 J. O. Besenhard and R. Schöllhorn, *J. Power Sources*, 1976, **1**, 267-276.

171 F. Bonino, L. P. Bicelli, B. Rivolta, M. Lazzari and F. Festorazzi, *Solid State Ionics*, 1985, **17**, 21-28.

172 F. W. Dampier, *J. Electrochem. Soc.*, 1974, **121**, 656-660.

173 S. Komaba, N. Kumagai, R. Kumagai, N. Kumagai and H. Yashiro, *Solid State Ionics*, 2002, **152–153**, 319-326.

174 N. Margalit, *J. Electrochem. Soc.*, 1974, **121**, 1460-1461.

175 M. S. Whittingham, *J. Electrochem. Soc.*, 1976, **123**, 315-320.

176 M. E. Spahr, P. Novák, O. Haas and R. Nesper, *J. Power Sources*, 1995, **54**, 346-351.

177 R. Schöllhorn, *Angew. Chem. Int. Ed.*, 1980, **19**, 983-1003.

178 T. Tsumura and M. Inagaki, *Solid State Ionics*, 1997, **104**, 183-189.

179 J. W. Bullard Iii and R. L. Smith, *Solid State Ionics*, 2003, **160**, 335-349.

180 J. O. Besenhard, J. Heydecke, E. Wudy, H. P. Fritz and W. Foag, *Solid State Ionics*, 1983, **8**, 61-71.

181 A. M. Hashem, M. H. Askar, M. Winter, J. H. Albering and J. O. Besenhard, *Ionics*, 2007, **13**, 3-8.

182 L. Q. Mai, B. Hu, W. Chen, Y. Y. Qi, C. S. Lao, R. S. Yang, Y. Dai and Z. L. Wang, *Adv. Mater.*, 2007, **19**, 3712-3716.

183 T. Tao, A. M. Glushenkov, C. Zhang, H. Zhang, D. Zhou, Z. Guo, H. K. Liu, Q. Chen, H. Hu and Y. Chen, *J. Mater. Chem.*, 2011, **21**, 9350-9355.

184 S. H. Choi and Y. C. Kang, *ChemSusChem*, 2014, **7**, 523-528.

185 A. C. Dillon, L. A. Riley, Y. S. Jung, C. Ban, D. Molina, A. H. Mahan, A. S. Cavanagh, S. M. George and S. H. Lee, *Thin Solid Films*, 2011, **519**, 4495-4497.

186 C. Feng, H. Gao, C. Zhang, Z. Guo and H. Liu, *Electrochim. Acta*, 2013, **93**, 101-106.

187 M. F. Hassan, Z. P. Guo, Z. Chen and H. K. Liu, *J. Power Sources*, 2010, **195**, 2372-2376.

188 S.-H. Lee, Y.-H. Kim, R. Deshpande, P. A. Parilla, E. Whitney, D. T. Gillaspie, K. M. Jones, A. H. Mahan, S. Zhang and A. C. Dillon, *Adv. Mater.*, 2008, **20**, 3627-3632.

189 J. F. Ni, G. B. Wang, J. Yang, D. L. Gao, J. T. Chen, L. J. Gao and Y. Li, *J. Power Sources*, 2014, **247**, 90-94.

190 L. A. Riley, A. S. Cavanagh, S. M. George, Y. S. Jung, Y. Yan, S.-H. Lee and A. C. Dillon, *ChemPhysChem*, 2010, **11**, 2124-2130.

191 L. A. Riley, A. S. Cavanagh, S. M. George, S.-H. Lee and A. C. Dillon, *Electrochem. Solid-State Lett.*, 2011, **14**, A29-A31.

192 L. A. Riley, S.-H. Lee, L. Gedvilias and A. C. Dillon, *J. Power Sources*, 2010, **195**, 588-592.

193 K. Sakaushi, J. Thomas, S. Kaskel and J. Eckert, *Chem. Mater.*, 2013, **25**, 2557-2563.

194 Y. Sun, J. Wang, B. Zhao, R. Cai, R. Ran and Z. Shao, *J. Mater. Chem. A*, 2013, **1**, 4736-4746.

195 Z. Wang, T. Chen, W. X. Chen, K. Chang, L. Ma, G. C. Huang, D. Y. Chen and J. Y. Lee, *J. Mater. Chem. A*, 2013, **1**, 2202-2210.

196 Z. Y. Wang, S. Madhavi and X. W. Lou, *J. Phys. Chem. C*, 2012, **116**, 12508-12513.

197 X. Y. Xue, Z. H. Chen, L. L. Xing, S. Yuan and Y. J. Chen, *Chem. Commun.*, 2011, **47**, 5205-5207.

198 L. C. Yang, W. L. Guo, Y. Shi and Y. P. Wu, *J. Alloy Compd.*, 2010, **501**, 218-220.

199 X. Zhao, M. Cao and C. Hu, *Mater. Res. Bull.*, 2013, **48**, 2289-2295.

200 P. A. Christian, J. N. Carides, F. J. DiSalvo and J. V. Waszczak, *J. Electrochem. Soc.*, 1980, **127**, 2315-2319.

201 J. P. Jegal, H. K. Kim, J. S. Kim and K. B. Kim, *J. Electroceramics*, 2013, **31**, 218-223.

202 Y. S. Jung, S. Lee, D. Ahn, A. C. Dillon and S.-H. Lee, *J. Power Sources*, 2009, **188**, 286-291.

203 P. Meduri, E. Clark, J. H. Kim, E. Dayalan, G. U. Sumanasekera and M. K.

Sunkara, *Nano Lett.*, 2012, **12**, 1784-1788.

204 H. Ohtsuka and Y. Sakurai, *Solid State Ionics*, 2001, **144**, 59-64.

205 R. H. Sanchez, L. Trevino, A. F. Fuentes, A. Martinez-de la Cruz and L. M. Torres-Martinez, *J. Solid State Electrochem.*, 2000, **4**, 210-215.

206 M. A. S. Ana, N. Mirabal, E. Benavente, P. Gomez-Romero and G. Gonzalez, *Electrochim. Acta*, 2007, **53**, 1432-1438.

207 M. Pasquali, G. Pistoia and F. Rodante, *Solid State Ionics*, 1982, **6**, 319-325.

208 M. Vasilopoulou, A. M. Douvas, D. G. Georgiadou, L. C. Palilis, S. Kennou, L. Sygellou, A. Soultati, I. Kostis, G. Papadimitropoulos, D. Davazoglou and P. Argitis, *J. Am. Chem. Soc.*, 2012, **134**, 16178-16187.

209 N. A. Chernova, M. Roppolo, A. C. Dillon and M. S. Whittingham, *J. Mater.Chem.*, 2009, **19**, 2526-2552.

210 G. Guzman, B. Yebka, J. Livage and C. Julien, *Solid State Ionics*, 1996, **86–88,** 407-413.

211 G. A. Nazri and C. Julien, *Ionics*, 1996, **2**, 1-6.

212 B. Yebka and C. Julien, *Ionics*, 1996, **2**, 196-200.

213 B. Yebka, C. Julien and G. A. Nazri, *Ionics*, 1999, **5**, 236-243.

214 N. Kumagai, N. Kumagai and K. Tanno, *Electrochim. Acta*, 1987, **32**, 1521-1526.

215 A. Martínez-de la Cruz and I. Juárez Ramírez, *J. Power Sources*, 2004, **133**, 268-271.

216 T. Buhrmester, N. N. Leyzerovich, K. G. Bramnik, H. Ehrenberg and H. Fuess, *Mater. Res. Soc. Symp. P*, 2003, **756**, 261-266.

217 C. T. Cherian, M. V. Reddy, S. C. Haur and B. V. R. Chowdari, *ACS Appl. Mater. Interfaces*, 2013, **5**, 918-923.

218 Y. Ding, Y. Wan, Y.-L. Min, W. Zhang and S.-H. Yu, *Inorg. Chem.*, 2008, **47**, 7813-7823.

219 S. S. Kim, S. Ogura, H. Ikuta, Y. Uchimoto and M. Wakihara, *Chem. Lett.*, 2001, **30**, 760-761.

220 S.-S. Kim, S. Ogura, H. Ikuta, Y. Uchimoto and M. Wakihara, *Solid State Ionics*, 2002, **146**, 249-256.

221 N. N. Leyzerovich, K. G. Bramnik, T. Buhrmester, H. Ehrenberg and H. Fuess, *J Power Sources*, 2004, **127**, 76-84.

222 Y. Liang, X. Han, Z. Yi, W. Tang, L. Zhou, J. Sun, S. Yang and Y. Zhou, *J. Solid State Electrchem.*, 2007, **11**, 1127-1131.

223 R. H. Sanchez, A. F. Fuentes, A. Martinez-De La Cruz and L. M. Torres-Martinez, *Bol. Soc. Esp. Ceram. V*, 1999, **38**, 421-425.

224 N. Sharma, G. V. S. Rao and B. V. R. Chowdari, *Electrochim. Acta*, 2005, **50**, 5305-5312.

225 N. Sharma, K. M. Shaju, G. V. Subba Rao, B. V. R. Chowdari, Z. L. Dong and T. J. White, *Chem. Mater.*, 2004, **16**, 504-512.

226 A. Yu, N. Kumagai, Z. Liu and J. Y. Lee, *Solid State Ionics*, 1998, **106**, 11-18.

227 G. Armstrong, A. R. Armstrong, P. G. Bruce, P. Reale and B. Scrosati, *Adv. Mater.*, 2006, **18**, 2597-2600.

228 W. Xiao, J. S. Chen, C. M. Li, R. Xu and X. W. Lou, *Chem. Mater.*, 2009, **22**, 746-754.

229 K. S. Park, S. D. Seo, H. W. Shim and D. W. Kim, *Nanoscale Res. Lett.*, 2012, **7**, 35.

230 B. Das, M. V. Reddy, C. Krishnamoorthi, S. Tripathy, R. Mahendiran, G. V. S. Rao and B. V. R. Chowdari, *Electrochim. Acta*, 2009, **54**, 3360-3373.

231 B. Das, M. V. Reddy, G. V. Subba Rao and B. V. R. Chowdari, *J. Solid State Electrchem.*, 2008, **12**, 953-959.

232 Y. M. Sun, X. L. Hu, W. Luo and Y. H. Huang, *J. Mater. Chem.*, 2011, **21**, 17229-17235.

233 Y. M. Sun, X.L. Hu, W. Luo, J. Shu and Y. H. Huang, *J. Mater. Chem. A*, 2013, **1**, 4468-4474.

234 R. L. Smith and G. S. Rohrer, *J. Catal.*, 1999, **184**, 49-58.

235 F. Leroux, G. R. Goward, W. P. Power and L. F. Nazar, *Electrochem. Solid-State Lett.*, 1998, **1**, 255-258.

236 F. Leroux and L. F. Nazar, *Solid State Ionics*, 2000, **133**, 37-50.

237 R. C. Haushalter, K. G. Strohmaier and F. W. Lai, *Science*, 1989, **246**, 1289-1291.

238 R. C. Haushalter and L. A. Mundi, *Chem. Mater.*, 1992, **4**, 31-48.

239 S. Natarajan and S. Mandal, *Angew. Chem. Int. Ed.*, 2008, **47**, 4798-4828.

240 R. Murugavel, A. Choudhury, M. G. Walawalkar, R. Pothiraja and C. N. R. Rao, *Chem. Rev.*, 2008, **108**, 3549-3655.

241 Y. Uebou, S. Okada and J. Yamaki, *J. Power Sources*, 2003, **115**, 119-124.

242 G. Hautier, A. Jain, S. P. Ong, B. Kang, C. Moore, R. Doe and G. Ceder, *Chem. Mater.*, 2011, **23**, 3495-3508.

243 B. H. Wen, N. A. Chernova, R. B. Zhang, Q. Wang, F. Omenya, J. Fang and M. S. Whittingham, *Chem. Mater.*, 2013, **25**, 3513-3521.

244 K. Ben-Kamel, N. Amdouni, H. Groult, A. Mauger, K. Zaghib and C. M. Julien, *J. Power Sources*, 2012, **202**, 314-321.

245 J. Barker, M. Y. Saidi and J. L. Swoyer, *Electrochem. Solid State Lett.*, 2003, **6**, A252-A256.

246 S. J. Hibble, I. D. Fawcett and A. C. Hannon, *Inorg. Chem.*, 1997, **36**, 1749-1753.

247 J. Barker, M. Y. Saidi and J. L. Swoyer, *Solid State Ionics*, 2003, **158**, 261-267.

248 D. Mikhailova, N. N. Bramnik, K. G. Bramnik, P. Reichel, S. Oswald, A. Senyshyn, D. M. Trots and H. Ehrenberg, *Chem. Mater.*, 2011, **23**, 3429-3441.

249 A. C. W. P. James and J. B. Goodenough, *J. Solid State Chem.*, 1988, **76**, 87-96.

250 Y. Takahashi, N. Kijima, H. Hayakawa, J. Awaka and J. Akimoto, *J. Phys. Chem. Solids*, 2008, **69**, 1518-1520.

251 H. Kobayashi, M. Tabuchi, M. Shikano, Y. Nishimura, H. Kageyama, T. Ishida, H. Nakamura, Y. Kurioka and R. Kanno, *J. Power Sources*, 1999, **81**, 524-529.

252 J. Ma, Y. N. Zhou, Y. R. Gao, X. Q. Yu, Q. Y. Kong, L. Gu, Z. X. Wang, X. Q. Yang and L. Q. Chen, *Chem. Mater.*, 2014, **26**, 3256-3262.

253 K. S. Park, D. Im, A. Benayad, A. Dylla, K. J. Stevenson and J. B. Goodenough, *Chem. Mater.*, 2012, **24**, 2673-2683.

254 J. Ma, Y. R. Gao, Z. X. Wang and L. Q. Chen, *J. Power Sources*, 2014, **258**, 314-320.

255 J. Lee, A. Urban, X. Li, D. Su, G. Hautier and G. Ceder, *Science*, 2014, **343**, 519-522.

256 M. Bouroushian, *Electrochemistry of Metal Chalcogenides*, Springer, Berlin ; London, 2010.

257 S. Balendhran, S. Walia, H. Nili, J. Z. Ou, S. Zhuiykov, R. B. Kaner, S. Sriram, M. Bhaskaran and K. Kalantar-zadeh, *Adv. Funct. Mater.*, 2013, **23**, 3952-3970.

258 M. Chhowalla, H. S. Shin, G. Eda, L. J. Li, K. P. Loh and H. Zhang, *Nat. Chem.*, 2013, **5**, 263-275.

259 X. Huang, Z. Y. Zeng and H. Zhang, *Chem. Soc. Rev.*, 2013, **42**, 1934-1946.

260 T. Stephenson, Z. Li, B. Olsen and D. Mitlin, *Energy Environ. Sci.*, 2014, **7**, 209-231.

261 Q. H. Wang, K. Kalantar-Zadeh, A. Kis, J. N. Coleman and M. S. Strano, *Nature Nanotechnology*, 2012, **7**, 699-712.

262 M. Chhowalla and G. A. J. Amaratunga, *Nature*, 2000, **407**, 164-167.

263 B. Radisavljevic, A. Radenovic, J. Brivio, V. Giacometti and A. Kis, *Nat. Nanotechnol.*, 2011, **6**, 147-150.

264 P. L. Sun, W. X. Zhang, X. L. Hu, L. X. Yuan and Y. H. Huang, *J. Mater. Chem. A*, 2014, **2**, 3498-3504.

265 J. Feng, X. F. Qian, C. W. Huang and J. Li, *Nat. Photonics*, 2012, **6**, 865-871.

266 H. I. Karunadasa, E. Montalvo, Y. J. Sun, M. Majda, J. R. Long and C. J. Chang, *Science*, 2012, **335**, 698-702.

267 C. F. Zhu, Z. Y. Zeng, H. Li, F. Li, C. H. Fan and H. Zhang, *J. Am. Chem. Soc.*, 2013, **135**, 5998-6001.

268 N. Imanishi, K. Kanamura and Z. I. Takehara, *J. Electrochem. Soc.*, 1992, **139**, 2082-2087.

269 C. Julien, S. I. Saikh and G. A. Nazri, *Mater. Sci. Eng.: B*, 1992, **15**, 73-77.

270 A. Y. Li, H. Y. Liu, Z. Z. Zhu, M. C. Huang and Y. Yang, *J. Mater. Sci. Technol.*, 2006, **22**, 40-44.

271 Y. Miki, D. Nakazato, H. Ikuta, T. Uchida and M. Wakihara, *J. Power Sources*, 1995, **54**, 508-510.

272 A. V. Murugan, M. Quintin, M. H. Delville, G. Campet, C. S. Gopinath and K. Vijayamohanan, *J. Power Sources*, 2006, **156**, 615-619.

273 M. A. Py and R. R. Haering, *Canadian J. Phys.*, 1983, **61**, 76-84.

274 V. Yufit, M. Nathan, D. Golodnitsky and E. Peled, *J. Power Sources*, 2003, **122**, 169-173.

275 Y. Chen, B. Song, X. Tang, L. Lu and J. Xue, *Small*, 2014, **10**, 1536-1543.

276 C. Q. Feng, J. Ma, H. Li, R. Zeng, Z. P. Guo and H. K. Liu, *Mater. Res. Bull.*, 2009, **44**, 1811-1815.

277 Y. N. Ko, Y. C. Kang and S. B. Park, *Nanoscale*, 2014, **6**, 4508-4512.

278 J. H. Kong, C. Y. Zhao, Y. F. Wei, S. L. Phua, Y. L. Dong and X. H. Lu, *J. Mater. Chem. A*, 2014, **2**, 15191-15199.

279 S. Q. Liang, J. Zhou, J. Liu, A. Q. Pan, Y. Tang, T. Chen and G. Z. Fang, *Crystengcomm*, 2013, **15**, 4998-5002.

280 Y. D. Liu, L. Ren, X. Qi, L. W. Yang, J. Li, Y. Wang and J. X. Zhong, *J. Energy Chem.*, 2014, **23**, 207-212.

281 U. K. Sen and S. Mitra, *ACS Appl. Mater. Interfaces*, 2013, **5**, 1240-1247.

282 M. Wang, G. Li, H. Xu, Y. Qian and J. Yang, *ACS Appl. Mater. Interfaces*, 2013, **5**, 1003-1008.

283 X. Xu, Z. Fan, S. Ding, D. Yu and Y. Du, *Nanoscale*, 2014, **6**, 5245-5250.

284 X. Cao, Y. Shi, W. Shi, X. Rui, Q. Yan, J. Kong and H. Zhang, *Small*, 2013, **9**, 3433-3438.

285 K. Chang, W. Chen, L. Ma, H. Li, H. Li, F. Huang, Z. Xu, Q. Zhang and J.-Y. Lee, *J. Mater. Chem.*, 2011, **21**, 6251.

286 K. Chang and W. X. Chen, *J. Mater. Chem.*, 2011, **21**, 17175-17184.

287 K. Chang and W. X. Chen, *ACS Nano*, 2011, **5**, 4720-4728.

288 K. Chang, D. Geng, X. Li, J. Yang, Y. Tang, M. Cai, R. Li and X. Sun, *Adv. Energy Mater.*, 2013, **3**, 839-844.

289 W. X. Chen and K. Chang, *Chem. Commun.*, 2011, **47**, 4252-4254.

290 Y. Gong, S. Yang, Z. Liu, L. Ma, R. Vajtai and P. M. Ajayan, *Adv. Mater.*, 2013, **25**, 3979-3984.

291 J. Guo, X. Chen, Y. J. Yi, W. Z. Li and C. H. Liang, *RSC Adv.*, 2014, **4**, 16716-16720.

292 H. Hwang, H. Kim and J. Cho, *Nano Lett.*, 2011, **11**, 4826-4830.

293 Y. C. Liu, Y. P. Zhao, L. F. Jiao and J. Chen, *J. Mater. Chem. A*, 2014, **2**, 13109-13115.

294 L. Ma, G. C. Huang, W. X. Chen, Z. Wang, J. B. Ye, H. Y. Li, D. Y. Chen and J. Y. Lee, *J. Power Sources*, 2014, **264**, 262-271.

295 K. Rana, J. Singh, J. T. Lee, J. H. Park and J. H. Ahn, *ACS Appl. Mater. Interfaces*, 2014, **6**, 11158-11166.

296 J. Xiao, X. J. Wang, X. Q. Yang, S. D. Xun, G. Liu, P. K. Koech, J. Liu and J. P. Lemmon, *Adv. Funct. Mater.*, 2011, **21**, 2840-2846.

297 H. L. Yu, C. Ma, B. H. Ge, Y. J. Chen, Z. Xu, C. L. Zhu, C. Y. Li, Q. Y. Ouyang, P. Gao, J. Q. Li, C. W. Sun, L. H. Qi, Y. M. Wang and F. H. Li, *Chem. Eur. J.*, 2013, **19**, 5818-5823.

298 X. F. Zhou, Z. Wang, W. X. Chen, L. Ma, D. Y. Chen and J. Y. Lee, *J. Power Sources*, 2014, **251**, 264-268.

299 X. S. Zhou, L. J. Wan and Y. G. Guo, *Chem. Commun.*, 2013, **49**, 1838-1840.

300 K. Bindumadhavan, S. K. Srivastava and S. Mahanty, *Chem. Commun.*, 2013, **49**, 1823-1825.

301 S. K. Das, *Mater. Lett.*, 2014, **130**, 240-244.

302 S. K. Das, R. Mallavajula, N. Jayaprakash and L. A. Archer, *J. Mater. Chem.*, 2012, **22**, 12988-12992.

303 S. Ding, J. S. Chen and X. W. Lou, *Chem. Eur. J.*, 2011, **17**, 13142-13145.

304 S. Hu, W. Chen, J. Zhou, F. Yin, E. Uchaker, Q. F. Zhang and G. Z. Cao, *J. Mater. Chem. A*, 2014, **2**, 7862-7872.

305 C. X. Lu, W. W. Liu, H. Li and B. K. Tay, *Chem. Commun.*, 2014, **50**, 3338-3340.

306 H. Luo, L. Z. Zhang and L. Yue, *Adv. Mater. Res.*, 2012, **531**, 471-477.

307 S. K. Park, S. H. Yu, S. Woo, B. Quan, D. C. Lee, M. K. Kim, Y. E. Sung and Y. Piao, *Dalton Trans.*, 2013, **42**, 2399-2405.

308 W. D. Qiu, J. Xia, S. X. He, H. J. Xu, H. M. Zhong and L. P. Chen, *Electrochim. Acta*, 2014, **117**, 145-152.

309 Y. M. Shi, Y. Wang, J. I. Wong, A. Y. S. Tan, C. L. Hsu, L. J. Li, Y. C. Lu and H. Y.

Yang, *Sci. Rep.*, 2013, **3**.

310 C. Wang, W. Wan, Y. H. Huang, J. T. Chen, H. H. Zhou and X. X. Zhang, *Nanoscale*, 2014, **6**, 5351-5358.

311 J.-Z. Wang, L. Lu, M. Lotya, J. N. Coleman, S.-L. Chou, H.-K. Liu, A. I. Minett and J. Chen, *Adv. Energy Mater.*, 2013, **3**, 798-805.

312 Q. Wang and J. H. Li, *J. Phys. Chem. C*, 2007, **111**, 1675-1682.

313 S. Q. Wang, X. Y. Jiang, H. Zheng, H. M. Wu, S. J. Kim and C. Q. Feng, *Nanosci. Nanotech. Lett.*, 2012, **4**, 378-383.

314 Y. Wang, G. Z. Xing, Z. J. Han, Y. M. Shi, J. I. Wong, Z. X. Huang, K. Ostrikov and H. Y. Yang, *Nanoscale*, 2014, **6**, 8884-8890.

315 L. C. Yang, S. N. Wang, J. J. Mao, J. W. Deng, Q. S. Gao, Y. Tang and O. G. Schmidt, *Adv. Mater.*, 2013, **25**, 1180-1184.

316 H. L. Yu, C. L. Zhu, K. Zhang, Y. J. Chen, C. Y. Li, P. Gao, P. P. Yang and Q. Y. Ouyang, *J. Mater. Chem. A*, 2014, **2**, 4551-4557.

317 C. Zhang, Z. Wang, Z. Guo and X. W. Lou, *ACS Appl. Mater. Interfaces*, 2012, **4**, 3765-3768.

318 C. F. Zhang, H. B. Wu, Z. P. Guo and X. W. Lou, *Electrochem. Commun.*, 2012, **20**, 7-10.

319 L. Zhang and X. W. Lou, *Chem. Eur. J.*, 2014, **20**, 5219-5223.

320 Q. F. Zhang, K. Yu, B. Zhao, Y. Wang, C. Q. Song, S. C. Li, H. H. Yin, Z. L. Zhang and Z. Q. Zhu, *RSC Adv.*, 2013, **3**, 10994-11000.

321 C. Y. Zhao, J. H. Kong, L. P. Yang, X. Y. Yao, S. L. Phua and X. H. Lua, *Chem. Commun.*, 2014, **50**, 9672-9675.

322 C. Y. Zhao, J. H. Kong, X. Y. Yao, X. S. Tang, Y. L. Dong, S. L. Phua and X. H. Lu, *ACS Appl. Mater. Interfaces*, 2014, **6**, 6392-6398.

323 X. Zhou, L. J. Wan and Y. G. Guo, *Nanoscale*, 2012, **4**, 5868-5871.

324 C. B. Zhu, X. K. Mu, P. A. van Aken, Y. Yu and J. Maier, *Angew. Chem. Int. Ed.*, 2014, **53**, 2152-2156.

325 X. P. Fang, X. W. Guo, Y. Mao, C. X. Hua, L. Y. Shen, Y. S. Hu, Z. X. Wang, F. Wu and L. Q. Chen, *Chem. Asian J.*, 2012, **7**, 1013-1017.

326 D. Ilić, K. Wiesener, W. Schneider, H. Oppermann and G. Krabbes, *J. Power Sources*, 1985, **14**, 223-229.

327 J. Morales, J. Santos and J. L. Tirado, *Solid State Ionics*, 1996, **83**, 57-64.

328 Y. F. Shi, C. X. Hua, B. Li, X. P. Fang, C. H. Yao, Y. C. Zhang, Y. S. Hu, Z. X. Wang, L. Q. Chen, D. Y. Zhao and G. D. Stucky, *Adv. Funct. Mater.*, 2013, **23**, 1832-1838.

329 J. Park, J. S. Kim, J. W. Park, T. H. Nam, K. W. Kim, J. H. Ahn, G. Wang and H. J. Ahn, *Electrochim. Acta*, 2013, **92**, 427-432.

330 M. Mortazavi, C. Wang, J. K. Deng, V. B. Shenoy and N. V. Medhekar, *J. Power Sources*, 2014, **268**, 279-286.

331 Z. Hu, L. Wang, K. Zhang, J. Wang, F. Cheng, Z. Tao and J. Chen, *Angew. Chem. Int. Ed.*, 2014, **126**, 13008-13012.

332 G. S. Bang, K. W. Nam, J. Y. Kim, J. Shin, J. W. Choi and S. Y. Choi, *ACS Appl. Mater. Interfaces*, 2014, **6**, 7084-7089.

333 Y. X. Wang, S. L. Chou, D. Wexler, H. K. Liu and S. X. Dou, *Chem. Eur. J.*, 2014, **20**, 9607-9612.

334 W.-H. Ryu, J.-W. Jung, K. Park, S.-J. Kim and I.-D. Kim, *Nanoscale*, 2014, **6**, 10975-10981.

335 Y. X. Wang, K. H. Seng, S. L. Chou, J. Z. Wang, Z. P. Guo, D. Wexler, H. K. Liu and S. X. Dou, *Chem. Commun.*, 2014, **50**, 10730-10733.

336 L. David, R. Bhandavat and G. Singh, *ACS Nano*, 2014, **8**, 1759-1770.

337 Y. N. Ko, S. H. Choi, S. B. Park and Y. C. Kang, *Nanoscale*, 2014, **6**, 10511-10515.

338 S.-G. Woo, J.-Y. Yoo, W. Cho, M.-S. Park, K. J. Kim, J.-H. Kim, J.-S. Kim and Y.-J. Kim, *RSC Adv.*, 2014, **4**, 59048-59055.

339 P. Saha, P. H. Jampani, M. K. Datta, C. U. Okoli, A. Manivannan and P. N. Kumta, *J. Electrochem. Soc.*, 2014, **161**, A593-A598.

340 T. Kaewmaraya, M. Ramzan, J. M. Osorio-Guillén and R. Ahuja, *Solid State Ionics*, 2014, **261**, 17-20.

341 T. Ichitsubo, S. Yagi, R. Nakamura, Y. Ichikawa, S. Okamoto, K. Sugimura, T.

Kawaguchi, A. Kitada, M. Oishi, T. Doi and E. Matsubara, *J. Mater. Chem.*, 2014, **2**, 14858-14866.

342 E. Levi, G. Gershinsky, D. Aurbach and O. Isnard, *Inorg. Chem.*, 2009, **48**, 8751-8758.

343 E. Levi, E. Lancry, A. Mitelman, D. Aurbach, G. Ceder, D. Morgan and O. Isnard, *Chem. Mater.,* 2006, **18**, 5492-5503.

344 E. Lancry, E. Levi, A. Mitelman, S. Malovany and D. Aurbach, *J.Solid State Chem.*, 2006, **179**, 1879-1882.

345 M. D. Levi, E. Lancry, H. Gizbar, Z. Lu, E. Levi, Y. Gofer and D. Aurbach, *J.Electrochem. Soc.*, 2004, **151**, A1044-A1051.

346 E. Levi, Y. Gofer, Y. Vestfreed, E. Lancry and D. Aurbach, *Chem. Mater.*, 2002, **14**, 2767-2773.

347 Y. L. Liang, R. J. Feng, S. Q. Yang, H. Ma, J. Liang and J. Chen, *Adv. Mater.,*2011, **23**, 640-643.

348 S. Q. Yang, D. X. Li, T. R. Zhang, Z. L. Tao and J. Chen, *J. Phys. Chem. C*, 2012, **116**, 1307-1312.

349 X. L. Li and Y. D. Li, *J. Phys. Chem. B*, 2004, **108**, 13893-13900.

350 Y. Liu, L. Jiao, Q. Wu, J. Du, Y. Zhao, Y. Si, Y. Wang and H. Yuan, *J. Mater. Chem. A*, 2013, **1**, 5822-5826.

351 G. Gershinsky, H. D. Yoo, Y. Gofer and D. Aurbach, *Langmuir*, 2013, **29**, 10964-10972.

352 L. L. Zhang and X. S. Zhao, *Chem. Soc. Rev.*, 2009, **38**, 2520-2531.

353 W. F. Wei, X. W. Cui, W. X. Chen and D. G. Ivey, *Chem. Soc. Rev.*, 2011, **40**, 1697-1721.

354 J. Rajeswari, P. S. Kishore, B. Viswanathan and T. K. Varadarajan, *Electrochem. Commun.*, 2009, **11**, 572-575.

355 F. L. Gao, L. J. Zhang and S. M. Huang, *Mater. Lett.*, 2010, **64**, 537-540.

356 P. X. Han, W. Ma, S. P. Pang, Q. S. Kong, J. H. Yao, C. F. Bi and G. L. Cui, *J. Mater. Chem. A*, 2013, **1**, 5949-5954.

357 K. M. Hercule, Q. Wei, A. M. Khan, Y. Zhao, X. Tian and L. Mai, *Nano Lett.*,

2013, **13**, 5685-5691.

358 X. Y. Li, J. Shao, J. Li, L. Zhang, Q. T. Qu and H. H. Zheng, *J. Power Sources*, 2013, **237**, 80-83.

359 L. Zheng, Y. Xu, D. Jin and Y. Xie, *J. Mater. Chem.*, 2010, **20**, 7135-7143.

360 Y. Zhou, C. W. Lee, S. K. Kim and S. Yoon, *Ecs Electrochem. Lett.*, 2012, **1**, A17-A20.

361 T. Brezesinski, J. Wang, S. H. Tolbert and B. Dunn, *Nat. Mater.*, 2010, **9**, 146-151.

362 T. Tao, Q. Y. Chen, H. P. Hu and Y. Chen, *Mater. Lett.*, 2012, **66**, 102-105.

363 I. Shakir, M. Shahid, H. W. Yang and D. J. Kang, *Electrochim. Acta*, 2010, **56**, 376-380.

364 R. Liang, H. Cao and D. Qian, *Chem. Commun.*, 2011, **47**, 10305-10307.

365 W. Tang, L. Liu, S. Tian, L. Li, Y. Yue, Y. Wu and K. Zhu, *Chem. Commun.*, 2011, **47**, 10058-10060.

366 J. B. Jiang, J. L. Liu, S. J. Peng, D. Qian, D. M. Luo, Q. F. Wang, Z. W. Tian and Y. C. Liu, *J. Mater. Chem. A*, 2013, **1**, 2588-2594.

367 B. Mendoza-Sanchez, T. Brousse, C. Ramirez-Castro, V. Nicolosi and P. S. Grant, *Electrochim. Acta*, 2013, **91**, 253-260.

368 G. R. Li, Z. L. Wang, F. L. Zheng, Y. N. Ou and Y. X. Tong, *J. Mater. Chem.*, 2011, **21**, 4217-4221.

369 Y. Liu, B. H. Zhang, Y. Q. Yang, Z. Chang, Z. B. Wen and Y. P. Wu, *J. Mater. Chem. A*, 2013, **1**, 13582-13587.

370 I. Shakir, M. Shahid, S. Cherevko, C. H. Chung and D. J. Kang, *Electrochim. Acta*, 2011, **58**, 76-80.

371 C. Liu, Z. Li and Z. Zhang, *Sci. Technol. Adv. Mater.*, 2013, **14**, 065005.

372 C. Liu, Z. C. Li and Z. J. Zhang, *Electrochim. Acta*, 2014, **134**, 84-91.

373 C. Liu, Z. Xie, W. P. Wang, Z. C. Li and Z. J. Zhang, *Electrochem. Commun.*, 2014, **44**, 23-26.

374 X. Xiao, T. P. Ding, L. Y. Yuan, Y. Q. Shen, Q. Zhong, X. H. Zhang, Y. Z. Cao, B. Hu, T. Zhai, L. Gong, J. Chen, Y. X. Tong, J. Zhou and Z. L. Wang, *Adv. Energy*

Mater., 2012, **2**, 1328-1332.

375 X. Xiao, T. Q. Li, Z. H. Peng, H. Y. Jin, Q. Z. Zhong, Q. Y. Hu, B. Yao, Q. P. Luo, C. F. Zhang, L. Gong, J. Chen, Y. Gogotsi and J. Zhou, *Nano Energy*, 2014, **6**, 1-9.

376 K. K. Purushothaman, M. Cuba and G. Muralidharan, *Mater. Res. Bull.*, 2012, **47**, 3348-3351.

377 M. C. Liu, L. B. Kong, X. J. Ma, C. Lu, X. M. Li, Y. C. Luo and L. Kang, *New J. Chem.*, 2012, **36**, 1713-1716.

378 B. Senthilkumar, K. V. Sankar, R. K. Selvan, M. Danielle and M. Manickam, *RSC Adv.*, 2013, **3**, 352-357.

379 D. Guo, H. M. Zhang, X. Z. Yu, M. Zhang, P. Zhang, Q. H. Li and T. H. Wang, *J. Mater. Chem. A*, 2013, **1**, 7247-7254.

380 Z. Q. Liu, L. Y. Tang, N. Li, K. Xiao, J. Wang, J. H. Zhang, Y. Z. Su and Y. X. Tong, *J. Electrochem. Soc.*, 2012, **159**, D582-D586.

381 G. K. Veerasubramani, K. Krishnamoorthy, R. Sivaprakasam and S. J. Kim, *Mater. Chem. Phys.*, 2014, **147**, 836-842.

382 D. Cai, D. Wang, B. Liu, Y. Wang, Y. Liu, L. Wang, H. Li, H. Huang, Q. Li and T. Wang, *ACS Appl. Mater. Interfaces*, 2013, **5**, 12905-12910.

383 D. Guo, P. Zhang, H. M. Zhang, X. Z. Yu, J. Zhu, Q. H. Li and T. H. Wang, *J. Mater. Chem. A*, 2013, **1**, 9024-9027.

384 D. Guo, Y. Z. Luo, X. Z. Yu, Q. H. Li and T. H. Wang, *Nano Energy*, 2014, **8**, 174-182.

385 D. P. Cai, B. Liu, D. D. Wang, Y. Liu, L. L. Wang, H. Li, Y. R. Wang, C. X. Wang, Q. H. Li and T. H. Wang, *Electrochim. Acta*, 2014, **115**, 358-363.

386 M. C. Liu, L. Kang, L. B. Kong, C. Lu, X. J. Ma, X. M. Li and Y. C. Luo, *RSC Adv.*, 2013, **3**, 6472-6478.

387 H. Z. Wan, J. J. Jiang, X. Ji, L. Miao, L. Zhang, K. Xu, H. C. Chen and Y. J. Ruan, *Mater. Lett.*, 2013, **108**, 164-167.

388 D. Ghosh, S. Giri and C. K. Das, *Nanoscale*, 2013, **5**, 10428-10437.

389 D. Ghosh, S. Giri, M. Moniruzzaman, T. Basu, M. Mandal and C. K. Das, *Dalton*

Trans., 2014, **43**, 11067-11076.

390 X. F. Xia, W. Lei, Q. L. Hao, W. J. Wang and X. Wang, *Electrochim. Acta*, 2013, **99**, 253-261.

391 M. Mandal, D. Ghosh, S. Giri, I. Shakir and C. K. Das, *RSC Adv.*, 2014, **4**, 30832-30839.

392 D. P. Cai, B. Liu, D. D. Wang, L. L. Wang, Y. Liu, H. Li, Y. R. Wang, Q. H. Li and T. H. Wang, *J. Mater. Chem. A*, 2014, **2**, 4954-4960.

393 M. C. Liu, L. B. Kong, C. Lu, X. J. Ma, X. M. Li, Y. C. Luo and L. Kang, *J. Mater. Chem. A*, 2013, **1**, 1380-1387.

394 L. Q. Mai, F. Yang, Y. L. Zhao, X. Xu, L. Xu and Y. Z. Luo, *Nat. Commun.*, 2011, **2**, 381.

395 B. Senthilkumar, D. Meyrick, Y. S. Lee and R. K. Selvan, *RSC Adv.*, 2013, **3**, 16542-16548.

396 L. J. Cao, S. B. Yang, W. Gao, Z. Liu, Y. J. Gong, L. L. Ma, G. Shi, S. D. Lei, Y. H. Zhang, S. T. Zhang, R. Vajtai and P. M. Ajayan, *Small*, 2013, **9**, 2905-2910.

397 E. G. da SilveiraFirmiano, A. C. Rabelo, C. J. Dalmaschio, A. N. Pinheiro, E. C. Pereira, W. H. Schreiner and E. R. Leite, *Adv. Energy Mater.*, 2014, **4**, n/a-n/a.

398 B. L. Hu, X. Y. Qin, A. M. Asiri, K. A. Alamry, A. O. Al-Youbi and X. P. Sun, *Electrochim. Acta*, 2013, **100**, 24-28.

399 K. J. Huang, L. Wang, Y. J. Liu, H. B. Wang, Y. M. Liu and L. L. Wang, *Electrochim. Acta*, 2013, **109**, 587-594.

400 K. J. Huang, L. Wang, J. Z. Zhang, L. L. Wang and Y. P. Mo, *Energy*, 2014, **67**, 234-240.

401 K. J. Huang, J. Z. Zhang, G. W. Shi and Y. M. Liu, *Electrochim. Acta*, 2014, **132**, 397-403.

402 K. Krishnamoorthy, G. K. Veerasubramani, S. Radhakrishnan and S. J. Kim, *Mater. Res. Bull.*, 2014, **50**, 499-502.

403 G. F. Ma, H. Peng, J. J. Mu, H. H. Huang, X. Z. Zhou and Z. Q. Lei, *J. Power Sources*, 2013, **229**, 72-78.

404 L. Ma, L. M. Xu, X. P. Zhou and X. Y. Xu, *Mater. Lett.*, 2014, **132**, 291-294.

405 A. Ramadoss, T. Kim, G. S. Kim and S. J. Kim, *New J. Chem.*, 2014, **38**, 2379-2385.

406 J. M. Soon and K. P. Loh, *Electrochem. Solid State Lett.*, 2007, **10**, A250-A254.

407 J. Wang, D. L. Chao, J. L. Liu, L. L. Li, L. F. Lai, J. Y. Lin and Z. X. Shen, *Nano Energy*, 2014, **7**, 151-160.

408 A. Winchester, S. Ghosh, S. M. Feng, A. L. Elias, T. Mallouk, M. Terrones and S. Talapatra, *ACS Appl. Mater. Interfaces*, 2014, **6**, 2125-2130.

409 X. P. Zhou, B. Xu, Z. F. Lin, D. Shu and L. Ma, *J. Nanosci. Nanotech.*, 2014, **14**, 7250-7254.